UCLA

UCLA Structural / Earthquake Engineering Research Laboratory

Ductile Reinforced Concrete Coupled Walls: FEMA P695 Study

Final Report

Negin A. Tauberg, Ph.D. Candidate, UCLA
Kristijan Kolozvari, Assistant Professor, CSU Fullerton
John W. Wallace, Professor and Director, UCLA

University of California, Los Angeles
Department of Civil and Environmental Engineering
5731C Boelter Hall
Los Angeles, California, 90095-1593

Project Sponsors:

CHARLES PANKOW FOUNDATION

aci Foundation
Knowledge to Practice®

UCLA SEERL
2019/01
July 2019

Ductile Reinforced Concrete Coupled Walls:
FEMA P695 Study

Final Report

Negin A. Tauberg, Ph.D. Candidate, UCLA
Kristijan Kolozvari, Assistant Professor, CSU Fullerton
John W. Wallace, Professor and Director, UCLA

University of California, Los Angeles
Department of Civil and Environmental Engineering
5731C Boelter Hall
Los Angeles, California, 90095-1593

Project Sponsors:

CHARLES PANKOW FOUNDATION

aci Foundation
Knowledge to Practice®

This page is intentionally left blank

Acknowledgements

The work presented in this report was supported by funds from the Charles Pankow Foundation under the Grant RGA#06-17, as well as in part by the American Concrete Institute Foundation. Special thanks to the independent peer review panel, Ron Hamburger, Anindya Dutta, Steve McCabe, and Charlie Kircher for their valuable comments, as well as our advisory group, which included Satyendra K. Ghosh, John Hooper, David Fields, Ron Klemencic, Andy Taylor, Jim Harris, and Kevin Aswegan, and members of the BSSC PUC IT4 committee who provided valuable input and support over the course of the research.

Any opinions, findings, and conclusions or recommendations expressed in this material are those of the authors and do not necessarily reflect those of the sponsoring organizations or the Regents of the University of California.

Table of Contents

Acknowledgements iii
Chapter 1 - Introduction 1
1.1 Background 1
1.2 Objectives 2
1.3 Report Organization 3
Chapter 2 - Archetype Design 5
2.1 Archetype Design Variations 5
2.2 Design Process 7
2.2.1 Coupling Beam Design 11
2.2.2 Wall Design 11
2.3 Initial Designs and Required Revisions 16
2.4 Archetype Designs 17
2.4.1 8-Story Archetypes 19
2.4.2 12-Story Archetypes 26
2.4.3 18-Story Archetypes 33
2.4.4 24-Story Archetypes 40
2.4.5 30-Story Archetypes 43
2.4.6 Comparison of RSA and ELF demands 46
2.4.7 Design Summary 48
Chapter 3 - Nonlinear Modeling 49
3.1 System and component modeling 49
3.1.1 System modeling 49
3.1.2 Component modeling 54
3.1.3 Coupling beam modeling 58
3.1.4 Damping 61
3.2 Model Validation 62
3.2.1 Model Validation - 1996 BRI 12-Story Coupled Wall Test 62
3.2.2 Model Validation – 1974 Test by Santhakumar 74
3.3 Summary 77
Chapter 4 - Failure Modes 78
4.1 Description of failure modes 78
4.1.1 Flexural failure via Drift Capacity Model 78
4.1.2 Shear Failure 80
4.1.3 Axial Failure 81
4.2 Assessment of Failure Modes 84
4.3 Summary 85

Chapter 5 - Nonlinear Structural Analyses 86
5.1 Analysis Procedure 86
5.2 Results of initial Archetype designs 91
5.2.1 Summary 94
5.3 Analysis Results of Final Archetype Designs 95
5.3.1 Pushover analysis results 95
5.3.2 IDA results 98
5.4 Assessment of the Deflection Amplification Factor, C_d 107
5.5 Shear at Peak Drift 109
5.6 Summary of Analysis Results 111
Chapter 6 - Additional Studies 113
6.1 D_{min} Archetypes 113
6.1.1 12-Story D_{min} Archetype Design 114
6.1.2 24-Story D_{min} Archetype Design 117
6.1.3 Analysis Results of D_{min} Archetypes 119
6.2 Uncoupled Shear Wall System 120
6.3 Low-rise Archetypes 123
6.3.1 6- and 4-Story Archetypes 123
6.3.2 2-Story Archetypes 125
6.4 Sensitivity studies with Shear-Flexure Interaction effects 128
Chapter 7 - Summary and Conclusions 130
Appendix 133
References 142

List of Symbols

A_g = Gross cross sectional area

A_s = Area of steel reinforcement

c = Neutral axis depth

C_0 = Modification factor relating the displacement of the control point to the displacement of a single degree of freedom system

C_s = Seismic response coefficient

C_u = Coefficient for upper limit for calculated period per ASCE 7

C_d = Deflection amplification factor per ASCE 7

D = Dead load

d_b = Diameter of reinforcing bar

E = Earthquake load

E_c = Concrete modulus of elasticity

E_s = Steel modulus of elasticity

f'_c = Concrete compressive strength

f_y = Steel yield strength

G = Shear modulus

h_w = Wall height

I = Moment of inertia

I_{eff} = Effective moment of inertia

L = Live load

l_d = Development length

l_n = Clear span

l_w = Wall length

P = Axial load

P_n = Nominal axial load capacity

P_u = Ultimate axial load

R = Response modification factor per ASCE 7

S_{D1} = Design spectral response acceleration parameter at a period of 1 second per ASCE 7

S_{DS} = Design spectral response acceleration parameter at short periods per ASCE 7

T = Design period

T_1 = Fundamental period

t_w = Wall thickness

V = Shear force

V_n = Nominal shear capacity

V_u = Ultimate shear load

α = Diagonal inclination angle

β = Uncertainty

δ = displacement

δ_u = Ultimate displacement

$\delta_{y,eff}$ = Effective yield displacement

Δ = Drift

ε_c = Compressive strain

ε_t = Tensile strain

φ = Strength reduction factor

θ = Rotation

μ = Ductility

ρ = Reinforcement ratio

Ω_0 = Overstrength factor per ASCE 7

Chapter 1 - Introduction

1.1 Background

Quantification of building system performance and response parameters, such as the Response Modification Factor (***R***), System Overstrength Factor ($\boldsymbol{\Omega_0}$), and Deflection Amplification Factor ($\boldsymbol{C_d}$), is required to design lateral force resisting systems per ASCE 7 (ASCE, 2016). The values of these parameters used in current design, e.g., ASCE/SEI 7-16, are mainly based on judgment and qualitative comparisons of the known response capabilities of these lateral-force resisting systems in earthquakes. The FEMA P695 (FEMA, 2009) methodology was developed to formalize the selection of building system response parameters for new systems, alternative configurations of existing systems, and for systems that utilize new materials.

Current ASCE 7 (ASCE, 2016) and ACI 318 (ACI, 2014) design requirements do not distinguish between different configurations used for reinforced concrete (RC) structural walls, i.e., a cantilever (uncoupled) wall is treated the same as a coupled wall. In addition, even for a coupled wall, current building system parameters do not vary with coupling beam reinforcement detailing, i.e., diagonally- and conventionally-reinforced coupling beams are treated the same even though it is well established that diagonally-reinforced beams have superior load-deformation behavior. Finally, current design parameters do not depend on coupling beam aspect ratio, which is known to influence the amount of overall system hysteretic energy dissipation, nor on the relative energy dissipation contribution between the special walls and coupling beams.

In coordination with ACI 318 and ASCE 7, a project was initiated to define a new ASCE 7 lateral system for ductile coupled walls having target values of $\boldsymbol{R} = 8$, $\boldsymbol{C_d} = 8$ and $\boldsymbol{\Omega_0} = 2.5$. A code change proposal has been approved for ACI 318-19 Sections 2.3 and 18.10.9 that defines a "Ductile Coupled Wall" as an assembly of walls with aspect ratio of total wall height to length (h_{wcs}/ℓ_w) greater than 2.0 which are linked by coupling beams having aspect ratios (ℓ_n/h) between 2.0 and 5.0. The limit on wall aspect ratio is intended to ensure that wall behavior at the critical section is governed by flexural yielding prior to shear failure, whereas the limit on coupling beam aspect ratio focuses on ensuring that a majority of the overall inelastic energy dissipation is provided by coupling beam yielding. Additional constraints are included to promote the intended response, i.e., at least 90% of the coupling beams of the lateral force resisting system of the building in the direction of load being considered must have aspect ratio less than 5.0, all coupling beams must have aspect ratio greater than 2.0, and primary longitudinal or/or diagonal reinforcement providing coupling beam strength must be developed to achieve $1.25f_y$ at each end of the coupling beam. In addition, for ASCE 7, a minimum height of 60 feet is proposed for Ductile Coupled Walls to ensure adequate participation of the coupling beams in the energy dissipation mechanism of the lateral force resisting system.

1.2 Objectives

The proposed study aims to justify the use of the proposed design parameters by applying the FEMA P695 approach to the newly defined lateral system. The primary objective of the study is to define a subset of conditions (design provisions) for which the proposed building system response parameters may be used for RC coupled walls. Target values for the Response Modification Factor ($\boldsymbol{R}$), System Overstrength Factor ($\boldsymbol{\Omega_0}$), and Deflection Amplification Factor ($\boldsymbol{C_d}$) are selected, as noted in the prior paragraph, and verified by application of the FEMA P695 methodology. An independent review panel of practicing engineers and researchers are peer reviewing the effort, and an advisory panel of practicing engineers and researchers active with ASCE 7 and ACI Committee 318 are providing input on the design and collapse assessment results.

Thirty-seven prototype RC coupled wall configurations (Archetypes) are assessed in this study for the Seismic Design Category (SDC) being considered, i.e., SDC D_{max}. The Archetypes considered address a range of variables expected to influence the collapse margin ratio, with primary variables of building height (6 to 30 stories), wall cross section (planar and flanged/core), coupling beam aspect ratio (l_n/h = 2.0 to 5.0), and coupling beam reinforcement arrangement (conventionally reinforced (CR) and diagonally reinforced (DR)). Each Archetype is designed using ASCE 7-16 and ACI 318-14 (including 318-19 approved code change proposals). Initially, a set of preliminary Archetypes were designed conforming to the wall shear provisions of ACI 318-14 and were assessed for conformance with the FEMA P695 acceptability criteria. Due to a high number of shear failures experienced during the collapse assessment process, these initial Archetypes had to be revised; the final Archetype designs conform instead to the wall shear provisions of ACI 318-19 code change proposal using amplified wall shear demands accounting for flexural overstrength and higher mode effects.

To assess the potential for collapse, a nonlinear model is created for each Archetype in an open-source computational platform OpenSees (McKenna et al., 2000) and subjected to ground acceleration response histories. New, state-of-the-art, approaches to predict collapse are implemented and evaluated/calibrated using existing test data. The established failure criteria account for flexural compression (concrete crushing, bar buckling, wall lateral instability), flexural tension (bar fracture), shear, and axial failures. For each Archetype, nonlinear static pushover (NSP) and nonlinear incremental dynamic analyses (IDA), subjected to the ATC-63 forty-four far-field ground motion record set, are conducted to obtain the overstrength/ductility and the collapse margin ratio values, respectively. The methodology prescribed in FEMA P695 is followed to establish limits on the adjusted collapse margin ratios (ACMRs) and to observe the vicinity of the obtained ACMRs to these limits in order to investigate the validity of the chosen R-value.

Initial findings indicated that Archetypes using $\boldsymbol{R} = 8$ and $\boldsymbol{C_d} = 8$ and designed conforming to current ACI 318-14 shear provisions, do not meet the FEMA P695 acceptability criteria due to a high number of shear failures experienced during incremental dynamic analysis. The Archetype designs were revised using $\boldsymbol{R} = 8$ and $\boldsymbol{C_d} = 8$ and amplified shear demands following an approved ACI 318-19 code change proposal that is similar to approaches used for wall shear amplification in CSA A23.3 (2014) and NZS 3101 (2006). Results for the final redesigned Archetypes meet the FEMA P695 acceptability criteria. Therefore, the revised design approach using $\boldsymbol{R} = 8$ and $\boldsymbol{C_d} = 8$ and amplified shear demands has been used for all Archetype designs.

1.3 Report Organization

This report summarizes the design, modeling, and collapse assessment results for a set of Ductile Coupled Wall Archetypes representative of common practice. Chapter 1 includes background information describing the purpose of the study and provides an overview of the report. Chapter 2 describes the design procedure and provides key details of the various Archetype designs. Chapter 3 describes details of the nonlinear modeling procedure and model validation studies, while Chapter 4 summarizes the failure models used for collapse assessment, along with the failure assessment procedure. Chapter 5 presents the results from nonlinear static pushover and incremental dynamic analyses including the collapse assessment results. Chapter 6 includes additional studies related to collapse assessment of Archetypes designed for SDC D_{min}, Archetypes designed with uncoupled cantilever walls, Archetypes designed with reduced coupling action (low-rise, i.e., six or fewer stories), and Archetypes analyzed using an advanced model that incorporates nonlinear shear-flexure interaction. Chapter 7 summarizes the general findings and conclusions of the study including recommendations for seismic response parameters of Ductile Coupled Walls as a lateral force resisting system in ASCE 7. An Appendix is used to provide additional information on the development of the Archetype designs.

Chapter 2 - Archetype Design

Collapse analyses are conducted on a series of coupled wall Archetype designs following the FEMA P695 methodology in order to reliably quantify the performance of ductile coupled wall systems and their respective seismic design coefficients including the Response Modification Factor ($\boldsymbol{R}$), the System Overstrength Factor ($\boldsymbol{\Omega_0}$), and the Deflection Amplification Factor ($\boldsymbol{C_d}$). The Archetypes represent designs that are near code limits, i.e., wall geometry and reinforcement that limits overstrength and is near the shear strength limits of ACI 318-19 and drift limits of ASCE 7-16, in order to limit unintended overstrength and ensure the design conditions are as close to design limits as possible. The configurations and design parameters of the Archetypes are presented in this chapter.

2.1 Archetype Design Variations

A series of Archetype coupled wall configurations with 6, 8, 12, 18, 24, and 30 stories (Table 2-1) are considered in this study. Two types of wall pier configurations are assessed: 1) rectangular walls for the 6, 8, and 12 story buildings, and 2) flanged (or core) walls for the 18, 24, and 30 story buildings. Coupling beam types consist of diagonally-reinforced (DR) with beam aspect ratios l_n/h = 2.0, 2.4, 3.0, and 3.3 and conventionally-reinforced (CR) coupling beams with l_n/h = 3.3, 4.0, and 5.0. These variations result in 16 planar and 21 flanged wall Archetypes that are organized into six performance groups.

The site seismic hazard is set as D_{max}. Archetypes designed for seismic hazard D_{min} can be similarly grouped; however, this study focuses on the more critical Archetypes designed for the maximum seismic load intensity per FEMA P695, i.e., SDC D_{max}. As observed in several studies noted in FEMA P695, Archetypes designed for lower seismic demand tend to have higher system overstrength due to the influence of gravity loads, while Archetypes designed for the highest seismic hazard tend to have the smallest collapse margins and higher collapse risk. The assumption of the D_{max} Archetype designs having lower ACMRs is confirmed with the studies summarized in section 6.2.

Table 2-1: Performance Groups for Evaluation of Ductile Coupled Wall Archetypes

Performance Group Summary					
Group No.	Grouping Criteria				Number of Archetypes
	Basic Configuration	Design Load Level		Period Domain	
		Gravity	Seismic		
PG-1	Planar walls, diagonally reinforced coupling beams with l_n/h = 2.0,2.4, 3.0, 3.3	Typical	SDC D_{max}	Short	9 (6, 8, 12 story)
PG-2	Planar walls, conventional reinforced coupling beams with l_n/h = 3.3, 4.0, 5.0	Typical	SDC D_{max}	Short	7 (6, 8, 12 story)
PG-3	Flanged walls, diagonally reinforced coupling beams with l_n/h = 2.0,2.4, 3.0, 3.3	Typical	SDC D_{max}	Short	4 (18 story)
PG-4				Long	8 (24 and 30 story)
PG-5	Flanged walls, conventional reinforced coupling beams with l_n/h = 3.3, 4.0, 5.0	Typical	SDC D_{max}	Short	3 (18 story)
PG-6				Long	6 (24 and 30 story)

A simple rectangular building floor plan is selected with two coupled walls providing lateral load resistance in each principal building direction (Figure 2.1). The floor plan is intended to provide an overall framework for the study such that floor plan areas, gravity column layout, and wall dimensions produce specific design objectives, i.e., maximum wall pier gravity axial stresses of about $0.3A_g f_c'$ under the load combination 1.2D+1.6L, and maximum unamplified wall shear stresses of about $4\sqrt{f'_c}$ (psi) under the governing seismic load combination $(1.2+0.2S_{DS})D+0.5L+1.0E$. Given these objectives, typical gravity axial stress under the FEMA P695 gravity load combination of 1.05D+0.25L are in the range of about $0.10A_g f_c'$ to $0.15A_g f_c'$. These targets are selected based on input from an industry advisory group. The relative area encased by the core compared to the building floor plan is selected to be about ten percent after a review of several recent drawings of coupled core wall buildings. Typical story heights are 10 ft, and an 8-inch thick post-tensioned slab with a 6 ft cantilevered slab overhang is assumed at all levels.

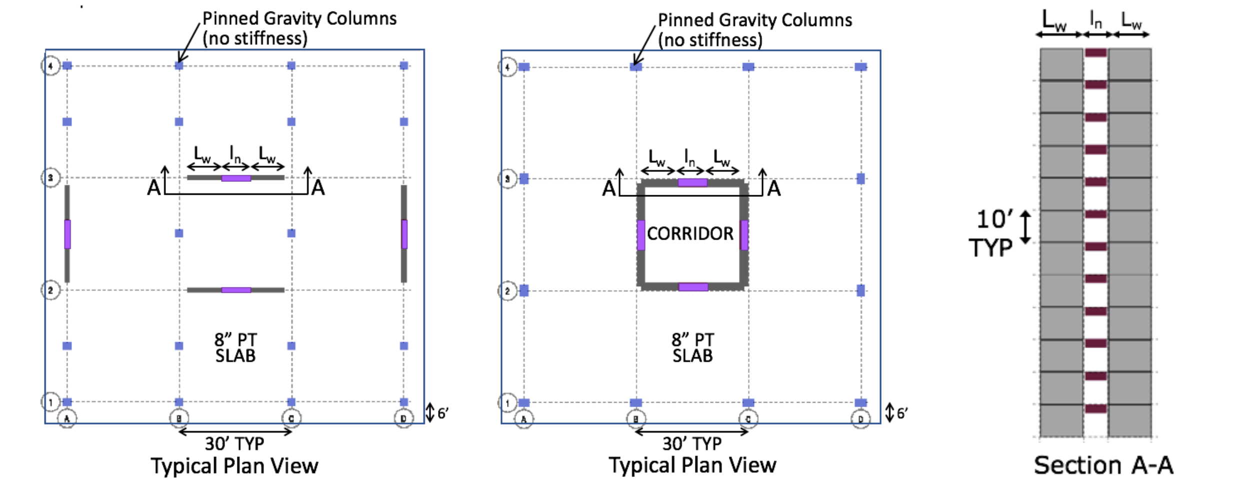

(a) Planar Walls (6, 8, 12 Story) (b) Flanged Walls (18, 24, 30 Story) (c) Elevation View

Figure 2.1: Archetype floor plans and typical wall elevation view

Design gravity loads consist of 100 psf of slab self-weight load plus an additional 25 psf of superimposed dead load (including perimeter and partition loading). Floor live loads (reducible) are taken as 40 psf for the residential buildings (coupling beam $l_n/h \leq 3.0$), 50 psf for the office buildings (coupling beam $l_n/h > 3.0$), and 20 psf for the roof per ASCE 7-16 Table 4-1. For the flanged wall prototypes, gravity loads inside the core consist of 100 psf dead load to account for the one-way slab framing and stairs as well as a non-reducible live load of 100 psf (applied as a line load).

2.2 Design Process

The Archetypes are designed following the provisions of ASCE 7-16, ACI 318-14 including ACI 318-19 approved code change proposals related to wall shear amplification (Section 18.10.3) and drift capacity (Section 18.10.6.2), and the seismic design parameters specified in FEMA P695 (importance factor, redundancy factor, and site class and spectral values). Seismic design forces are determined using the Response Spectrum Analysis (RSA) method of ASCE 7 §12.9.1, subject to scaling the base shear to 100% of the Equivalent Lateral Force base shear of ASCE 7 §12.8 for a period $T = C_u T_a$. Use of the RSA method is permitted by the FEMA P695 methodology, and it also is likely to be used in engineering practice; therefore, it is adopted for this study. Modal damping ratio is assumed to be 5 percent, and the Complete Quadratic Combination (CQC) method is used to combine modal responses.

The trial seismic response parameters are defined as $\boldsymbol{R}$ = 8, $\boldsymbol{C_d}$ = 8, and $\boldsymbol{\Omega_0}$ = 2.5. The designs are for Risk Category I or II structures with an importance factor I_e = 1.0. The soil is assumed to be Site Class D, as specified in FEMA P695 §5.2.2. Seismic spectral acceleration values are S_{DS}=1.0g and S_{D1}=0.6g for seismic design category D_{max} as specified in FEMA P695. The redundancy factor ρ is taken equal to 1.0 per FEMA P695 §11.1.4, since the use of a larger value would increase seismic loads (and capacities), and produce more conservative Archetype designs, which might not be representative for all applications of the proposed system. Story drifts are checked to be less than the two percent drift limit using the fundamental period ($\boldsymbol{T_1}$) with $\boldsymbol{C_d} = \boldsymbol{R}$ as prescribed by FEMA P695 Section 7.7.

The Archetype buildings are modeled using an elastic 3D structural analysis program and subjected to dead, live, and seismic loads. A fixed base is assumed, i.e., soil-structure interaction effects are neglected, and a rigid diaphragm is assumed at each floor level. The wall piers are modeled as 2D elements having an elastic in-plane bending and shear stiffness and an elastic out-of-plane bending stiffness. The wall piers are connected by elastic coupling beam elements having a specified flexural effective stiffness, as described in the following paragraph. Gravity columns with zero lateral stiffness (pinned at each end) are included to account for P-Δ effects for gravity loads not applied to the walls. The gravity columns are distributed around the floor plan to consider the in-plan distribution of the gravity loads.

Effective stiffness values are established based on a review of code provisions and with input from an advisory committee of practicing engineers as summarized in Table 2-2. The wall flexural in-plane and out-of-plane stiffness values are taken as $0.75I_g$ and $0.10I_g$, respectively, while the out-of-plane bending stiffness of the floor diaphragm is set to a negligible value of $0.05I_g$. The value of $0.75I_g$ is selected based on experience and input from the advisory committee such that lateral story drifts for DE level shaking do not exceed lateral drifts for MCE level shaking computed from NL-RHA and to achieve slightly larger wall demands (design base shear). The relatively low value for out-of-plane bending stiffness is selected to minimize this contribution to lateral stiffness. Shear stiffness of walls and coupling beams are set to $0.4E_cA_g$ based on common practice of using gross section shear stiffness for design.

Table 2-2: Effective Stiffness Values for Archetype Designs

Element	Flexural Rigidity	Shear Rigidity	Axial Rigidity
Walls	0.75 E_cI_g (in-plane) 0.10 E_cI_g (out-of-plane)	0.4 E_cA_g	E_cA_g
Coupling beams	(0.07*l_n/h) E_cI_g	0.4 E_cA_g	-- *

* Rigid in-plane diaphragm is assumed.

The coupling beams are modeled as elastic beams with an effective flexural stiffness based on the relation in the PEER TBI (2017) and LATBSDC (2017) guidelines, i.e., $E_cI_{eff}/E_cI_g = 0.07l_n/h$, which represents the secant stiffness to yield, and includes the stiffening impact of the slab and the post-tensioning stress. This expression is based on a review of experimental results for 46 conventionally-reinforced and 58 diagonally-reinforced coupling beam specimens reported in the literature from 1969 to 2016 (Lim and Hwang et al. (2016); Naish (2010); Lequesne (2009); Zhu, et al. (2008); Fortney (2005); Brena and Ihtiyar (2011); Canbolat (2005); Zhou (2003); Dugas (2003); Kwan and Zhao (2002); Adebar (2001); Galano and Vignoli (2000); Bristowe (2000); Tassios (1996); Teshigawara et al. (1996); Kanakubo (1996); Kimura (1991); Tegos and Penelis (1988); Barney (1980); Binney, et al. (1972); Paulay (1972)). This trend and the data used to derive this relationship are shown in Figure 2.2 for conventional- and diagonally- reinforced coupling beams. It is noted that the effective stiffness values represent an average value, and that effective stiffness was increased by 20% to account for the potential influence of scale on bar slip (Naish et al., 2013) and by 20% to account the in-plane stiffness of a slab.

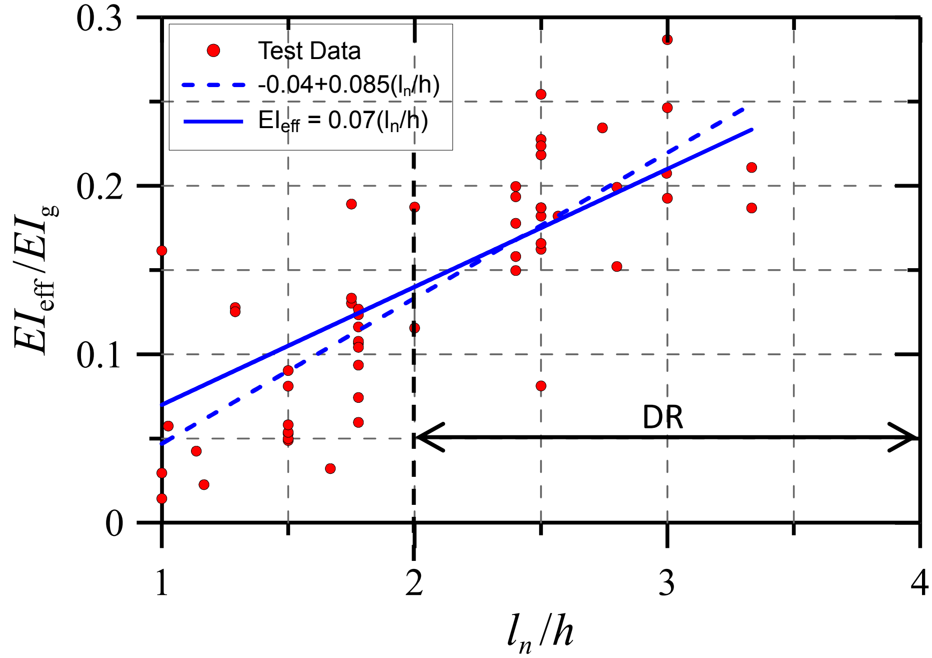

(a) Diagonally Reinforced Coupling Beams

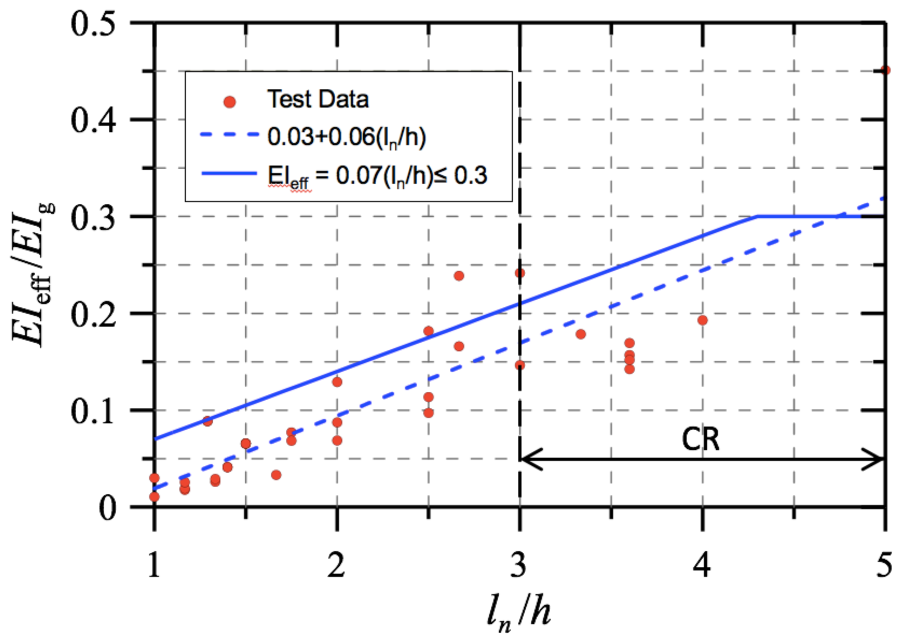

(b) Conventionally Reinforced Coupling Beams

Figure 2.2: Validation of coupling beam effective stiffness relation $0.07l_n/h$

2.2.1 Coupling Beam Design

Coupling beams with diagonal reinforcement are designed to satisfy the provisions of ACI 318-14 §18.10.7.4 such that the shear demand (V_u) does not exceed the reduced strength (ϕV_n). The beam shear strength is a function of the design diagonal bar area A_{vd}, the reinforcement yield stress f_y, and angle of inclination α of the diagonal reinforcement, where the beam nominal strength should not exceed $10\sqrt{f'_c}bd$.

$$\phi V_n = 0.85\left(2A_{vd}f_y sin\alpha\right) < 8.5\sqrt{f'_c}bd \tag{2-1}$$

Conventionally-reinforced coupling beams are designed to satisfy the provisions of 18.10.7.1.

2.2.2 Wall Design

For the 6, 8 and 12 story Archetypes with planar walls, the lateral load demand is considered only in the direction parallel to the length of the walls (Figure 2.3a). For the flanged wall configurations, demands at the centroid of the L-shaped wall group are obtained, and the impact of bi-directional loading is considered by combining 100 percent of the force in one direction and 30 percent of the force in the orthogonal direction (Figure 2.3b) as required by ASCE 7-16 Section 12.5.3.1. Although accidental torsion effects are considered for all Archetypes through offsetting the center of mass by 5 percent in each direction to check for horizontal irregularity, force demands with or without accidental torsion effects do not vary significantly (less than 5% difference) since the coupled walls are near the center of mass in the floor plan.

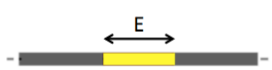

a) Planar Walls

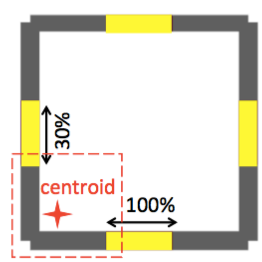

b) Flanged Walls

Figure 2.3: Determination of seismic demands (E) for wall piers

Strength of the wall piers is based on the ACI 318 requirements for special structural walls (§18.10.5) to ensure that the P_u-M_u demand pairs for all load combinations do not exceed the axial and moment capacities ΦP_n-ΦM_n that are reduced with the appropriate strength reduction factors. Governing load combinations for strength design are taken as:

$$(1.2 + 0.2S_{DS})D + E + 0.5L \tag{2-2a}$$

$$(0.9 - 0.2S_{DS})D - E \qquad \text{(2-2b)}$$

The quantities of boundary longitudinal reinforcement and shear reinforcement are reduced over the wall height, typically every two stories, to optimize the design as demands decrease; however, longitudinal reinforcement within the plastic hinge region is not decreased to ensure the critical section forms at the base of the wall, as intended in the design for the provided detailing (as required by ACI 318-14, §18.10.6.2). The wall boundary longitudinal reinforcement ratio exceeds the minimum limit of $6\sqrt{f_c'}/f_y$ per ACI 318-19 §18.10.2.4.

The displacement-based detailing approach of §18.10.6.2 is used to assess whether special boundary elements (SBE) are required since all wall pier aspect ratios exceed 2.0 and because it is less conservative than the stress-based approach per §18.10.6.3. Based on §18.10.6.2, given the wall maximum neutral axis depth ($\boldsymbol{c}$) computed for the maximum axial load, the wall boundary compression zone must be reinforced with special boundary elements when:

$$c \geq l_w/\left[600\left(1.5\delta_u/h_w\right)\right] \qquad \text{(2-3)}$$

Transverse reinforcement at the wall boundaries is based on the approved provisions of ACI 318-19 §18.10.6.4 and 18.10.6.5 that require overlapping hoops as well as crossties with 135-degree hooks at both ends. The wall web vertical reinforcement is also laterally supported by crossties with seismic hooks for a distance above and below the critical section per §18.10.6.2. Termination of wall longitudinal reinforcement is per approved provisions of ACI 318-19 §18.10.2.3 and typically results in extensions of longitudinal reinforcement of l_d above the next floor level beyond the theoretical cut-off point.

The lateral drift capacity of the building is also checked using a new code provision adopted in ACI 318-19 §18.10.6.2. This drift capacity check is derived from a comprehensive database (Abdullah and Wallace, 2019) and is applied in design of Archetypes to ensure a low probability of lateral strength loss due to flexural failure by checking that the drift demand estimated for DE level shaking does not exceed the wall lateral drift capacity (see Equation 2-4a). For this check, the lateral drift at the top of a wall pier, amplified by a factor of 1.5 to represent the mean drift demand for MCE level shaking, must be less than the drift capacity δ_c/h_w at the top of the wall determined from an expression derived using the database (Abdullah and Wallace, 2019). The drift capacity relation derived from the database is a function of wall length (l_w), wall compression zone thickness (b), the maximum design neutral axis depth (c), the concrete compressive strength (f'_c), and the maximum wall shear demand ($v_{u,max}$).

$$\frac{1.5\delta_u}{h_w} \leq \frac{\delta_c}{h_w} \tag{2-4a}$$

$$\frac{\delta_c}{h_w}(\%) = 4.0 - \frac{cL_w}{50b^2} - \frac{v_{u,max}}{10\sqrt{f'_c}} \tag{2-4b}$$

Wall shear reinforcement for the final Archetype designs conforms to the requirements of the ACI 318-19 §18.10.3 ACI 318-19 (Public Comment Version, December 2018) using an amplified shear demand V_e to account for the increase in shear demand due to flexural over-strength and the effects of higher modes. It is noted that a moderately more conservative provision was adopted for 318-19 based on Public Comments which would lead to slightly higher ACMRs. The wall shear reinforcement ratio (ρ_t) is selected to resist the amplified shear demand using $\phi_v = 0.75$ since wall piers with (h_{wcs}/ℓ_w) > 2.0 with amplified shear demand tend to have nominal shear strength greater than the shear corresponding to the development of flexural strength.

$$\rho_t \geq (V_e/(0.75 l_w t_w) - 2\sqrt{f'_c})/f_y \geq 0.0025 \tag{2-5}$$

The proposed approach amplifies the code level shear force (V_u) by a flexural overstrength factor (Ω_v) and a dynamic shear amplification factor (ω_v) that accounts for higher modes, resulting in:

$$V_e = \Omega_v \omega_v V_u \tag{2-6}$$

The dynamic shear amplification factor (ω_v), depends on number of stories (n_s) as:

$$\omega_v = 1.3 + n_s/30 \leq 1.8, for\ n_s > 6\ stories \tag{2-7}$$

The overstrength factor (Ω_v) is the ratio of probable moment strength M_{pr} to code required strength M_u, and shall not be taken less than 1.5 per ACI 318-19 §R18.10.3. In this study, the flexural overstrength ratio of M_{pr}/M_u was taken as 1.5 for all designs so that the Archetypes would not be overdesigned for shear strength and represent the governing case for collapse analysis. In general, overstrength values exceed 1.5 for coupled walls as summarized in the next paragraph. Table 2-3 summarizes the shear amplification factors for the Archetypes in this project.

Table 2-3: Summary of Shear Amplification for Final Archetype Designs

Shear Amplification	8-Story	12-Story	18-Story	24-Story	30-Story
ω_v	1.57	1.7	1.8	1.8	1.8
$V_e=\varphi_0 \cdot \omega_v \cdot V_u$	$V_e=2.35 \cdot V_u$	$V_e=2.55 \cdot V_u$	$V_e=2.7 \cdot V_u$	$V_e=2.7 \cdot V_u$	$V_e=2.7 \cdot V_u$

Actual ratios of M_{pr} to M_u tend to be higher than 1.5 because required reinforcement for the load case producing wall tension (or minimum compression) typically produces significant overstrength for the load case that causes large wall compression. The ratios of M_{pr}/M_u were computed for a subset of Archetypes at the critical section (base of the coupled walls) as presented in Table 2-4. M_{pr} was typically computed as 1.25 times M_n, where M_n is the moment strength at the considered axial load demand; where the axial load exceeded the balance point in the P_n-M_n strength interaction diagram (e.g., 18-story Archetypes), M_{pr} was taken equal to M_n. Table 2-4 includes sample determinations of M_n and M_{pr} from the *P-M* interaction diagram of the wall section. The results for the ratios of M_{pr}/M_u indicate a mean value of 2.3 and a maximum wall pier value of 3.75. Although the minimum value of $\Omega_v = 1.5$ was used in this study, designs using the largest ratio of M_{pr}/M_u from the worst-case wall pier would have appreciably higher overstrength; the results suggest that the maximum amplification of $\Omega_v \omega_v = 3$ per ACI 318-19 would apply to all Archetypes in this study greater than 60 ft (proposed minimum height).

Table 2-4: Ratios of M_{pr} to M_u for a subset of Archetypes

Archetype	$(0.9\text{-}0.2S_{DS})D$ - E		$(1.2+0.2S_{DS})D + 0.5L$ +E	
	Tension Wall	Compression Wall	Tension Wall	Compression Wall
8H-DR-2.4	1.58	2.98	2.05	2.90
8H-DR-3.3	1.63	2.72	2.07	2.74
12H-DR-2.4	1.37	2.89	1.74	2.75
12H-DR-3.3	1.35	2.77	1.94	2.74
18H-DR-2.4	1.53	3.75	1.53	2.93
18H-DR-3.3	1.49	3.37	2.14	2.67
Mean:	**1.49**	**3.08**	**1.91**	**2.79**
	2.3			

RSA	$(0.9\text{-}0.2S_{DS})D$ - E Tension Wall			
Archetype	$P_{u,min}$ (k)	M_u (k-ft)	M_{pr} (k-ft)	M_{pr}/M_u
8H-DR-2.4	-798	5989	9442	1.58
8H-DR-3.3	-546	6432	10495	1.63
12H-DR-2.4	-1406	7509	10250	1.37
12H-DR-3.3	-992	8730	11743	1.35
18H-DR-2.4	-1075	13799	21082	1.53
18H-DR-3.3	-582	15333	22794	1.49

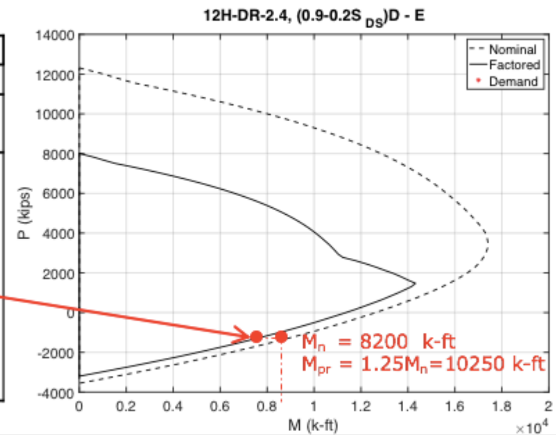

RSA	$(1.2+0.2S_{DS})D$ +0.5L + E Compression Wall			
Archetype	$P_{u,max}$ (k)	M_u (k-ft)	M_{pr} (k-ft)	M_{pr}/M_u
8H-DR-2.4	2694	5994	17386	2.90
8H-DR-3.3	2515	6423	17607	2.74
12H-DR-2.4	3295	7508	20670	2.75
12H-DR-3.3	3152	8746	23942	2.74
18H-DR-2.4	9205	13936	40809	2.93
18H-DR-3.3	8869	15403	41087	2.67

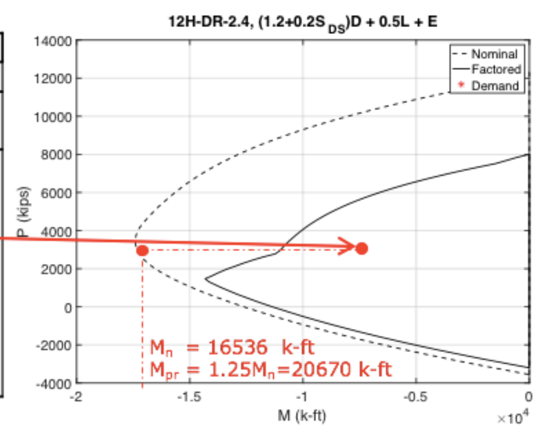

2.3 Initial Designs and Required Revisions

The Archetypes were originally designed following the wall shear provisions of ACI 318-14 using $\phi_v = 0.75$ without considering shear amplification to assess if current code provisions would achieve the project objectives. Once a subset of Archetype designs were completed for several building heights (as presented in Table 2-5) preliminary analyses were conducted. The preliminary incremental dynamic analysis (IDA) results indicated that Archetypes designed using ACI 318-14 shear provisions experienced a high number of wall shear failures at collapse margin ratios that did not satisfy the FEMA P695 acceptability criteria as summarized in Section 4b. Using $\phi_v = 0.60$ would not have improved the ACMRs appreciably; therefore, the Archetypes were redesigned to include wall shear demand amplification, as discussed in Section 2.2 of this report. Typically, web shear reinforcement is increased to account for the increase in demand; however, in all cases, wall thickness at the lower levels is increased to keep the contribution of V_s below $8\sqrt{f'_c}bd$. Comparisons between a subset of the preliminary designs versus the revised designs are summarized in Table 2-6.

Table 2-5: Summary of a Subset of Preliminary Designs Following ACI 318-14 Shear Provisions

Archetype	Total Height	V_b (kips)	Wall Pier Dimensions	Wall Reinf. at base	Coupling Beam	CB Reinforcement
8H-DR-3.0 Planar walls	80’	1186 C_s=0.100	l_w = 8.5’ L2-8: t_w = 10” L1: t_w = 12	A_{sb}: 34#10 ρ_t = 0.42%	l_n/h = 3.0 10”x30” L1: 12”x30”	L2-7: 6#10 L8-R: 6#9
12H-DR-3.0 Planar walls	120’	1349 C_s=0.074	l_w = 9.25’ t_w = 12”	A_{sb}: 38#11 ρ_t = 0.37%	l_n/h = 3.0 12”x30”	L2-6: 6#11, L7-10: 6#10, L11-R: 6#9
18H-DR-3.0 Flanged walls	180’	1463 C_s=0.0545	l_w = 9’ t_w = 16”	A_{sb}: 3#10@5” ρ_t = 0.48%	l_n/h = 3.0 16”x30”	L2-11: 6#11, L12-15:6#10, L16-17: 6#9, L18-R: 6#8
24H-DR-3.0 Flanged walls	240’	1740 C_s=0.044	l_w = 10’ L20-R: t_w = 18” L1-18: t_w = 24”	A_{sb}: 3#10@5” ρ_t = 0.29%	l_n/h = 3.0 18”x30” 24”x30”	L2-10: 8#11, L11-12:8#10, L13-20: 6#11, L21-23: 6#9, L23-R: 6#8
30H-DR-3.0 Flanged walls	300’	2160.5 C_s=0.044	l_w = 11.25’ L16-30: t_w =24” L1-15: t_w = 30”	A_{sb}: 3#10@5” ρ_t = 0.26%	l_n/h = 3.0 24”x30” 30”x30”	L2-14: 8#11, L15-16:8#10, L17-19:6#11, L20-27:6#10, L28-29: 6#9, L30-R: 6#8

Table 2-6: Sample Comparisons of Archetype Design Revisions

Example	Preliminary Design			Revised Design		
	t_w (in.)	Wall ρ_t (%)	$V_u/(\sqrt{f'_c}A_{cv})$	t_w (in.)	Wall ρ_t (%)	$V_u/(\sqrt{f'_c}A_{cv})$
8H-DR-3, Level 1	12	0.42	3.19	14	1.05	2.96
12H-DR-3, Level 1	12	0.37	3.44	16	0.92	2.59

2.4 Archetype Designs

Details of the Archetype designs are presented in this section. The design concrete compressive strength (f'_c) is 6.0 ksi for the 6, 8, and 12-story planar wall Archetypes and 8.0 ksi for the taller 18, 24, and 30-story flanged wall Archetypes. The reinforcement yield stress (f_y) is set at 60 ksi. The coupling beam widths match the wall thickness at each floor level. For walls 12 in. thick or less, the wall thickness may not be sufficient to fit the coupling beam reinforcement into the wall core using diagonal confinement (ACI 318-14 §18.10.7.4(c)), which requires a slightly wider beam than full-section confinement (ACI 318-14 §18.10.7.4(d)). A wider wall is not used to ensure the Archetypes represent the worst-case design condition. A summary of key design parameters are presented in Table 2-7 for a subset of Archetype designs including the total building height, design period, base shear, degree of coupling (DOC), typical wall pier dimensions, and the maximum and minimum wall axial stresses. The degree of coupling is computed using the seismic axial force couple due to overturning (T), the moment arm (l) between the centerline of the tension and compression piers, and the seismic moments M_1 and M_2 at the base of each wall pier using the equation:

$$DOC = (Tl)/(Tl + M_1 + M_2) \tag{2-8}$$

DOC decreases with shorter building heights and with increasing coupling beam aspect ratio l_n/h. Although DOCs greater than 0.6 have been reported to produce large axial stresses on the wall piers (Table 2-7), the DOCs of the Archetypes in this study are relatively high since the coupling beam shear stresses are close to ACI limits to represent the worst-case design for collapse assessment; however, the axial stresses are not unreasonably high because a thicker wall is required to satisfy the new ACI 318-19 provisions for wall shear demand amplification and for the drift capacity check. As noted above, a thicker wall might also be required to fit coupling beam reinforcement inside of wall boundary longitudinal reinforcement (i.e., to avoid congestion).

Table 2-7: Summary of a Select Set of Archetype Designs

Archetype	Total Height	T_1 (s)	$T=C_uT_a$ (s)	V_b (kips)	DOC	Wall Pier Dimensions	$P_{u,1}$[1] $/A_g f'_c$	$P_{u,2}$[2] $/A_g f'_c$	$P_{u,3}$[3] $/A_s f_y$
6H-DR-2 (planar walls)	60’	0.83	0.604	1,062 $C_s = 0.124$	0.60	$l_w = 8.0'$ $t_{w,L1\text{-}4} = 14''$ $t_{w,L5\text{-}6} = 10''$	0.16	0.28	-0.31
8H-DR-3 (planar walls)	80’	1.27	0.749	1,201 $C_s = 0.100$	0.61	$l_w = 8.5'$ $t_{w,L1\text{-}4} = 14''$ $t_{w,L5} = 12''$ $t_{w,L6\text{-}8} = 10''$	0.14	0.27	-0.27
12H-DR-3 (planar walls)	120’	2.14	1.015	1,360 $C_s = 0.074$	0.66	$l_w = 9.25'$ $t_{w,L1\text{-}4} = 16''$ $t_{w,L5\text{-}12} = 12''$	0.13	0.30	-0.33
18H-DR-3 (flanged walls)	180’	3.14	1.376	1,489.5 $C_s = 0.0545$	0.66	$l_w = 9.0'$ $t_{w,L1\text{-}5} = 24''$ $t_{w,L6\text{-}8} = 20''$ $t_{w,L5\text{-}12} = 16''$	0.13	0.19	-0.07
24H-DR-3 (flanged walls)	240’	3.39	1.707	1,654 $C_s = 0.044$	0.69	$l_w = 10.0'$ $t_{w,L1\text{-}18} = 24''$ $t_{w,L19\text{-}24} = 18''$	0.17	0.23	-0.03
30H-DR-3 (flanged walls)	300’	3.62	2.018	2,112 $C_s = 0.044$	0.68	$l_w = 11.25'$ $t_{w,L1\text{-}10} = 30''$ $t_{w,L11\text{-}20} = 24''$ $t_{w,L21\text{-}30} = 18''$	0.13	0.20	-0.06

1 $P_{u,1}$* is the gravity axial stress under load combination 1.2D+1.6L
2 $P_{u,2}$* is the maximum axial stress under load combination $(1.2+0.2S_{DS})$D+0.5L+1.0E
3 $P_{u,3}$* is the minimum (net tensile) axial stress under load combination $(0.9-0.2S_{DS})$D-1.0E

Prior to considering amplified wall shear demands, the proportioning of wall cross sections for the preliminary Archetypes was typically governed by drift; however, for the final designs, the thickness of the wall piers had to be increased at the lower levels to ensure that the wall pier shear strength did not exceed the ACI 318 limit of $10\sqrt{f'_c}A_{cv}$.

In the following subsections, designs of different height buildings with beam aspect ratio of 3.0 are presented. The key design details of all Archetypes are summarized in Appendix A.

2.4.1 8-Story Archetypes

The 8-story Archetype buildings (Figure 2.4) are each 80 feet tall and consist of planar wall piers with l_w equal to 8.5 ft. The walls have to be at least 12 in. thick at Level 1 due to the wall special boundary element (SBE) requirements of ACI 318-14 §18.10.6.4(c), which requires a minimum wall thickness for piers that are not tensioned-controlled. The preliminary 8-story designs as described in Section 2.3 had walls that were 12 in. thick at Level 1 and 10 in. thick at the upper levels. However, when the wall shear reinforcement was increased to meet the amplified shear demands, the wall thickness was increased to 14 in. at Levels 1-4 and 12 in. at Level 5 to keep the contribution of shear strength from horizontal web reinforcement (V_s) below the $8\sqrt{f'_c}A_{cv}$ limit.

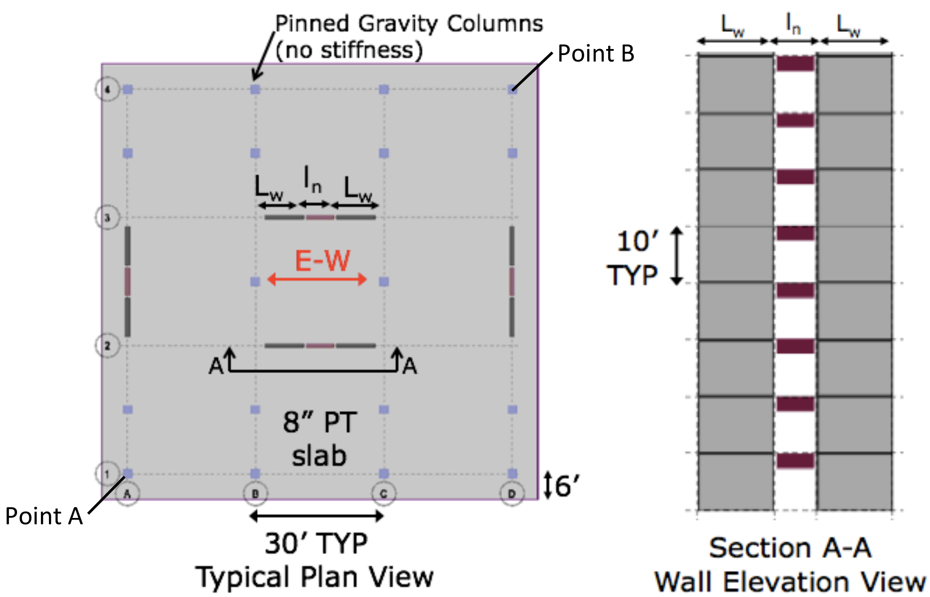

Figure 2.4: 8-Story Archetype

Details of the Archetype with coupling beam aspect ratio l_n/h = 3.0 (8H-DR-3.0) are presented in this section. The coupling beams have a clear span (l_n) of 7.5 ft and a depth of 30 in., resulting in a beam reinforcement diagonal angle (α) of about 15 degrees. Axial stresses at the wall base for each pier are $0.14A_gf'_c$ under the governing gravity load combination 1.2D+1.6L and $0.27A_gf'_c$ when seismic load effects are included under the governing load combination $(1.2+0.2S_{DS})$D+0.5L.+1.0E. The governing wall net tension force is about $-0.1A_gf'_c$ for the piers near the base of wall. The wall unamplified shear stresses are about $3\sqrt{f'_c(psi)}$ while the amplified shear stresses range from $5.1 - 7\sqrt{f'_c(psi)}$. Higher shear stress levels could not be achieved using reduced wall section sizes without violating the story drift limit.

The fundamental period (T_1) of the building is 1.27 seconds, and the period for design (T) per ASCE 7-16 is the minimum of T_1 and $C_u T_a$ = 0.75 seconds. The resulting governing seismic coefficient is $C_s = (SD_1/T)/(R/I_e) = 0.10$. With a seismic weight of 11,989 kips, the base shear V_b is 1201 kips. The story drifts at the center of mass (CM) and corner points (see Figure 2.4) as presented in Figure 2.5 are less than the maximum allowable value of 2.0%, and no extreme torsional irregularity exists ($\Delta_{max}/\Delta_{avg} = 1.23 < 1.4$).

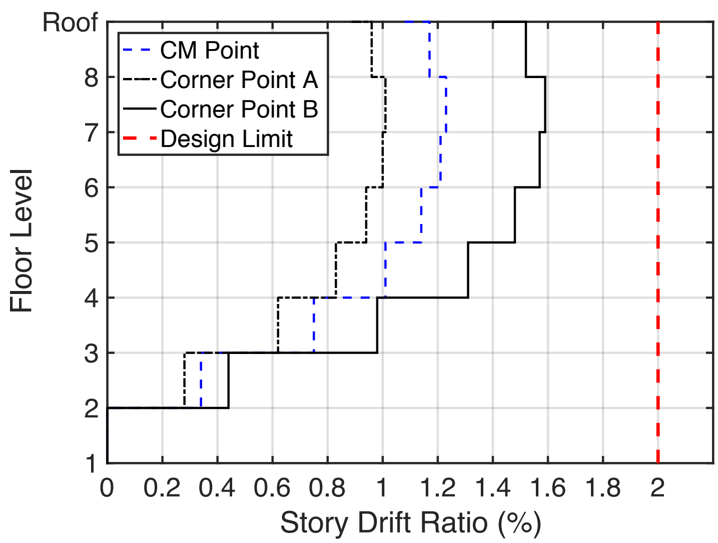

Figure 2.5: Archetype 8H-DR-3.0 Story Drifts

A summary of demands, capacities, and design limits for this Archetype are summarized in Figure 2.7 and Table 2-8. The coupling beams are designed according to ACI 318-14 §18.10.7.4, and the diagonal reinforcement is optimized based on the shear demand. The maximum coupling beam shear stress is less than $7\sqrt{f'_c}bd$. The diagonal reinforcement for the diagonally-reinforced coupling beams is embedded into the wall boundaries as required to develop $1.25f_y$.

The wall shear reinforcement ratio (ρ_t) ranges from 1.05% at the wall base to 0.62% at the upper levels, exceeding the ACI 318 code minimum reinforcement ratio of 0.25% at all levels. The wall shear strength per ACI 318, $\phi V_n = 0.75 l_w t_w \left(2\sqrt{f'_c} + \rho_t f_{yt}\right)$= 852.4 kips at the lower levels exceeds the maximum amplified shear demand V_e = 815 kips. The wall boundary longitudinal reinforcement (A_{sb}) is selected to satisfy *P-M* interaction diagram limits (Figure 2.6) with the design controlled by the load combination with the governing moment demand M_u and the governing net tensile axial force $P_{u,min}$.

The wall piers at Level 1 require special boundary elements since the maximum neutral axis depth c = 46.3 in. exceeds the limit $l_w/(600(1.5\delta_u/h_w))$ = 8.6 in., and SBE detailing extends up the height of the first floor based on ACI 318-14 §18.10.6.2.b. Since boundary longitudinal reinforcement ratios at floor levels above the special boundary element exceed the limit of $400/f_y$, ordinary boundary elements conforming to ACI 318-14 §18.10.6.5 are required over the entire wall height.

Table 2-8: Archetype 8H-DR-3.0 Design Summary

Level	f'_c (ksi)	$t_w=b$ (in.)	Coupling Beam Design			Wall Shear Design		Wall Longit. Reinf.		
			Diagonal Bars	Shear D/C	$V_u/(\sqrt{f'_c}\,A_g) < \varphi*10$	Wall f_v $V_e/(\sqrt{f'_c}A_v)$	Wall ρ_t (%)	Outer A_{sb}	Middle A_{sb}	Inner A_{sb}
8	6000	10	6#8	0.91	5.1	5.10	0.62	6#7	10#4	6#4
7	6000	10	6#9	0.82	5.8	5.99	0.78	6#7	10#4	6#4
6	6000	10	6#9	0.92	6.5	6.98	0.98	8#9	16#4	6#5
5	6000	12	6#10	0.91	6.7	6.61	0.92	8#9	16#4	6#5
4	6000	14	6#11	0.87	6.7	6.31	0.90	12#10	16#5	6#6
3	6000	14	6#11	0.83	6.4	6.84	0.97	12#10	16#5	6#6
2	7000	14	6#11	0.77	5.5	6.82	1.05	16#11	12#6	6#7
1	7000	14	6#11	0.52	3.7	6.44	1.05	16#11	12#6	6#7

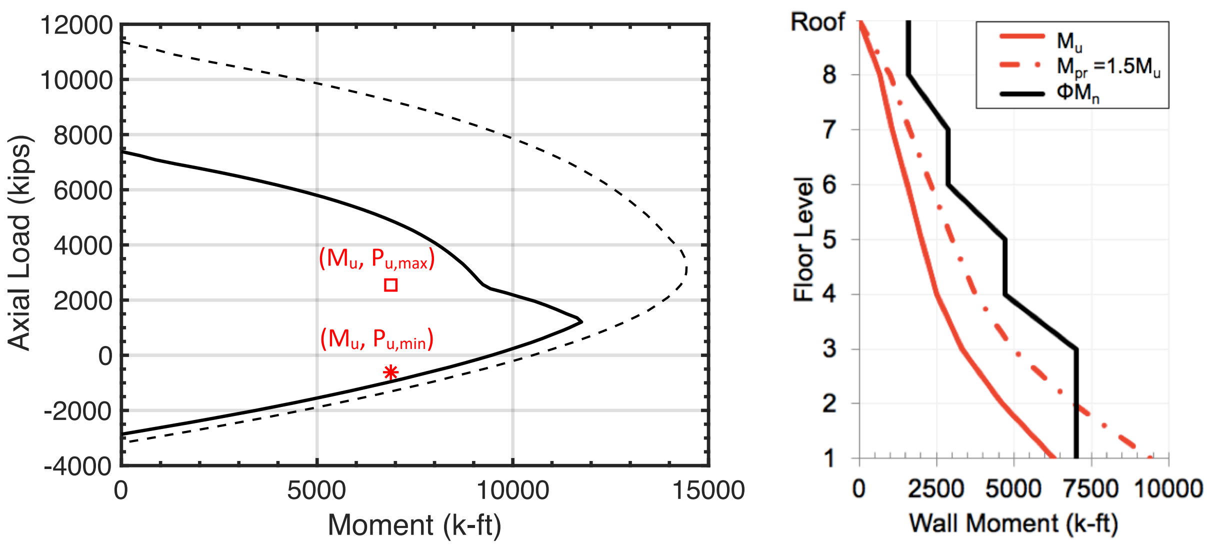

(a) (b)

Figure 2.6: Archetype 8H-DR-3.0 Wall design (a) Level 1 Wall *P-M* interaction diagram; (b) Moment profile along wall height

Following the design of the 8H-DR-3.0 Archetype, the coupling beam aspect ratio (l_n/h) was varied from 3.0 to 3.3 by increasing the length of the coupling beam from 7.5 ft to 8.25 ft. For the design of Archetype 8H-DR-3.3, the coupling beam demand generally decreased due to the increase in coupling beam length resulting in a more flexible structure. However, since angle (***α***) decreases, the coupling beam shear capacity decreases for the same quantity of diagonal reinforcement used for Archetype 8H-DR-3.0 (Figure 2.7a). As a result, the same coupling beam diagonal reinforcement used for 8H-DR-3.0 is used for 8H-DR-3.3, except at the roof level. Since there were negligible changes to the axial, moment, and shear wall demands (Figure 2.7b, c), the wall pier design also remained the same as the 8H-DR-3.0 Archetype.

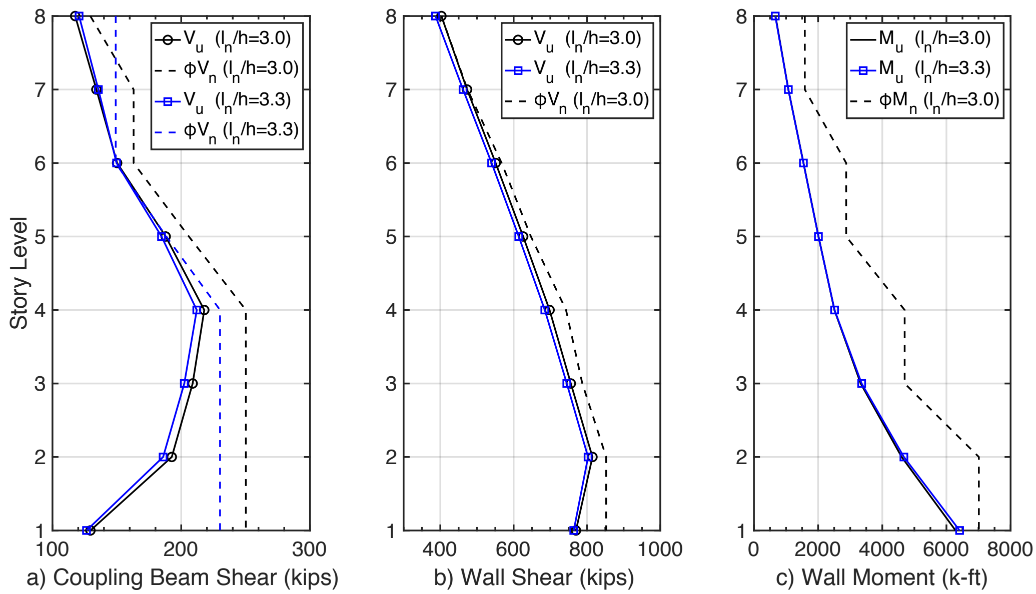

Figure 2.7: 8H-DR-3.3 Archetype Demands

Coupling beam reinforcement for the diagonally-reinforced Archetype with l_n/h = 3.3 (8H-DR-3.3) and the conventionally-reinforced (8H-CR-3.3) are summarized in Table 2-9. The longitudinal reinforcement for the conventionally-reinforced coupling beams are embedded into the wall boundaries as required to develop 1.25f_y.

Table 2-9: Coupling Beam Reinforcement Design for 8H-DR-3.3 and 8H-CR-3.3

Level	Diagonally Reinforced (DR)				Conventionally Reinforced (DR)	
	Diagonal Bars	**α (°)**	**Shear D/C**	**$V_u/(\sqrt{f'_c}\, A_g) < \varphi*10$**	**Longitudinal Bars**	**Flexure D/C**
Roof	6#9	14.10	0.89	5.7	4#10	0.88
8	6#9	14.10	1.00	6.4	4#10	1.00
7	6#10	14.03	0.88	7.2	4#11	0.91
6	6#10	14.03	0.93	7.6	4#11	0.97
5	6#11	13.87	0.96	7.3	5#11	0.97
4	6#11	13.87	1.0	6.7	5#11	1.0
3	6#11	13.87	0.88	5.7	5#11	0.88
2	6#11	13.87	0.60	3.9	5#11	0.58

As the coupling beam aspect ratio is varied for the different Archetypes, the coupling beam and wall demands change only slightly. Therefore, for most Archetypes, the same wall shear and longitudinal reinforcement required for the 8H-DR-3.0 Archetype also work for the other Archetypes. At some floor levels, the wall shear reinforcement and boundary longitudinal reinforcement are reduced due to the slightly reduced demands.

For all Archetypes, maximum story drifts are less than the maximum allowed story drift of 0.02; drift ratios were largest for Archetype 8H-CR-5.0. Key design parameters of the 8-Story Archetypes are summarized in Table 2-10 including the roof drift at which the drift capacity model predicts significant strength loss using the maximum design wall shear demand (V_e) and maximum neutral axis depth. The increase in wall thickness due to amplified shear demands leads to higher roof drift capacity at strength loss (about 3% roof drift) which leads to larger ACMR values. The importance of the drift capacity check is discussed in Chapter 4 where the detailed modeling approaches for NL-RHA are discussed.

Table 2-10: Design Summary of 8-Story Archetypes

<table>
<tr><th>Archetype</th><th>T_1 (s)</th><th>V_b (kips)</th><th>CB h (ft)</th><th>CB l_n (ft)</th><th>Wall l_w (ft)</th><th>Wall t_w</th><th>Drift Capacity</th></tr>
<tr><td>8H-DR-2.0</td><td>1.19</td><td>1199</td><td>2.75</td><td>5.50</td><td rowspan="7">8.5</td><td rowspan="7">L1-4: 14”
L5: 12”
L6-8: 10”</td><td>2.59 %</td></tr>
<tr><td>8H-DR-2.4</td><td>1.24</td><td>1199</td><td>2.50</td><td>6.00</td><td>2.65%</td></tr>
<tr><td>8H-DR-3.0</td><td>1.27</td><td>1201</td><td>2.50</td><td>7.50</td><td>2.71%</td></tr>
<tr><td>8H-DR-3.3</td><td rowspan="2">1.29</td><td rowspan="2">1202</td><td rowspan="2">2.50</td><td rowspan="2">8.25</td><td rowspan="2">2.75%</td></tr>
<tr><td>8H-CR-3.3</td></tr>
<tr><td>8H-CR-4.0</td><td>1.33</td><td>1204</td><td>2.50</td><td>10.00</td><td>2.76%</td></tr>
<tr><td>8H-CR-5.0</td><td>1.43</td><td>1204</td><td>2.25</td><td>11.25</td><td>2.80%</td></tr>
</table>

Overall, as the coupling beam aspect ratio (l_n/h) increases, the buildings become more flexible and wall axial and moment demands decrease due to the reduced coupling action and lower coupling beam shear forces. Therefore, for Archetype 8H-CR-4.0, the wall longitudinal boundary reinforcement at Level 1 was slightly reduced to 14#11 outer boundary bars (versus 16#11 outer boundary bars for Archetype 8H-DR-3.0). Moreover, as the beam aspect ratio increases and the beams become more flexure-dominant, the coupling beam shear demands decrease and beam moment demands increase. For example, the design for Archetype 8H-CR-4.0 requires more beam longitudinal reinforcement at the Roof and Level 6 than that required for Archetype 8H-CR-3.3. A sample coupling beam detail is depicted in Figure 2.8, and variations in coupling beam designs for the 8-story Archetypes are summarized in Table 2-11.

Table 2-11: 8-Story Archetype design variations

8-Story Archetypes	**Coupling Beam Design Variations**						
	Diagonal Reinforcement				**Conventional Reinforcement**		
Level	**8H-DR-2**	**8H-DR-2.4**	**8H-DR-3**	**8H-DR-3.3**	**8H-CR-3.3**	**8H-CR-4**	**8H-CR-5**
Roof	6#7	6#7	6#8	6#9	4#9	4#10	4#10
8th	6#8	6#8	6#9	6#9	4#10	4#10	4#10
7th	6#8	6#9	6#9	6#9	4#10	4#10	4#11
6th	6#9	6#10	6#10	6#10	4#11	5#11	5#11
5th	6#10	6#10	6#11	6#11	5#11	5#11	5#11
4th	6#10	6#10	6#11	6#11	5#11	5#11	5#11
3rd	6#10	6#10	6#11	6#11	5#11	5#11	5#11
2nd	6#10	6#10	6#11	6#11	5#11	5#11	5#11

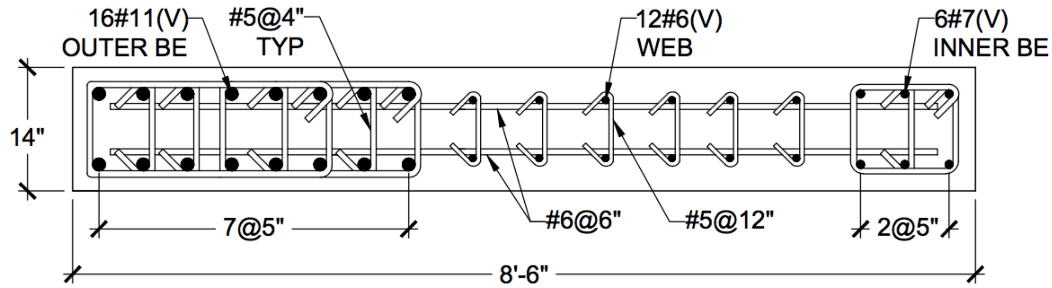

a) Wall detail at Level 1

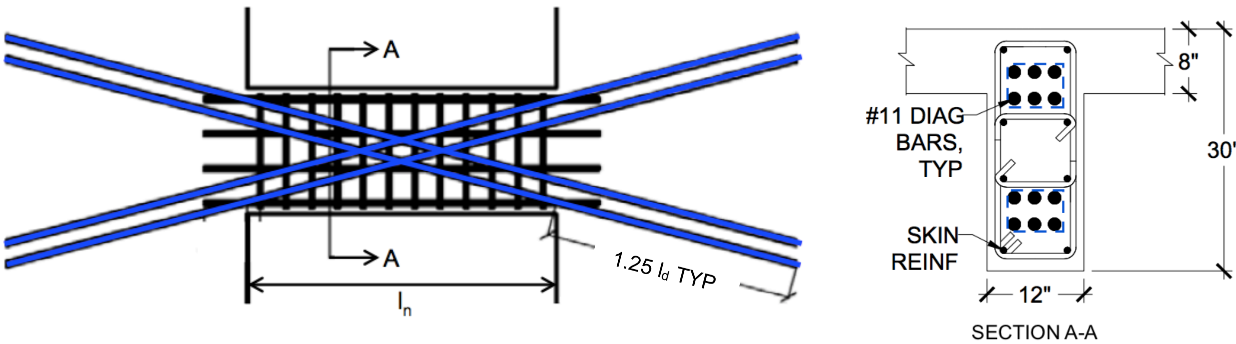

b) Coupling beam detail at Level 5

Figure 2.8: Archetype 8H-DR-3.0 Wall and Coupling Beam Details

2.4.2 12-Story Archetypes

The 12-story Archetype buildings (Figure 2.9) are each 120 feet tall and consist of planar wall piers that are 9.25 feet in length. The preliminary 12-story designs had walls that were 12 in. thick; however, when the wall shear reinforcement was increased due to amplified wall shear demands, the wall thickness was increased to 16 in. at Levels 1-4 to keep the contribution of shear strength from horizontal web reinforcement (V_s) below the $8\sqrt{f_c'}A_{cv}$ limit.

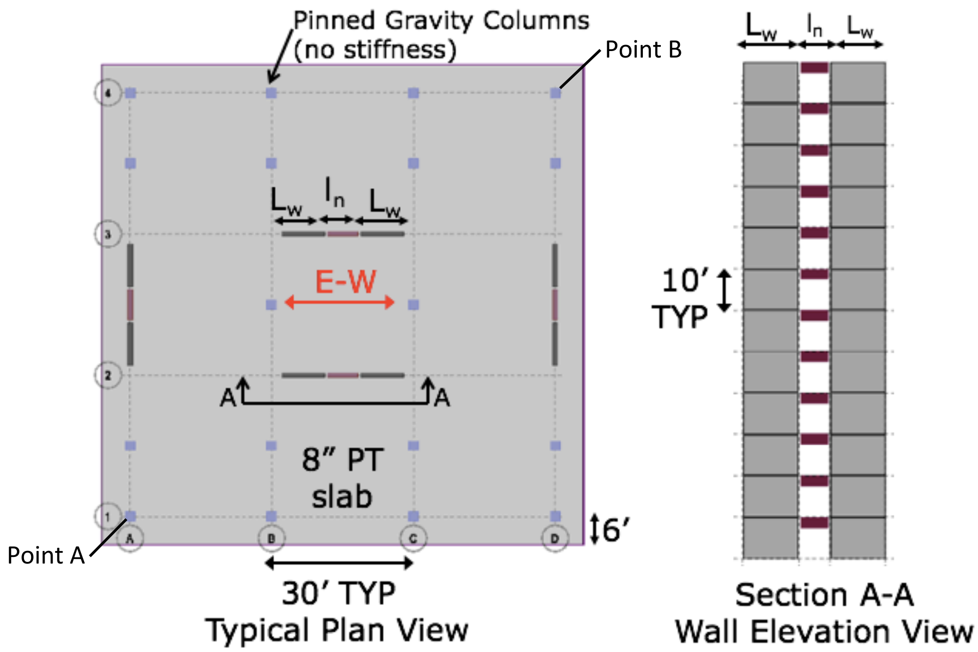

Figure 2.9: 12-Story Archetype

Details of the Archetype with coupling beam aspect ratio l_n/h = 3.0 (12H-DR-3.0) are presented in this section. The peak axial stress at the wall base is $0.13A_gf'_c$ under the governing gravity load combination 1.2D+1.6L and $0.30A_gf'_c$ when seismic load effects are included under the governing load combination (1.2+0.2S_{DS})D+0.5L+1.0E. The governing net tension force at the wall base is about $-0.11A_gf'_c$ for the piers near the base of the wall. As noted earlier, these limits of about 15 to 20% under gravity load combinations and approximately 25 to 30% under combined gravity and earthquake load combinations, were based on input from an industry advisory group. Wall amplified shear stresses range from $3.3\sqrt{f'_c(psi)}$ at the upper levels to $6.8\sqrt{f'_c(psi)}$ at the lower levels. Higher wall shear demands could not be achieved by using a smaller wall cross-section without violating story drift limits.

The fundamental period (T_1) of the building is 2.14 seconds, and the period for design (T) per ASCE 7-16 is the minimum of T_1 and C_uT_a = 1.015 seconds. The resulting governing seismic coefficient is $C_s = (SD_1/T)/(R/I_e) = 0.074$. With a seismic weight of 18,404 kips, the base shear V_b is 1360 kips. The maximum story drifts presented in Figure 2.10 are less than the maximum allowable value of 2.0%, and no extreme torsional irregularity exists ($\Delta_{max}/\Delta_{avg}$ =1.23 < 1.4).

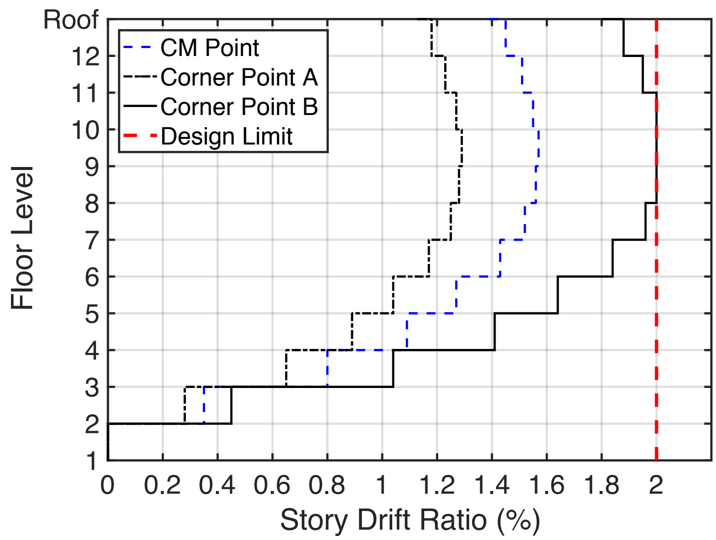

Figure 2.10: Archetype 12H-DR-3.0 Story Drifts

The coupling beam and wall reinforcement details are summarized in Table 2-12. Maximum coupling beam shear stresses range from 3.5 to $7\sqrt{f'_c(psi)}$ and do not exceed the code limit stress of $8.5\sqrt{f'_c(psi)}$.

The wall shear reinforcement ratio ($\boldsymbol{\rho_t}$) using 2 legs of #6 or #5 bars ranges from 0.92% at the wall base to 0.32% at the upper levels, exceeding the ACI 318 code minimum reinforcement ratio of 0.25%. The maximum wall shear demand V_e = 934 kips (amplified by a factor of 2.55 to account for shear amplification) does not exceed the reduced shear strength computed at the base, $\phi V_n = 0.75 l_w t_w \left(2\sqrt{f_c'} + \rho_t f_{yt}\right)$ = 939 kips. The wall shear demands as compared to the ACI 318 requirements are presented in Figure 2.11.

Table 2-12: Archetype 12H-DR-3.0 Design Summary

Level	f'_c (ksi)	t_w=b (in.)	Coupling Beam Design: Diagonal Bars	Coupling Beam Design: Shear D/C	Coupling Beam Design: $V_u/(\sqrt{f'_c}\,A_g) < \varphi*10$	Wall Shear Design: Wall f_v $V_e/(\sqrt{f'_c}A_v)$	Wall Shear Design: Wall ρ_t (%)	Wall Longit. Reinf.: Outer A_{sb}	Wall Longit. Reinf.: Middle A_{sb}	Wall Longit. Reinf.: Inner A_{sb}
12	6000	12	6#8	0.92	4.3	3.27	0.32	8#5	14#4	8#4
11	6000	12	6#9	0.82	4.8	4.35	0.52	8#5	14#4	8#4
10	6000	12	6#9	0.93	5.4	5.09	0.65	12#7	14#4	8#4
9	6000	12	6#10	0.81	6.0	5.48	0.73	12#7	14#4	8#4
8	6000	12	6#10	0.86	6.4	5.71	0.73	12#8	14#5	8#5
7	6000	12	6#10	0.91	6.7	5.97	0.81	12#8	14#5	8#5
6	6000	12	6#10	0.94	6.9	6.45	0.92	14#9	14#6	8#6
5	6000	12	6#10	0.95	7.0	7.05	0.98	14#9	14#6	8#6
4	6000	16	6#11	0.99	6.7	5.92	0.92	16#10	14#7	8#7
3	6000	16	6#11	0.93	6.3	6.42	0.92	16#10	6#9	16#9
2	6000	16	6#11	0.79	5.4	6.79	0.92	22#11	10#8	8#8
1	6000	16	6#11	0.52	3.5	6.60	0.92	22#11	10#8	8#8

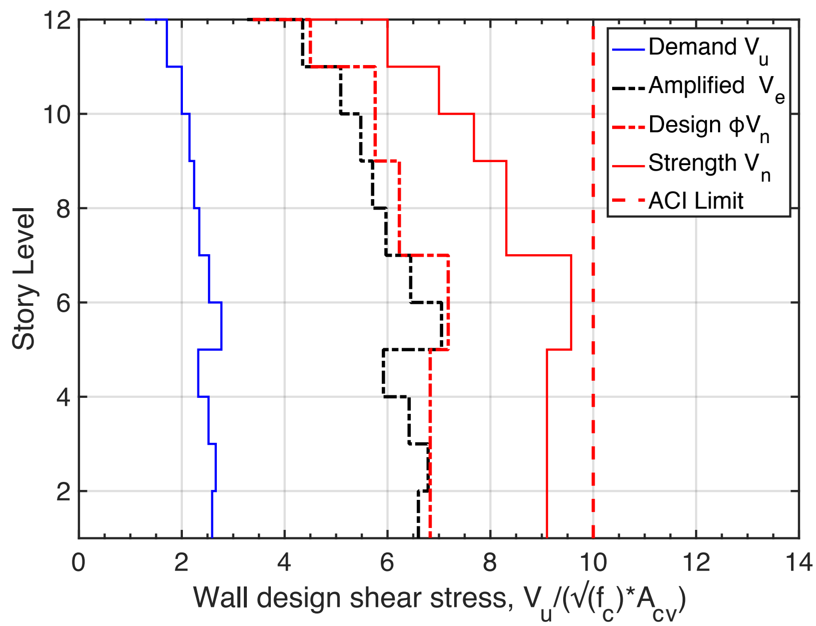

Figure 2.11: Archetype 12H-DR-3.0 Wall Shears

The wall boundary longitudinal reinforcement (A_{sb}) is designed to resist the worst-case net-tension load and the moment demand. A *P-M* interaction section analysis is done at every level to compute the flexural strength and determine the maximum neutral axis depth of the wall. A sample wall detail at Level 1 along with its *P-M* interaction surface is presented in Figure 2.12.

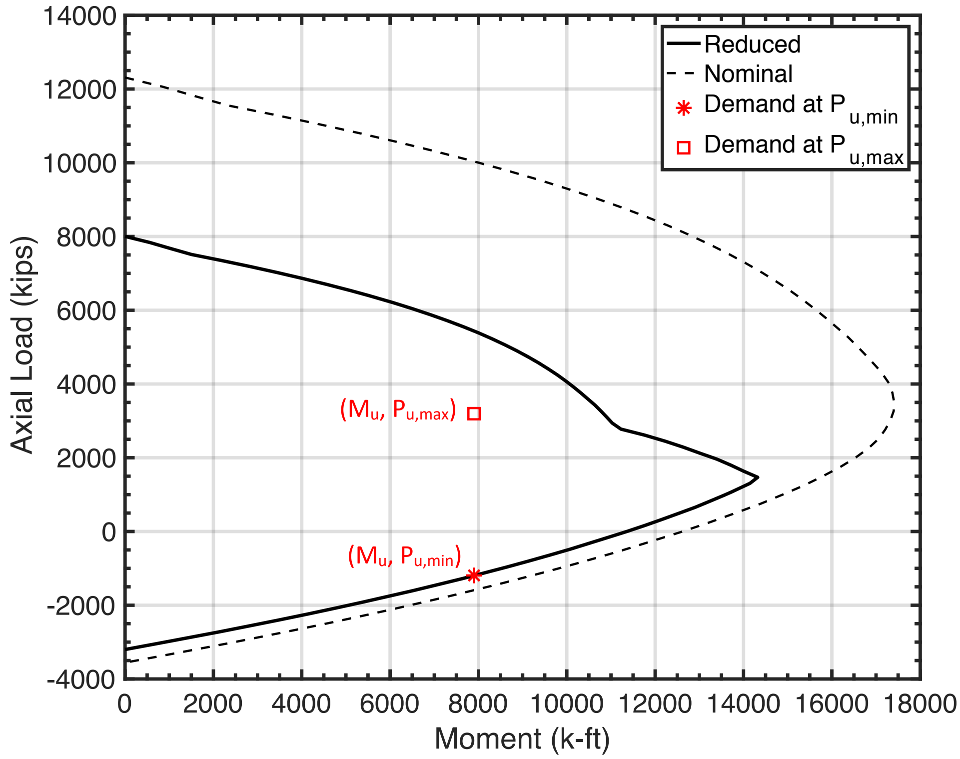

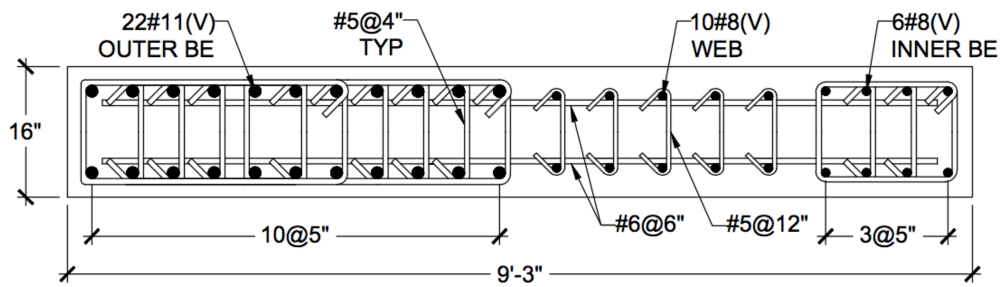

Figure 2.12: Archetype 12H-DR-3.0 Level 1 Wall Detail and *P-M* Interaction

The displacement-based approach of ACI 318-14 §18.10.6.2 is used to determine whether special boundary elements are required. At the wall base, since the maximum neutral axis depth c = 64.5 in. exceeds the limit $l_w/(600(1.5\delta_u/h_w))$ = 7.4 in., special boundary elements are required. The length of the special boundary element (SBE) is 44 in., computed according to §18.10.6.4(a) as the maximum of $\{c\text{-}0.1l_w, c/2\}$. The SBE extends from the critical section at the base of the wall to the top of the first story, a height of 10 feet (i.e., $h_{SBE} \geq \max\{l_w, M/(4V)\}$ = 9.25 ft). Boundary transverse reinforcement for the SBE consists of #5 ties spaced at 4 in. on center per ACI 318 §18.10.6.4(e) and (f). Moreover, since the boundary longitudinal reinforcement ratios above the SBE exceed the limit of $400/f_y$, ordinary boundary elements conforming to ACI 318 §18.10.6.5(a) are required over the entire wall height.

Design variations from Archetype 12H-DR-3.0 for several 12-story Archetypes are summarized in Table 2-13 and described in the subsequent pages.

Table 2-13: 12-Story Archetype Design Variations

Archetype	T_1 **(s)**	V_b **(kips)**	**CB** h **(ft)**	**CB** l_n **(ft)**	**CB Reinforcement**	l_w **(ft)**	**Wall Reinf.**	**Drift Capacity**
12H-DR-2.0	2.06	1358	2.75	5.50	L2-5:6#10, L6-9:6#10, L10-L11:6#8, L12-R:6#7	9.25	T2.11	2.59%
12H-DR-2.4	2.12	1357	2.50	6.00	L2-5:6#11, L6-8:6#10 L9-11:6#9, L12-R:6#8	9.25	T2.11	2.61%
12H-DR-3.0	2.14	1360	2.50	7.50	L2-5:6#11, L6-10:6#10 L11-12:6#9, R:6#8	9.25	T2.11	2.62%
12H-DR-3.3	2.00	1369	2.50	8.33	L2-5: 6#11, L6-11:6#10, L12-R:6#9	10	T2.12	2.66%
12H-CR-3.3					L2-5:5#11, L6-10:4#11, L11-12:4#10, R:4#9			
12H-CR-4.0	2.04	1372	2.50	10.00	L2-8:5#11, L9-11:4#11, L12-R:4#10	10	T2.12	2.68%
12H-CR-5.0	2.10	1375	2.50	12.50	L2-5:6#11, L6-9:4#11 L10-12:4#11, R:4#10	10	T2.12	2.72%

For the development of the Archetype 12H-DR-2.4, the coupling beam aspect ratio (l_n/h) of 2.4 is achieved by decreasing the length of the coupling beam from 7.5 feet to 6 feet. For the development of the Archetype 12H-DR-2.0, a coupling beam cross section of 12 in. by 33 in. is selected with a clear span of 5.5 feet resulting in l_n/h=2.0; the beam depth is chosen as 33 in. based on 10 ft story heights considering that door openings are typically not shorter than 7.25 ft.

In general, as l_n/h decreases from 3.0 to 2.4 and 2.0, the coupling beam shear demands increase due to shorter coupling beam lengths producing a stiffer structure. However, the beam shear strengths also increase due to a higher diagonal inclination angle ($\boldsymbol{\alpha}$); thus, the diagonal reinforcement areas are reduced at the levels indicated as summarized in Table 2-14.

For the wall piers, as l_n/h decreases, the wall axial forces due to seismic lateral forces increase but the wall moment demands tend to decrease as presented in Figure 2.13. Since there are negligible changes to the wall demands, the design of the wall piers for Archetypes 12H-DR-2.4 and 12H-DR-2.0 remain the same as that for Archetype 12H-DR-3.0.

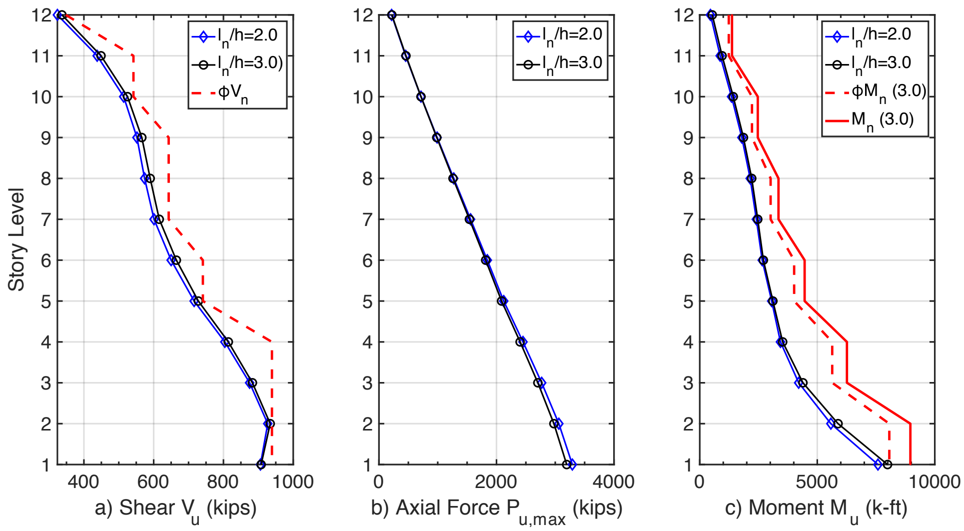

Figure 2.13: Comparison of Wall Demands for 12-Story Archetypes with low l_n/h

Table 2-14: Archetypes 12H-DR-2.4 and 12H-DR-2.0 Beam Reinforcement Design

CB Design			12H-DR-2.4				12H-DR-2.0			
Level	**f'_c (ksi)**	**b (in.)**	**Diagonal Bars**	**α (°)**	**Shear D/C**	**$V_u / (\sqrt{f'_c}\, A_g)$**	**Diagonal Bars**	**α (°)**	**Shear D/C**	**$V_u / (\sqrt{f'_c}\, A_g)$**
Roof	6	12	6#8	19.1	0.77	4.36	*6#7*	23.1	0.81	3.80
12	6	12	*6#8*	19.1	0.89	5.07	*6#7*	23.1	0.98	4.59
11	6	12	6#9	19.1	0.82	5.86	*6#8*	23.0	0.88	5.44
10	6	12	*6#9*	19.1	0.91	6.49	*6#8*	23.0	0.99	6.11
9	6	12	*6#9*	19.1	0.97	6.96	*6#9*	22.9	0.85	6.60
8	6	12	6#10	19.0	0.86	7.35	*6#9*	22.9	0.90	7.00
7	6	12	6#10	19.0	0.90	7.68	*6#9*	22.9	0.95	7.37
6	6	12	6#10	19.0	0.93	7.87	*6#9*	22.9	0.98	7.63
5	6	16	6#11	18.9	0.91	7.58	6#10	22.8	1.01	7.41
4	6	16	6#11	18.9	0.87	7.25	6#10	22.8	0.98	7.21
3	6	16	6#11	18.9	0.76	6.31	6#10	22.8	0.87	6.42
2	6	16	6#11	18.9	0.51	4.23	6#10	22.8	0.60	4.41

In the development of the Archetypes with coupling beam aspect ratios of 3.3, 4.0, and 5.0, the coupling beam lengths increase to 8.33 ft, 10 ft, and 12.5 ft, respectively. As l_n/h increases, the beam flexural demands increase, and the reinforcement is selected along the building height as summarized in Table 2-13. With increasing l_n/h, the Archetypes also become more flexible, and additional stiffness is required to meet the 2% design drift limit; therefore, for Archetypes with l_n/h = 3.3, 4.0, and 5.0, the length of the wall piers had to be increased from 9.25 ft. to 10 ft. The design details for the 10 ft. wall piers of Archetype 12H-CR-5.0 are presented in Table 2-15.

Although beam reinforcement is optimized for the different Archetypes, the wall pier design for Archetypes 12H-CR-3.3 and 12H-CR-4.0 are the same as that outlined for the 12H-CR-5.0 Archetype, since the wall pier demands do not vary significantly among these Archetypes as shown in Figure 2.14.

Table 2-15: Archetype 12H-CR-5.0 Shear Wall Design

Floor Level	Governing Demands			Longitudinal Reinforcement				Shear Reinforcement	
	$P_{u,max}$ (kips)	$P_{u,min}$ (kips)	M_u (k-ft)	Outer A_{sb}	Middle A_{sb}	Inner A_{sb}	Flexure D/C	A_{sh}	Wall f_v $V_e/(\sqrt{f'_c}A_v)$
12	222	-32	683	8#5	14#4	8#4	0.44	2#4@12"	2.93
11	459	-71	1205	8#5	14#4	8#4	0.87	2#5@10"	4.02
10	705	-119	1722	10#7	14#4	8#5	0.71	2#5@8"	4.71
9	958	-173	2175	10#7	14#4	8#5	0.98	2#5@8"	5.11
8	1215	-232	2532	12#8	14#4	8#5	0.75	2#6@10"	5.37
7	1473	-291	2790	12#8	14#4	8#5	0.89	2#6@10"	5.64
6	1728	-348	3055	12#9	14#5	8#6	0.74	2#6@8"	6.09
5	1977	-399	3548	12#9	14#5	8#6	0.90	2#6@8"	6.64
4	2256	-468	4179	14#10	14#6	8#7	0.67	2#6@7"	5.53
3	2520	-522	5356	14#10	14#6	8#7	0.88	2#6@7"	5.97
2	2760	-552	7197	18#11	14#7	8#8	0.87	2#6@6"	6.29
1	2962	-544	9592	18#11	14#7	8#8	0.94	2#6@6"	6.15

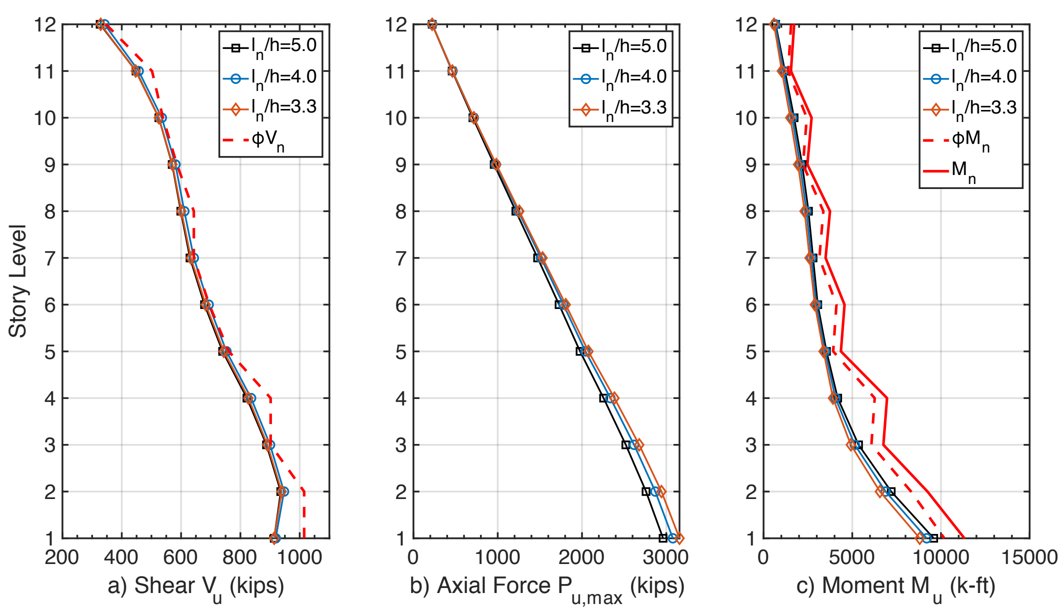

Figure 2.14: Comparison of Wall Demands for 12-Story Archetypes with high l_n/h

2.4.3 18-Story Archetypes

The 18-story Archetype buildings are each 180 feet tall and consist of flanged wall piers that are 9 ft in length as shown in Figure 2.15. The preliminary 18-story designs had walls that were 16 in. thick. However, when the wall shear reinforcement was increased due to the amplified shear demands, the wall thickness at the lower nine levels had to be increased to keep the shear strength from horizontal web reinforcement (V_s) below the $8\sqrt{f'_c}A_{cv}$ limit.

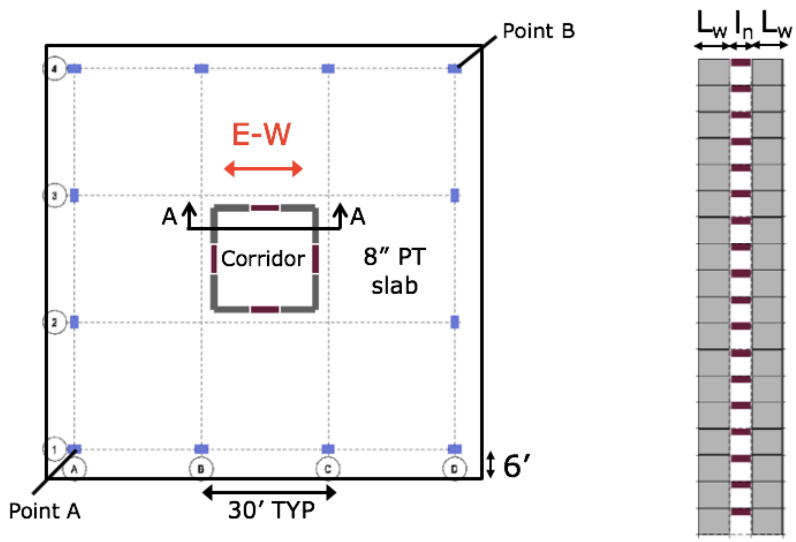

Figure 2.15: 18-Story Archetype

Details of the 18-story Archetype with coupling beam aspect ratio l_n/h = 3.0 (18H-DR-3.0) are presented in the following paragraphs. The fundamental mode of the building is torsional, with a period of 3.14 seconds, whereas the fundamental translational period is 2.06 seconds. The period for design (T) per ASCE 7-16 is the minimum of T_1 and C_uT_a = 1.37 seconds. The resulting governing seismic coefficient is $C_s = (S_{D1}/T)/(R/I_e) = 0.0545$. With a seismic weight of 27,327 kips, the base shear V_b is 1490 kips. The maximum story drifts presented in Figure 2.16 are less than the maximum allowable value of 2.0%, and no extreme torsional irregularity exists ($\Delta_{max}/\Delta_{avg} = 1.21 < 1.4$). The Archetype has a design drift capacity of 3.1% (per equation (2-4b) in Section 2.2 of this report) computed using the neutral axis depth for the worst-case condition when the wall flange is in tension.

The coupling beams are designed as described in Section 2.2. For design of the flanged walls, demands are determined at the centroid of the L-shaped wall group, and bi-directional effects are accounted for by combining 100% of the wall group resultant seismic force in one direction plus

30% of the wall group resultant seismic force in the orthogonal direction. The impact of accidental torsion is also included in the designs.

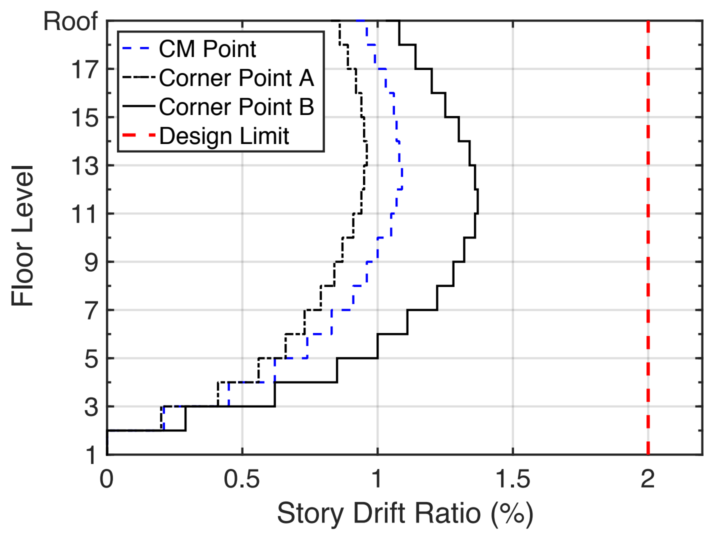

Figure 2.16: Archetype 18H-DR-3.0 Story Drifts

Wall boundary longitudinal reinforcement (A_{sb}) is selected to resist the worst-case net-tension load and the moment demand on a wall pier using a uniform layout of equally spaced longitudinal reinforcement. A biaxial *P-M* interaction diagram is computed at every floor level to determine the section strength and to verify that the design is adequate as illustrated in the example for the wall at Level 1 in Wall Detail at Level 12

Figure 2.18.

The displacement-based approach of ACI 318-14 §18.10.6.2 is used to determine whether special boundary elements are required. At the wall critical section (base), since the maximum neutral axis depth with the wall flange in tension exceeds the limit $l_w/(600(1.5\delta_u/h_w))$, special boundary elements are required almost throughout the entire wall length at the first story because the required confined length computed as the maximum of $\{c/2, c\text{-}0.1l_w\}$ is about $0.6l_w$ when the flange is in tension and about $0.1l_w$ when the flange is in compression. Boundary transverse reinforcement for the SBE is #5 ties spaced at 4 in. on center per ACI 318 §18.10.6.4(e) and (f). Moreover, for the levels where the boundary longitudinal reinforcement ratios exceed the limit of $400/f_y$, confined ordinary boundary elements are required with transverse reinforcement conforming to ACI 318 §18.10.6.5. The governing loads and longitudinal reinforcement along the wall height are summarized in Table 2-16.

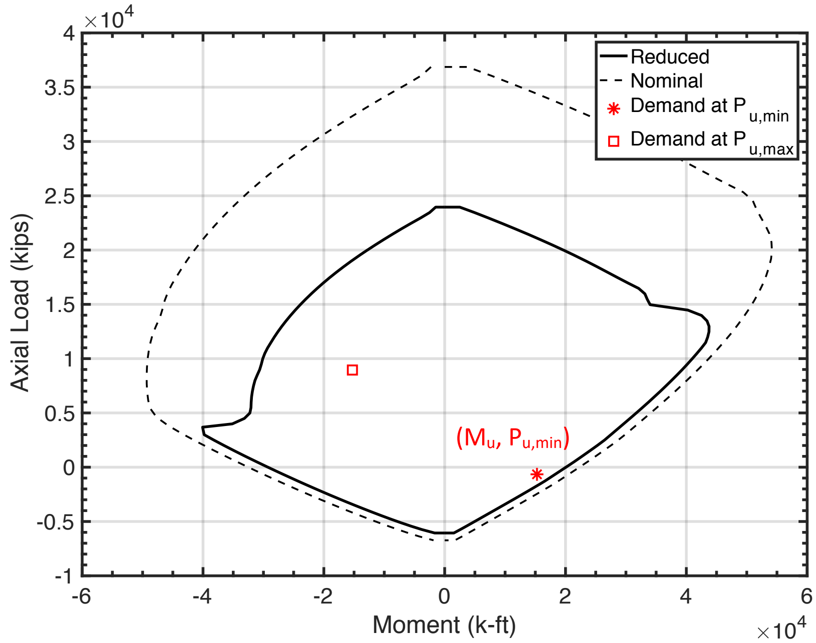

a) *P-M* interaction diagram at Level 1

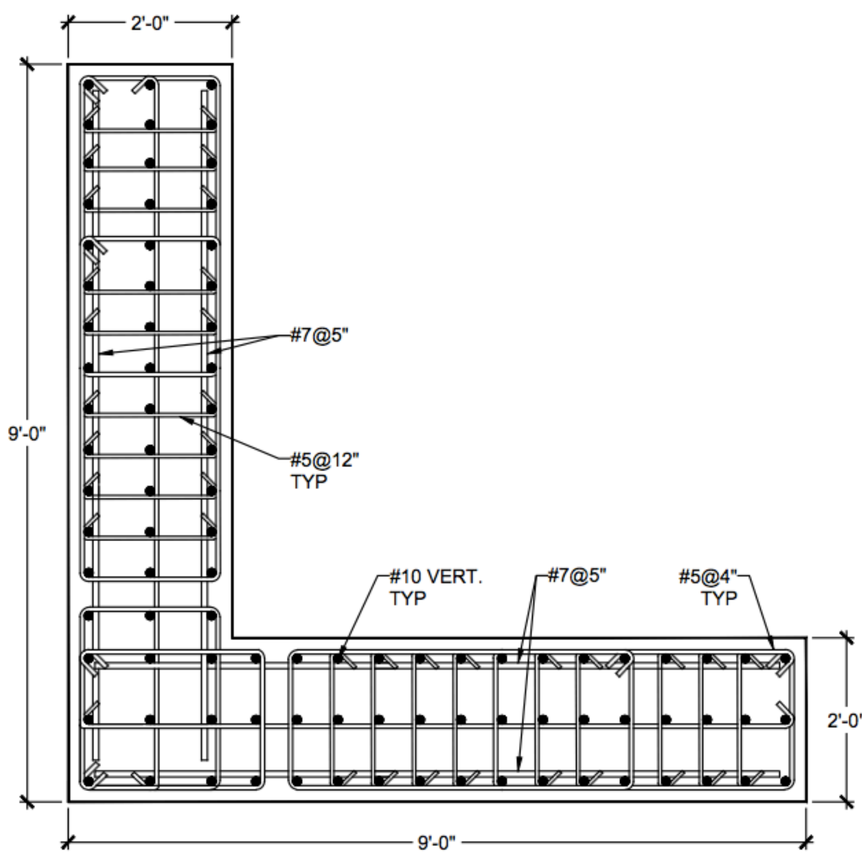

a) Wall Detail at Level 1

Figure 2.17: Archetype 18H-DR-3.0 Wall Detail and *P-M* Interaction

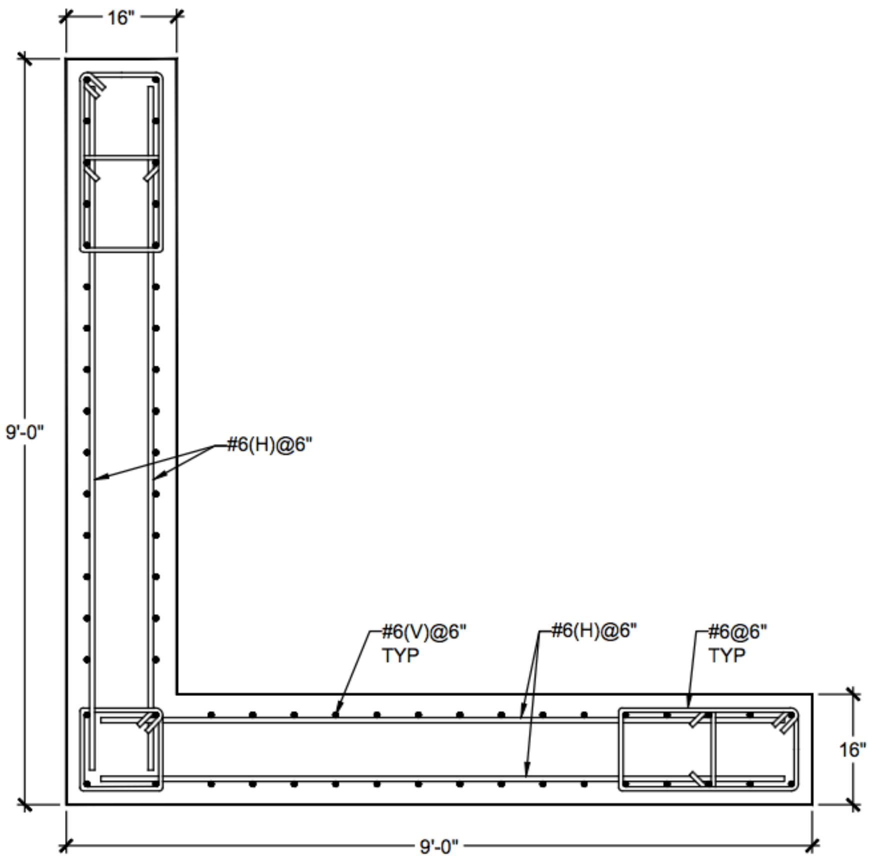

a) Wall Detail at Level 12

Figure 2.18 continued: Archetype 18H-DR-3.0 Wall Detail and *P-M* Interaction

Table 2-16: Archetype 18H-DR-3.0 Design Summary

Level	$b=t_w$ (in.)	Wall Design		Coupling Beam Design		
		Shear ρ_{tr}	Longitudinal A_{sb}	Diag. Bars	Shear D/C	$V_u/(\sqrt{f'_c}\, A_g)$ < φ*10
18	16	0.28	2#5 @12"	6#8	0.86	2.6
17	16	0.69	2#5 @12"	6#8	0.96	2.9
16	16	0.69	2#5 @9"	6#9	0.85	3.2
15	16	0.92	2#5 @9"	6#9	0.94	3.6
14	16	0.92	2#6 @6"	6#10	0.80	3.9
13	16	0.92	2#6 @6"	6#10	0.85	4.1
12	16	1.10	2#6 @6"	6#10	0.89	4.3
11	16	1.10	2#7 @6"	6#10	0.92	4.4
10	16	1.10	2#7 @6"	6#10	0.94	4.5
9	16	1.10	2#7 @6"	6#10	0.96	4.6
8	20	1.00	3#7 @6"	6#11	0.96	4.5
7	20	1.00	3#7 @6"	6#11	0.96	4.5
6	20	1.00	3#7 @6"	6#11	0.95	4.4
5	24	1.00	3#9 @6"	8#10	0.99	4.2
4	24	1.00	3#9 @6"	8#10	0.94	4.0
3	24	1.00	3#9 @6"	8#10	0.84	3.6
2	24	1.00	3#10 @6"	8#10	0.69	2.9
1	24	1.00	3#10 @6"	8#10	0.44	1.9

As the beam aspect ratio is varied between the Archetype designs, the coupling beam reinforcement is optimized for the revised demands; however, the same wall reinforcement used in Archetype 18H-DR-3.0 is typically sufficient for the other Archetypes since the wall demands do not vary significantly among the Archetypes, except as noted in Table 2-17. Variations in design for the 18-story Archetypes are summarized in Table 2-19. To present an example, the optimal beam diagonal reinforcement designs for Archetype 18H-DR-2.4 are summarized in Table 2-18; although beam shear demands increase relative to 18H-DR-3.0, beam shear strengths increase due to the larger diagonal inclination angle allowing for some optimization.

Table 2-17: Wall Reinforcement Variations for 18-Story Archetypes

		Longitudinal Reinforcement, A_{sb}		
Level	**t_w (in.)**	**18H-CR-3.3**	**18H-CR-4.0**	**18H-CR-5.0**
4	24	3#9 @6"	3#9 @6"	3#10 @6"
3	24	3#9 @6"	3#9 @6"	3#10 @6"
2	24	3#10 @6"	3#10 @6"	3#11 @6"
1	24	3#10 @6"	3#10 @6"	3#11 @6"

Table 2-18: Diagonal Reinforcement Design for Archetype 18H-DR-2.4

Level	Wall and CB f'_c (ksi)	$b = t_w$ (in.)	Diagonal Bars	α (°)	Shear D/C	$V_u/(\sqrt{f'_c}\,A_g) < \varphi*10$
18	8	16	6#7	19.2	0.88	2.49
17	8	16	6#8	19.2	0.77	2.86
16	8	16	6#8	19.2	0.89	3.31
15	8	16	6#9	19.1	0.80	3.73
14	8	16	6#9	19.1	0.88	4.10
13	8	16	6#9	19.1	0.94	4.38
12	8	16	6#9	19.1	0.99	4.60
11	8	16	6#10	19.0	0.81	4.79
10	8	16	6#10	19.0	0.84	4.94
9	8	16	6#10	19.0	0.86	5.05
8	8	20	6#11	18.9	0.87	5.03
7	8	20	6#11	18.9	0.89	5.11
6	8	20	6#11	18.9	0.90	5.18
5	8	24	6#11	18.9	0.90	4.30
4	8	24	6#11	18.9	0.87	4.16
3	8	24	6#11	18.9	0.79	3.81
2	8	24	6#11	18.9	0.65	3.14
1	8	24	6#11	18.9	0.42	2.00

Table 2-19: 18-Story Archetype Design Variations

Archetype	T_1 (s)	V_b (kips)	CB h (ft)	CB l_n (ft)	CB Reinforcement	l_w (ft)	Drift Capacity
18H-DR-2.0	2.76	1496	2.75	5.50	L2-7:6#11, L8-9:6#10, L10-14:6#9, L15-17:6#8, L18:6#7, R:6#6	9.0	3.05%
18H-DR-2.4	3.03	1494	2.50	6.00	L2-6:6#11, L7-9:6#11, L10-12:6#10, L13-16:6#9, L17-18:6#8, R:6#7		3.07%
18H-DR-3.0	3.14	1490	2.50	7.50	L2-6:8#10, L7-9:6#11, L10-15:6#10, L16-17:6#9, L18-R:6#8		3.09%
18H-DR-3.3	3.26	1485	2.50	8.33	L2-6:8#10, L7-9:8#10, L10-12:6#11, L13-16:6#10, L17-18:6#9, R:6#8		3.09%
18H-CR-3.3					L2-9:6#11, L10-12:5#11, L13-15:4#11, L16-18:4#10, R:4#9		
18H-CR-4.0	3.34	1479	2.50	10.00	L2-9:6#11, L10-14:5#11, L15-17:4#11, L18-R:4#10		3.11%
18H-CR-5.0	3.37	1468	2.50	12.50	L2-9:8#10, L10-12:6#11, L13-16:5#11, L17-R:4#11		3.12%

2.4.4 24-Story Archetypes

The 24-story Archetype buildings are each 240 feet tall and consist of flanged wall piers that are 10 ft in length. The design process for the 24-story flanged wall Archetypes are the same as described in section 2.2 and outlined for the 18-story designs.

Details of the Archetype with beam aspect ratio l_n/h = 3.0 (24H-DR-3.0) are presented in this section (see Table 2-20) . The fundamental mode of the building is torsion having a period of 3.39 seconds while the first translational period of the building is 2.78 seconds. The period for design (T) per ASCE 7-16 is the minimum of T_1 and C_uT_a = 1.71 seconds. The resulting governing seismic coefficient is $C_s = 0.044S_{DS}I_e = 0.044$. With a seismic weight of 37,586 kips, the base shear V_b is 1654 kips. The maximum story drifts presented in Figure 2.19 are less than the 2% allowable drift value, and no extreme torsional irregularity exists ($\Delta_{max}/\Delta_{avg}$ =1.22 < 1.4).

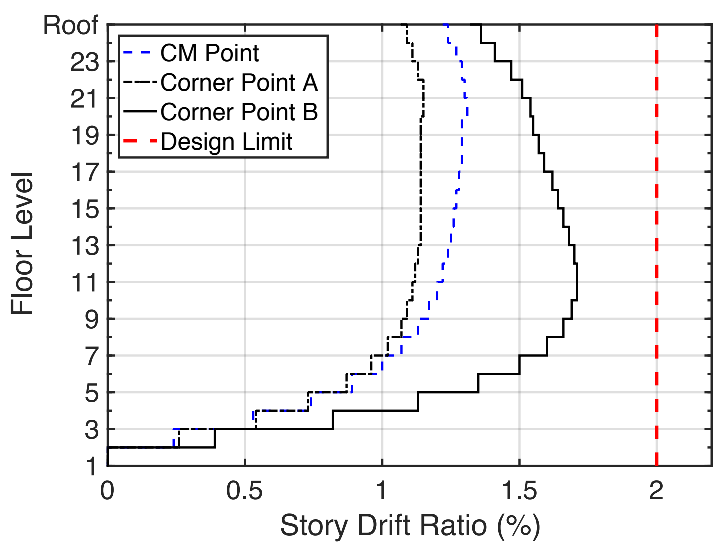

Figure 2.19: Archetype 24H-DR-3.0 Story Drifts

The coupling beams are designed according to ACI 318-14 §18.10.7.4, and the beam reinforcement is optimized based on the shear or flexure demands. The maximum coupling beam shear stress is less than $6\sqrt{f'_c(psi)}$. For design of the flanged walls, demands are determined from combining 100% of the wall group resultant seismic force in one direction plus 30% of the wall group resultant seismic force in the orthogonal direction. The impact of accidental torsion is considered in determining the design demands.

Wall boundary longitudinal reinforcement (A_{sb}) is selected to resist the governing axial and moment demand as described in section 2.2.2, as well as the minimum required by ACI 318-19. A P-M interaction diagram is computed at every floor level to determine the section strength and to verify that the design is adequate. Special boundary elements are needed for Level 1 wall piers with boundary transverse reinforcement consisting of #5 ties spaced at 4 inches. Transverse reinforcement satisfying ACI 318 §18.10.6.5 is provided at Levels 1-10 where the boundary longitudinal reinforcement ratios exceed the limit of $400/f_y$. The resulting wall and coupling beam designs are summarized in Table 2-20.

Table 2-20: Archetype 24H-DR-3.0 Wall and Coupling Beam Design

Level	$b=t_w$ (in.)	Wall Design		Coupling Beam Design		
		Shear A_{tr}	Longitudinal A_{sb}	Diag. Bars	Shear D/C	$V_u/(\sqrt{f'_c}\,A_g)$
24	18	2#5@12"	2#4@12"	6#8	0.87	2.3
23	18	2#5@12"	2#4@12"	6#8	0.96	2.6
22	18	2#5@6"	2#4@12"	6#9	0.84	2.8
21	18	2#5@6"	2#6@12"	6#9	0.92	3.1
20	18	2#6@6"	2#6@12"	6#9	0.98	3.3
19	18	2#6@6"	2#6@12"	6#10	0.80	3.4
18	24	2#6@6"	3#6@12"	6#11	0.87	3.4
17	24	2#6@6"	3#6@12"	6#11	0.88	3.5
16	24	2#6@6"	3#7@12"	6#11	0.90	3.5
15	24	2#6@6"	3#7@12"	6#11	0.92	3.6
14	24	2#6@6"	3#7@12"	6#11	0.94	3.7
13	24	2#7@8"	3#7@12"	6#11	0.97	3.8
12	24	2#7@8"	3#7@12"	6#11	0.99	3.9
11	24	2#7@6"	3#7@12"	8#10	0.95	4.0
10	24	2#7@6"	3#8@12"	8#10	0.98	4.2
9	24	2#7@6"	3#8@12"	8#11	0.83	4.3
8	24	2#7@6"	3#8@12"	8#11	0.86	4.5
7	24	2#8@6"	3#8@6"	8#11	0.88	4.6
6	24	2#8@6"	3#8@6"	8#11	0.89	4.6
5	24	2#8@6"	3#8@6"	8#11	0.87	4.5
4	24	2#8@6"	3#9@6"	8#11	0.83	4.3
3	24	2#8@6"	3#9@6"	8#11	0.74	3.9
2	24	2#8@6"	3#10@6"	8#11	0.60	3.1
1	24	2#8@6"	3#10@6"	8#11	0.39	2.0

Among the 24-story Archetype variations, the wall reinforcement selected for Archetype 24H-DR-3.0 is typically satisfactory for the other Archetypes, except in a few cases. As coupling beam aspect ratio and flexibility increases, the wall flexural demands increase thus requiring increased wall longitudinal reinforcement to resist the wall P_u-M_u demand pairs. For example, Archetypes 24H-CR-4.0 and 24H-CR-5.0 require 2#5@12” longitudinal bars at Level 22.

Moreover, Archetype 24H-CR-5.0 requires at least 2#7@12” at Level 19 and 3#8@6” at Level 4 in order to meet wall flexure demands. The key parameters of the design variations among the 24-story Archetypes are summarized in Table 2-21.

Table 2-21: 24-Story Archetype Design Variations

<table>
<tr><th>Archetype</th><th>T_1 (s)</th><th>V_b (kips)</th><th>CB h (ft)</th><th>CB l_n (ft)</th><th>CB Reinforcement</th><th>l_w (ft)</th><th>Drift Capacity</th></tr>
<tr><td>24H-DR-2.0</td><td>2.87</td><td>1662</td><td>2.75</td><td>5.50</td><td>L2-8:6#11, L9-13:6#10, L14-19:6#9, L20-22:6#8, L23-24:6#7, R:6#6</td><td rowspan="7">10</td><td>2.92%</td></tr>
<tr><td>24H-DR-2.4</td><td>3.16</td><td>1659</td><td>2.50</td><td>6.00</td><td>L2-7:8#10, L8-12:6#11, L13-19:6#10, L20-21:6#9, L22-23:6#8, L24-R:6#7</td><td>2.92%</td></tr>
<tr><td>24H-DR-3.0</td><td>3.39</td><td>1654</td><td>2.50</td><td>7.50</td><td>L2-10:8#11, L11-12:8#10, L13-19:6#11, L20:6#10, L21-23:6#9, L24-R:6#8</td><td>2.94%</td></tr>
<tr><td>24H-DR-3.3</td><td rowspan="2">3.50</td><td rowspan="2">1651</td><td rowspan="2">2.50</td><td rowspan="2">8.33</td><td>L2-10:8#11, L11-12:8#10, L13-19:6#11, L20:6#10, L21-23:6#9, L24-R:6#8</td><td rowspan="2">2.99%</td></tr>
<tr><td>24H-CR-3.3</td><td>L2-11:6#11, L12-19:5#11, L20-22: 5#11, L23-R: 4#9</td></tr>
<tr><td>24H-CR-4.0</td><td>3.61</td><td>1644</td><td>2.50</td><td>10.00</td><td>L2-9:8#10, L10-15:6#11, L16-19: 5#11, L20-21:4#11, L22-L24:4#10, R: 4#9</td><td>3.01%</td></tr>
<tr><td>24H-CR-5.0</td><td>3.71</td><td>1632</td><td>2.50</td><td>12.50</td><td>L2-13:8#11, L14-16:8#10, L17-19:6#11, L20-21: 5#11, L22-L24:4#11, R: 4#10</td><td>2.99%</td></tr>
</table>

2.4.5 30-Story Archetypes

The 30-story Archetype buildings are each 300 feet tall and consist of flanged wall piers that are 11.25 ft in length. The floor plan layout and loading are similar to that of the 18-story Archetypes. The walls are 30 in. thick at the lower 10 levels, 24 in. thick at Levels 11-20, and 18 in. thick at the upper 10 levels. The design process for the 30-story flanged wall Archetypes are the same as described in section 2.2 and outlined for the 18-story designs. The key parameters of the design variations among the 24-story Archetypes are summarized in Table 2-23.

The main difference between the 30-story Archetype designs is that the wall piers in Archetype 30H-CR-5.0 are lengthened from 11.25 ft to 12 ft in order for the design to meet the 2% story drift limit.

Details of the Archetype with coupling beam aspect ratio l_n/h = 3.0 (30H-DR-3.0) are presented in this section. The fundamental mode of the building is torsion with a period of 3.62 seconds while the first translational period is 3.37 seconds. The period for design (T) per ASCE 7-16 is the minimum of T_1 and C_uT_a = 2.02 seconds. With a seismic weight of 48,006 kips and a governing seismic coefficient $C_s = 0.044S_{DS}I_e = 0.044$, the base shear V_b is 2112 kips. The maximum story drifts presented in Figure 2.20 are less than the maximum allowable 2% value, and no torsional irregularity exists ($\Delta_{max}/\Delta_{avg}$ =1.13 < 1.2).

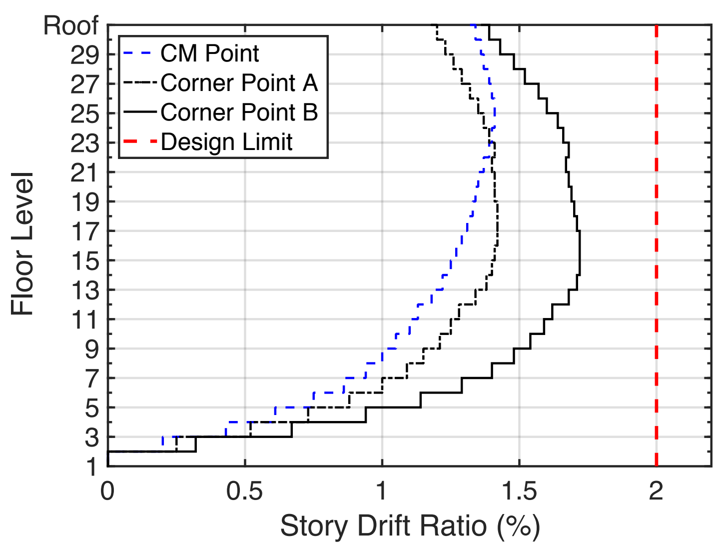

Figure 2.20: Archetype 30H-DR-3.0 Story Drifts

The coupling beams designed according to ACI 318-14 §18.10.7.4 have shear stresses less than $5\sqrt{f'_c(psi)}$. For design of the flanged walls, the L-shaped wall group resultant seismic demands, including accidental torsion effects, are determined, and the wall longitudinal reinforcement (A_{sb}) is designed to resist the worst-case net-tension load and the moment demand. Special boundary elements are needed at the lower level wall piers at Level 1 with #5 ties spaced at 4 inches; the SBE extends up to Level 2 based on the minimum SBE height taken as the maximum of $\{l_w, (M_u/(4V_u)\}$ = 11.25 feet . Transverse reinforcement required by ACI 318 §18.10.6.5 is provided at Levels 2-24, where the longitudinal reinforcement ratios exceed the limit of $400/f_y$. The resulting wall pier and coupling beam designs are summarized in Table 2-22.

Table 2-22: Archetype 30H-DR-3.0 Design Results

Floor	***b=t_w* (in.)**	**Wall Design**		**Coupling Beam Design**		
		Shear A_{tr}	**Longitudinal** A_{sb}	**Diag. Bars**	**Shear D/C**	$V_u/(\sqrt{f'_c}\,A_g)$ < φ*10
30	18	2#5@10"	2#4@9"	6#8	0.89	2.4
29	18	2#5@10"	2#4@9"	6#8	0.96	2.6
28	18	2#6@8"	2#5@9"	6#9	0.84	2.8
27	18	2#6@8"	2#5@9"	6#9	0.92	3.1
26	18	2#6@6"	2#6@9"	6#9	1.00	3.4
25	18	2#6@6"	2#6@9"	6#10	0.84	3.6
24	18	2#6@6"	2#7@9"	6#10	0.88	3.8
23	18	2#7@7"	2#7@9"	6#10	0.92	3.9
22	18	2#7@7"	2#8@9"	6#10	0.94	4.0
21	18	2#7@7"	2#8@9"	6#10	0.96	4.1
20	24	2#7@7"	3#6@6"	6#11	0.91	3.5
19	24	2#7@7"	3#6@6"	6#11	0.91	3.6
18	24	2#7@7"	3#6@6"	6#11	0.92	3.6
17	24	2#7@7"	3#6@6"	6#11	0.94	3.7
16	24	2#7@7"	3#6@6"	6#11	0.95	3.7
15	24	2#7@7"	3#6@6"	6#11	0.97	3.8
14	24	2#7@6"	3#6@6"	6#11	0.99	3.9
13	24	2#7@6"	3#7@6"	8#10	0.92	3.9
12	24	2#7@5.5"	3#7@6"	8#10	0.94	4.0
11	24	2#7@5.5"	3#7@6"	8#10	0.95	4.0
10	30	2#8@7"	3#7@6"	8#11	0.96	4.0
9	30	2#8@7"	3#7@6"	8#11	0.97	4.0
8	30	2#8@6"	3#8@6"	8#11	0.97	4.0
7	30	2#8@6"	3#8@6"	8#11	0.96	4.0
6	30	2#8@6"	3#9@6"	8#11	0.94	3.9
5	30	2#8@5.5"	3#9@6"	8#11	0.90	3.8
4	30	2#8@5.5"	3#10@6"	8#11	0.83	3.5
3	30	2#8@5.5"	3#10@6"	8#11	0.73	3.0
2	30	2#8@5.5"	3#11@6"	8#11	0.57	2.4
1	30	2#8@5.5"	3#11@6"	8#11	0.35	1.4

Table 2-23: 30-Story Archetype Design Variations

Archetype	T_1 (s)	V_b (kips)	CB h (ft)	CB l_n (ft)	CB Reinforcement	l_w (ft)	Drift Capacity
30H-DR-2.0	3.29	2124	2.75	5.50	L2-11:8#10, L12-15:6#11, L16-21:6#10, L22-25:6#9, L26-28: 6#8, L29-R:6#7	11.25	3.10%
30H-DR-2.4	3.35	2120	2.50	6.00	L2-11:8#11, L12-16:6#11, L17-23:6#10, L24-27:6#9, L28-30: 6#8, R:6#7		3.12%
30H-DR-3.0	3.17	2112	2.50	7.50	L2-11:8#11, L12-14:8#10, L15-21:6#11, L22-26:6#10, L27-29:6#9, L30-R:6#8		3.11%
30H-DR-3.3	3.76	2108	2.50	8.33	L2-11:10#11, L12-17:8#11, L18-21:8#10, L22-25:6#11, L26-29:6#10, L30-R:6#9		3.11%
30H-CR-3.3					L2-9: 6#11, L10-11: 5#11, L12-15: 4#11, L16-30: 4#10, Roof: 4#9		
30H-CR-4.0	3.93	2099	2.50	10.00	L2-11: 8#11, L12-18: 8#10, L19-22: 6#11, L23-27: 5#11, L28-30: 4#11, Roof: 4#10		3.12%
30H-CR-5.0	3.72	2130	2.50	12.50	L2-11: 10#11, L12-19: 8#11, L20-21: 8#10, L22-25: 6#11, L26-30: 5#11, Roof: 4#11	12.00	3.13%

2.4.6 Comparison of RSA and ELF demands

Seismic design forces for this study were determined using the RSA method of ASCE 7-16 §12.9.1 as described in Section 2.2. In addition to RSA being the more likely method of analysis used in practice, design axial and moment demands and story drifts from RSA tend to be lower than those of ELF. Table 2-24 presents the difference in demands between RSA and ELF methods of analyses of a subset of Archetypes, i.e., 8, 12, and 18 story Archetypes with diagonally reinforced coupling beams having aspect ratio $l_n/h = 2.4$ and 3.3. The demands are compared for the tension and compression pier of the coupled wall for the two governing seismic load combinations for worst-case net tension and maximum compression. Although the RSA base shear is scaled to 100% of the ELF base shear per ASCE 7-16 §12.9.1.4, ELF axial and moment demands exceed those of RSA as summarized by the ratios presented in Table 2-25 (e.g., ELF moments are on average 15 percent higher than RSA moment demands).

Table 2-24: Comparison of RSA and ELF design demands

RSA	**$(0.9-0.2S_{DS})D$ - E**				**$(1.2+0.2S_{DS})D + 0.5L + E$**			
	Tension Wall		**Compression Wall**		**Tension Wall**		**Compression Wall**	
Archetype	$P_{u,min}$ (k)	M_u (k-ft)	$P_{u,max}$ (k)	M_u (k-ft)	$P_{u,min}$ (k)	M_u (k-ft)	$P_{u,max}$ (k)	M_u (k-ft)
8H-DR-2.4	-798	5989	1987	5996	-96	5979	2694	5994
8H-DR-3.3	-546	6432	1758	6415	211	6424	2515	6423
12H-DR-2.4	-1406	7509	2593	7505	-704	7505	3295	7508
12H-DR-3.3	-992	8730	2327	8739	167	8723	3152	8746
18H-DR-2.4	-1075	13799	6128	13877	2002	13740	9205	13936
18H-DR-3.3	-582	15333	5685	15371	2602	15300	8869	15403

ELF	**$(0.9-0.2S_{DS})D$ - E**				**$(1.2+0.2S_{DS})D + 0.5L + E$**			
	Tension Wall		**Compression Wall**		**Tension Wall**		**Compression Wall**	
Archetype	$P_{u,min}$ (k)	M_u (k-ft)	$P_{u,max}$ (k)	M_u (k-ft)	$P_{u,min}$ (k)	M_u (k-ft)	$P_{u,max}$ (k)	M_u (k-ft)
8H-DR-2.4	-935	6445	2124	6435	-233	6455	2830	6433
8H-DR-3.3	-666	6936	1883	6928	81	6947	2636	6928
12H-DR-2.4	-2195	9130	3386	9132	-1502	9127	4084	9133
12H-DR-3.3	-1533	10354	2869	10363	-710	10346	3693	10369
18H-DR-2.4	-2454	16345	7507	16266	623	16403	10584	16208
18H-DR-3.3	-1729	17922	6833	17884	1455	17954	10016	17851

Table 2-25: Ratio of ELF to RSA design demands

ELF/RSA	$(0.9\text{-}0.2S_{DS})D$ - E				$(1.2+0.2S_{DS})D + 0.5L + E$			
	Tension Wall		**Compression Wall**		**Tension Wall**		**Compression Wall**	
Archetype	$P_{u,min}$ (k)	M_u (k-ft)	$P_{u,max}$ (k)	M_u (k-ft)	$P_{u,min}$ (k)	M_u (k-ft)	$P_{u,max}$ (k)	M_u (k-ft)
8H-DR-2.4	1.17	1.08	1.07	1.07	2.43	1.08	1.05	1.07
8H-DR-3.3	1.22	1.08	1.07	1.08	0.38	1.08	1.05	1.08
12H-DR-2.4	1.56	1.22	1.31	1.22	2.13	1.22	1.24	1.22
12H-DR-3.3	1.55	1.19	1.23	1.19	4.24	1.19	1.17	1.19
18H-DR-2.4	2.28	1.18	1.23	1.17	0.31	1.19	1.15	1.16
18H-DR-3.3	2.97	1.17	1.20	1.16	0.56	1.17	1.13	1.16
Average	1.79	1.15	1.18	1.15	1.68	1.15	1.13	1.15

2.4.7 Design Summary

Designs for the 8-, 12-, 18-, 24- and 30-story Archetypes were summarized in section 2.4. Typically, detailed information was presented for each building height for a coupling beam aspect ratio of 3.0, and variations in the designs relative to this Archetype were summarized. In general, as the coupling beam aspect ratio is varied for the different Archetypes, the beam and wall demands do not vary significantly; therefore, only slight modifications are typically required to the coupling beam reinforcement and wall reinforcement along the building height. For all Archetypes, maximum story drifts are less than the allowable 2.0 percent story drift limit, expect for a couple of the Archetypes with high beam aspect ratios that require increased wall pier lengths in order to satisfy the drift requirements (namely, Archetypes 12H-CR-3.3, -4.0, -5.0, and 30H-CR-5.0). For the Archetypes with conventionally reinforced coupling beams, the beam flexural demand increases with increasing aspect ratio due to the increase in coupling beam length resulting in a more flexible structure; therefore, the beam longitudinal reinforcement needs to be upsized at a particular level compared to the design with l_n/h = 3.0.

In terms of wall demands, as the coupling beam aspect ratio increases, the wall shear and axial forces typically decrease due to reduced coupling action whereas the wall flexural demands typically increase due to increased beam flexibility. For many of the Archetype designs with increased aspect ratios, the same longitudinal reinforcement at that floor level from the Archetype with l_n/h=3.0 satisfies the P_u-M_u demand pairs because while the flexure demand M_u increases, the axial demand P_u decreases resulting in a higher ΦM_n below the P-M interaction diagram balanced point. Similarly, for Archetypes with reduced aspect ratios than 3.0, the same or slightly reduced longitudinal reinforcement than for the Archetype with l_n/h = 3.0 typically satisfies the P_u-M_u demand pairs because of slightly reduced wall flexural demands.

The Appendix A presents the key details for each of the design variations.

Chapter 3 - Nonlinear Modeling

3.1 System and component modeling

Nonlinear analysis is performed using the two-dimensional OpenSees Multi-Vertical-Line-Element-Model (MVLEM) for RC walls implemented by Kolozvari et al. (2018). The following subsections describe the nonlinear model in more detail.

3.1.1 System modeling

Analytical models for the lateral-load-resisting system of each Archetype are generated in the structural analysis software OpenSees (McKenna et al., 2000) according to the adopted geometry, cross-sections, and expected material properties of the structural walls and coupling beams summarized in Chapter 2. Given the wall locations in the building plan and relatively large spans between the vertical structural components (walls and columns), it is assumed that the out-of-plane stiffness of the 8 in. (200 mm) thick floor slab is small and that insignificant axial forces are imposed on walls via wall-wall or wall-column outrigger interaction. Symmetry is used such that a two-dimensional model consists of two walls and coupling beams. Analysis is performed for in-plane loads only. The approach is described by Kolozvari et al. (2018b).

Lateral displacement degrees-of-freedom at each floor level are slaved to simulate the behavior of a rigid diaphragm. Moreover, the effect of out-of-plane deformation of the wall on the in-plane force and deformation capacities are not considered because analytical models are not available and experimental data are scarce. Although these assumptions are commonly used in nonlinear modeling of RC walls, they represent important issues that require additional analytical and experimental studies.

The conceptual modeling approach is presented in Figure 3.1. Tributary mass is assigned at the element nodes at each story level, while gravity load (dead and live) is assigned at the same nodes based on corresponding tributary areas (Figure 3.1a). P-delta effects are considered via a P-delta column for one half of the building represented by an elastic element with axial and negligible bending stiffness corresponding to gravity columns (Figure 3.1a). The wall piers with defined material force-deformation relations (Figure 3.1b) are connected by rigid coupling beam elements having a nonlinear shear hinge located at the beam midspan (Figure 3.1c). The wall shear response (Figure 3.1d) is simulated using a linear elastic spring with an effective shear stiffness of 0.5G. Additional sensitivity studies are conducted (see Section 6.4) using a model with shear-flexure interaction (SFI-MVLEM) as described in section 3.1.2 which allows coupling of axial/flexural and shear behavior to better predict shear demands in the wall plastic hinge regions for the Archetype buildings.

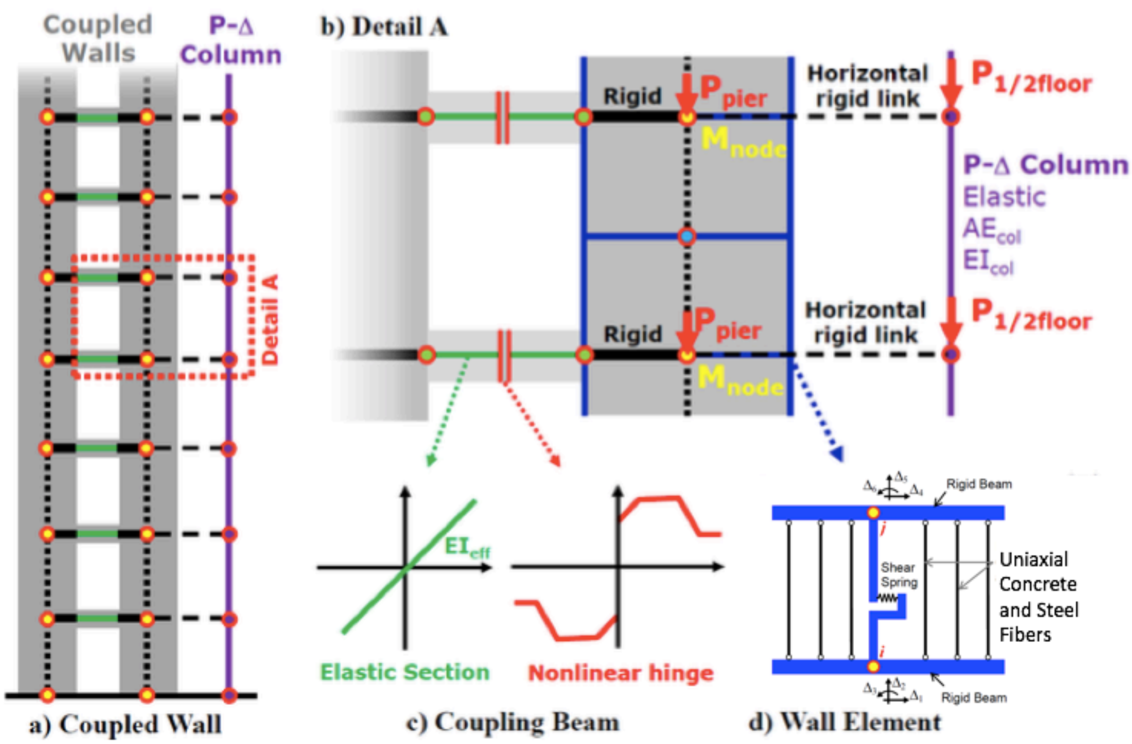

Figure 3.1: Modeling approach for coupled wall system (Kolozvari et al., 2018b)

The wall piers are modeled in OpenSees using the *Multiple-Vertical-Line-Element-Model* (MVLEM; implemented and validated by Orakcal et al., 2004; Orakcal and Wallace, 2006; Kolozvari et al., 2015c) as presented in Figure 3.2. The axial/flexural response of the model element is simulated by a series of uniaxial elements (macro-fibers) distributed along the wall cross-section and connected to rigid beams at the top and bottom of the element to enforce plane-section assumption, as illustrated in Figure 3.2a. The MVLEM is similar to a displacement-based beam-column element model, except that the deformations and forces in the element fibers are obtained using average strains and stresses developing within each macro-fiber in order to minimize convergence issues and improve numerical stability. The stiffness properties and force-deformation relations of the uniaxial elements are obtained using the hysteretic stress-strain relations for concrete and reinforcing steel (Figure 3.2b) and the tributary area assigned to each uniaxial element. Moreover, element flexure and shear responses are uncoupled (Figure 3.2b).

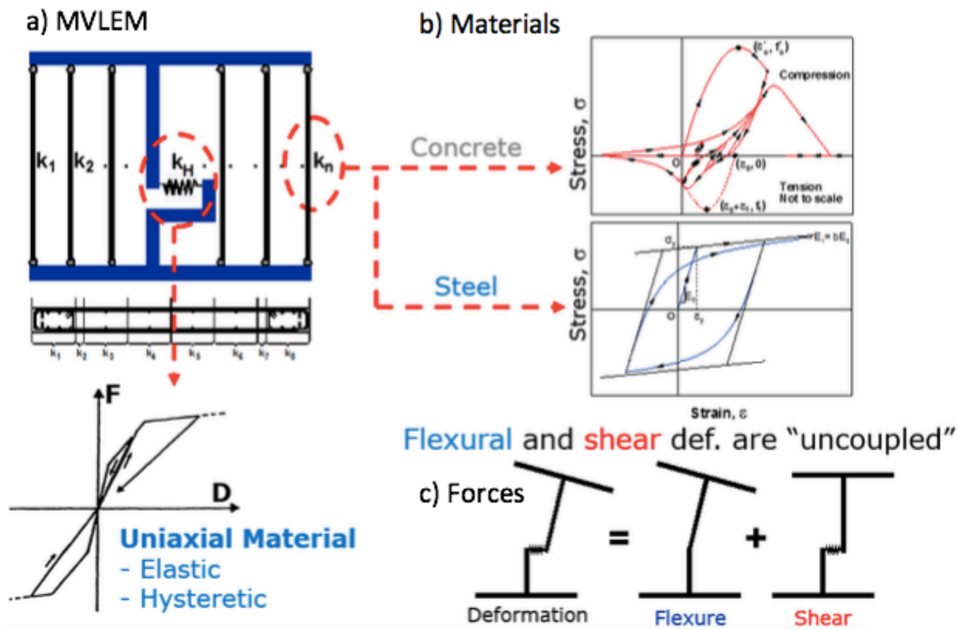

Figure 3.2: MVLEM wall model: a) wall macro-fibers, b) fiber material stress-strain relations, c) decoupled element flexural and shear forces

Within each macro-fiber, the axial stresses developing in concrete and reinforcement steel and the shear force developing in the horizontal spring are used to obtain the internal force vector of the MVLEM element in order to simulate element response. The relative rotation between top and bottom boundaries of the model element is concentrated at the element center of rotation defined at the same location as the shear spring. The distribution of curvature is assumed to be constant along the element height, hence an appropriate number of elements should be used over the anticipated plastic hinge region in order to reasonably predict local deformation responses.

Wall discretization in the horizontal direction include sufficient number of fibers typically 5 inches wide to reasonably represent wall cross-section and reinforcement configuration in the boundaries and web of the wall. Discretization in the vertical direction includes two wall elements per story height which has been investigated to be appropriate (Kolozvari et al., 2018b) since wall damage is correlated to global engineering demand parameters such as drift that are not sensitive to wall discretization. Discretization in the horizontal direction is established based on comparing analytical results for an 8-story Archetype (8H-DR-3.0) between two models having fibers that are 2.5 inches versus 5 inches wide at the wall boundaries. Nonlinear pushover results as presented in Figure 3.3 indicate that the neutral axis depth of the model with 2.5 inch wide fibers is less than 2% larger than the neutral axis depth of the model with 5 inch wall fibers. Since the wall local and global responses do not vary much between these two levels of discretization, using fiber sizes about 5 in. is appropriate for modeling the Archetypes, and is more computationally efficient.

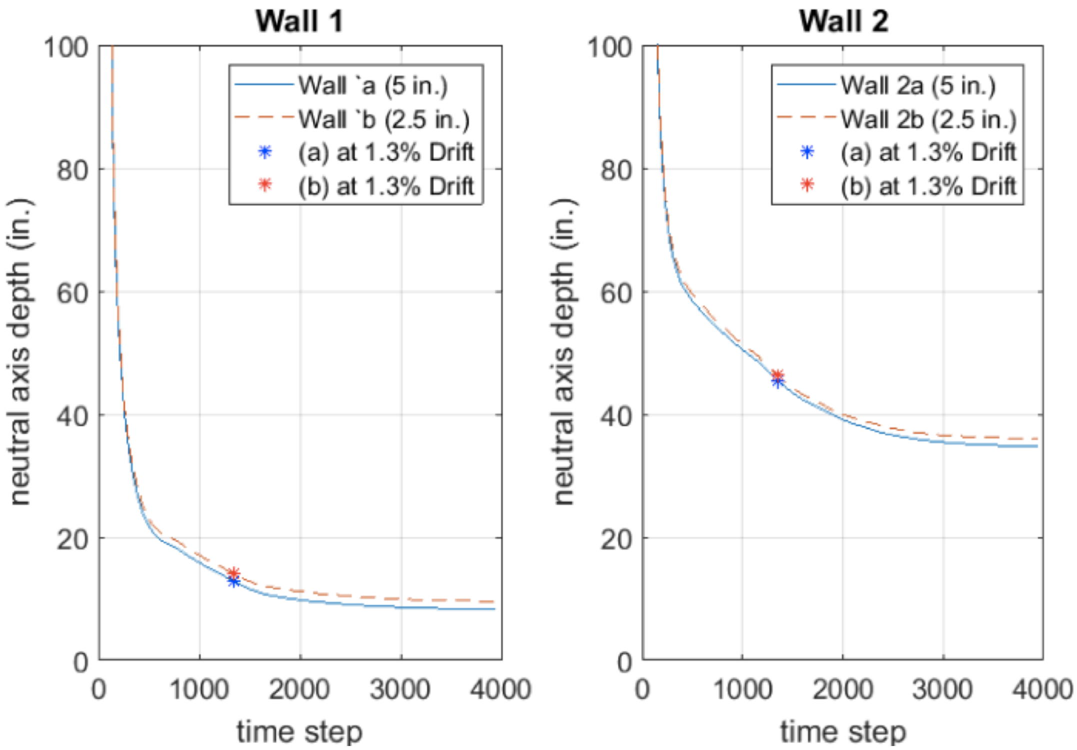

Figure 3.3: Fiber size sensitivity study

Shear response of the model element is simulated by a horizontal spring connected to the top and the bottom rigid beams via vertical rigid strut, with behavior typically described by ad-hoc force-deformation rules (e.g., linear-elastic, bi-linear, origin-oriented hysteresis models, etc.). Based on current design/evaluation provisions (e.g., ASCE 41; LATBSDC, 2015; PEER/ATC 72, 2010) an elastic spring with a cracked effective shear stiffness of $0.5GA_w$ is used to represent shear behavior of uncoupled modeling approaches, which is the most commonly used approach in engineering practice. Since axial/flexural and shear responses are described independently, there is no coupling between these responses in the MVLEM element (Figure 3.2c).

Alternatively, the *Shear-Flexure Interaction MVLEM* (SFI-MVLEM developed and validated by Kolozvari et al., 2015a,b,c, and Kolozvari et al., 2018) incorporates biaxial constitutive RC panel behavior (Ulugtekin, 2010), described with the fixed-strut angle approach, into a two-dimensional macroscopic fiber-based model formulation of the MVLEM (Figure 3.4). Axial-shear coupling is achieved at each macro-fiber (panel) level through two-dimensional constitutive RC panel material model, which further allows coupling of axial/flexural and shear responses under cyclic loading at the SFI model element level. Since shear behavior is governed by RC panel elements, the shear spring is removed from the element formulation. Similar to the MVLEM, panel strains/stresses are treated in the average sense, the element rotation occurs at the center of rotation, and constant distribution of curvature is assumed over the element height. Biaxial behavior of concrete within each RC panel element is described using a uniaxial stress-strain relationship for concrete applied along fixed compression struts, where mechanisms representing compression softening (Vecchio and Collins, 1993), hysteretic biaxial damage (Mansour et al, 2002), and tension stiffening effects (Belarbi and Hsu, 1994) are used. The implemented uniaxial constitutive relationship for reinforcing steel is applied along vertical and horizontal reinforcement directions. The RC panel model also incorporates two shear-resisting mechanisms to resist shear stresses along concrete cracks including: a) shear aggregate interlock effects (Orakcal et al., 2012), and b) reinforcement dowel action (Kolozvari *et al*, 2015a). In the SFI-MVLEM, wall shear stiffness and strength of the element evolve according to computed RC panel responses and assumed material behavior. Therefore, explicit definition of shear modeling parameters is not necessary in SFI-MVLEM, as opposed to commonly used wall models with uncoupled shear and axial/flexural behavior, such as the displacement-based beam-column element (OpenSees, Taucer 1991) or the shear wall element (Perform 3D, CSI).

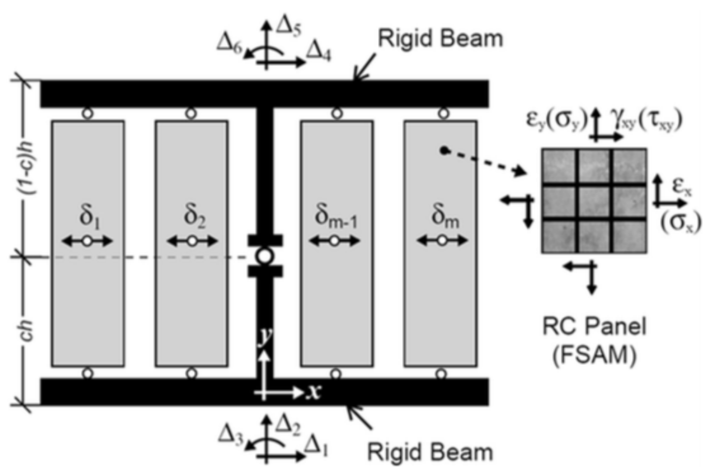

Figure 3.4: SFI-MVLEM wall model

3.1.2 Component modeling

The wall piers are modeled in OpenSees using the MVLEM described in Section 3.1.1 consisting of fiber elements with defined material stress-strain relations for concrete and steel. The constitutive relationships implemented in the MVLEM for concrete and reinforcing steel described in the following paragraphs have been calibrated using the procedure described by Orakcal and Wallace (2006) to match corresponding specimen material properties obtained from uniaxial material tests of slender RC walls with rectangular and T-shaped cross sections. Using this procedure, the validated cyclic stress-strain behavior of steel and concrete including parameters for confinement and tension stiffening result in an effective modeling approach for predicting the flexural response of slender RC walls (Orakcal and Wallace, 2006).

The unconfined concrete stress-strain values specified for each wall fiber element is based on the model by Hognestad (1951) while the confined concrete relationship is based on the confinement model by Saatcioglu and Razvi (1992). The strain history of the unconfined concrete consists of loading to a strain of 0.002 until reaching the peak concrete compressive stress (f'_c) and then decreasing the stress until it drops to zero. The strain history of the confined concrete consists of the strain increasing with constant stress until the peak confined compressive stress (f'_{cc}) is reached and decreasing thereafter until the stress drops to twenty percent of the peak confined compressive stress. The quantity and distribution of transverse reinforcement in the confined wall boundaries is used to determine the appropriate uniaxial concrete stress versus strain relations for confined concrete. The design longitudinal reinforcement is assigned for each fiber along the wall length to represent the steel stress-strain relations.

A uniaxial hysteretic model (*Concrete02* in OpenSees) proposed by Yassin (1994) is used in this study to simulate the behavior of concrete material. The material envelope curve in compression follows the monotonic stress-strain relationship model of Kent and Park (1971) as extended by Scott, Park and Priestley (1982). Therefore, concrete degradation in compression is modeled directly with the concrete constitutive material model (Figure 3.5). In the model implementation used in this study, the compression envelope is defined by strain and stress values corresponding to concrete peak compressive capacity (ε_0, f'_c) and post-peak residual capacity of concrete (ε_{cu}, σ_{cu}), where ascending branch of the curve ($0 < \varepsilon_c < \varepsilon_0$) follows the quadratic relationship, descending post-peak branch is described with a linear relationship

($\varepsilon_0 < \varepsilon_c < \varepsilon_u$), and residual capacity of concrete is described as constant ($\varepsilon_c > \varepsilon_u$), as illustrated in Figure 3.5.

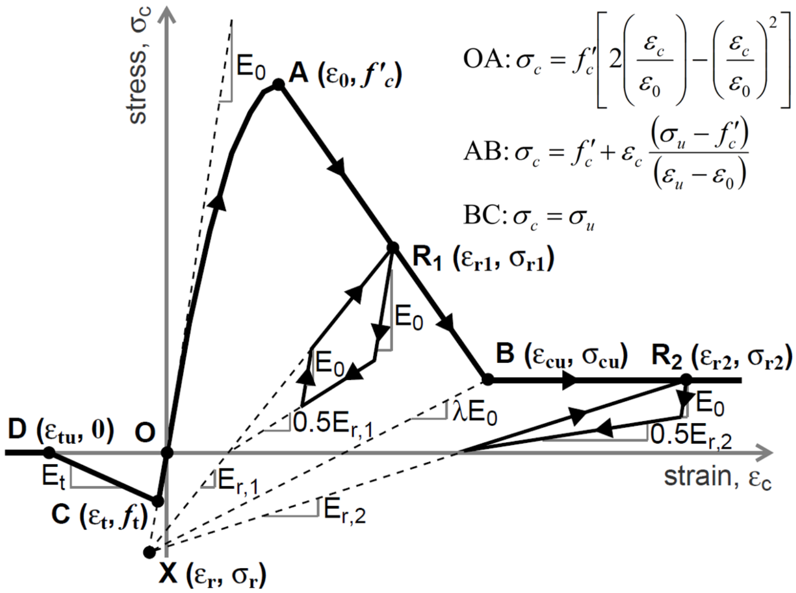

Figure 3.5: Concrete material model (Yassin, 1992)

The hysteretic unloading and reloading rules are adopted according to a set of linear stress-strain relationships. All reloading lines intersect at a common point X determined by the intersection of the tangent to the monotonic envelope curve at the origin (E_0) and the projection of the unloading line from point corresponding to ε_{cu} and σ_{cu} at a slope of λE_0, where λ is user-defined parameter that takes values between 0.0 and 1.0 (Figure 3.5). For each point on the compression envelope R_i from which unloading occurs, a reloading line X-R_i can be defined, and the corresponding reloading stiffness $E_{r,i}$ can be calculated. As shown in Figure 3.5, the unloading from point R_i starts with slope E_0 and transitions into a slope $0.5E_{r,i}$, while reloading to the compression envelope starts with slope E_0 and transitions to the reloading line X-R_i.

The tensile strain-stress envelope of the model follows a straight line with slope of E_0 from the origin until the user-defined peak tensile strength of concrete f_t (and corresponding strain ε_t) is reached. For tensile strains larger than the cracking strain ε_t, tensile envelope follows a straight line at a slope E_t, which allows modeling of tension stiffening effect; a value of $E_t = 0.05 \cdot E_0$ was used in this study as suggested by Yassin (1994). The model assumes that tensile stress can occur anywhere along the strain axis, either as a result of initial tensile loading or as a result of unloading from a compressive state, and it accounts for degradation of the unloading and reloading stiffness for increasing values of maximum tensile strain after initial cracking.

The constitutive model for concrete proposed by Yassin (*Concrete02* in OpenSees) takes into account important behavioral characteristics of the material behavior such as concrete damage, tension stiffening, and hysteretic behavior, but it is also relatively simple, computationally efficient, and numerically stable. Given the large number of analyses conducted for this study, use of an efficient concrete material model is essential. The primary shortcoming of this constitutive model is its inability to simulate gradual gap closure due to progressive contact stresses within the cracks in concrete. Despite this limitation, this concrete model is sufficient to meet the objectives of this study.

The uniaxial hysteretic constitutive model (*SteelMPF* in OpenSees, Kolozvari et al., 2018) for reinforcing steel proposed by Menegotto and Pinto (1973), as extended by Filippou et al. (1983) to include isotropic strain hardening effects, is used in this study for simulating the hysteretic stress-strain behavior of reinforcing steel bars. The strain-stress relationship is in the form of curved transitions, each from a straight-line asymptote with slope E_0 (modulus of elasticity) to another straight-line asymptote with slope $E_1 = b \cdot E_0$ (yield modulus) where b is the strain hardening ratio (Figure 3.6). The curvature of the transition curve between the two asymptotes is governed by a cyclic curvature parameter R, which permits the Bauschinger effect to be represented, and is dependent on the absolute strain difference between the current asymptote intersection point (ε_0,σ_0) and the previous maximum or minimum strain reversal point (ε_r,σ_r) depending whether the current strain is increasing or decreasing, respectively. The strain and stress pairs (ε_r,σ_r) and (ε_0,σ_0) shown on Figure 3.6 are updated after each strain reversal.

The implementation of the hysteretic model for steel used in this study involves two improvements to the original model formulation introduced by Kolozvari et al. (2017): 1) degradation of the cyclic curvature parameter R is implemented for strain reversals in both pre- and post- yielding regions of the hysteretic stress-strain behavior, which enables improved prediction of yield capacity, and 2) the issues related to stress overshooting after partial unloading/reloading (possible under dynamic loading or stress re-distribution due to concrete cracking or local crushing), acknowledged by Filippou et al. (1983), are fixed for improved prediction of strain hardening and stress values under cyclic loading as illustrated in Figure 3.6.

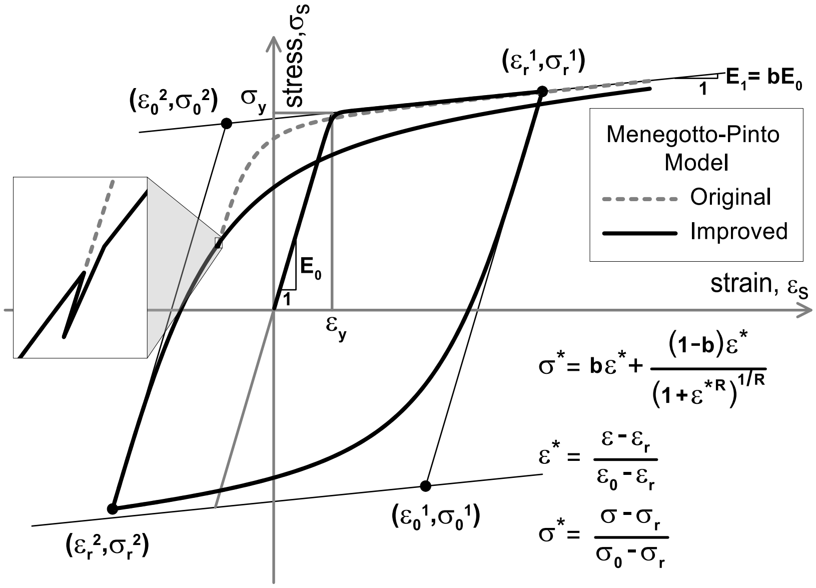

Figure 3.6: Material model for steel (Kolozvari et al., 2017)

3.1.3 Coupling beam modeling

Coupling beams are connected to wall piers via rigid beam elements defined between centerline of the walls and the ends of the coupling beam element. The deformation of the coupling beams are modeled using elastic beam elements with an effective flexural stiffness of $0.07(l_n/h)I_g$ per LATBSDC (2017), while nonlinear hysteretic behavior was captured using a nonlinear shear hinge located in the center of the beam as illustrated in Figure 3.7a. The behavior of the shear hinge is modeled using the *Pinching4* material available in OpenSees (Figure 3.7b) comprised of the following four points: Point 1 representing the yield point, Point 2 representing ultimate shear, Point 3 as the point at which the shear begins to degrade, and Point 4 as the point of reaching the residual force.

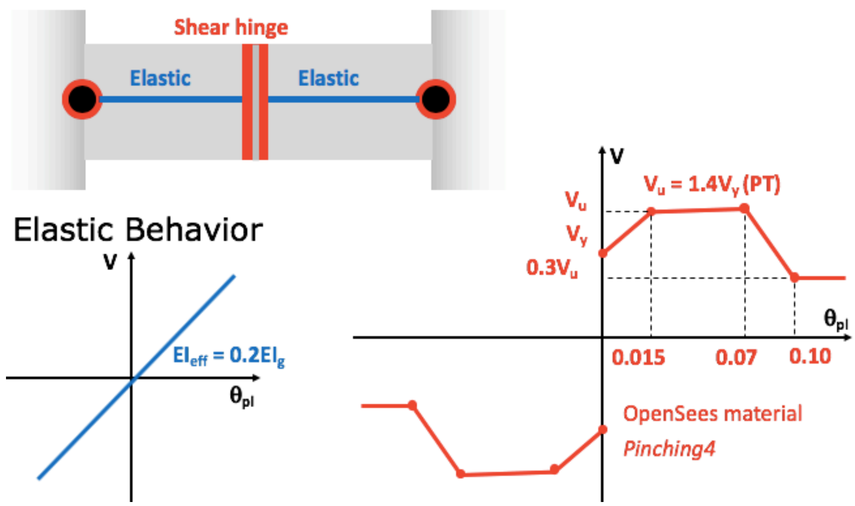

a) Typical modeling approach for coupling beams

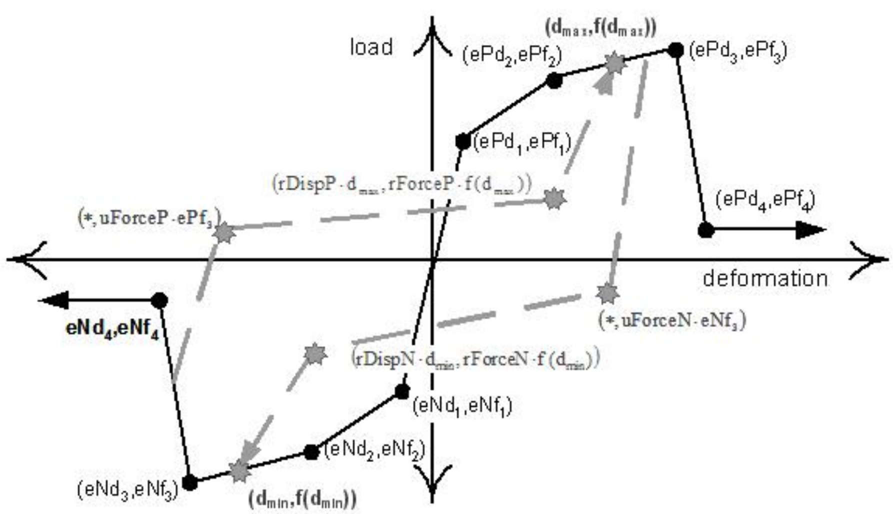

b) OpenSees Pinching4 Model (opensees.berkeley.edu)

Figure 3.7: Coupling beam model

The coupling beam hysteretic behavior is calibrated using the coupling beam specimen tested by Naish et al. (2013). Figure 3.8 illustrates that a good match between analytical and experimental load-deformation responses is obtained for each validation and summarizes the calibrated values used in this study from the test specimen. For this project, the calibrated coupling beam hysteretic responses are derived from specimen CB24F-PT with a post-tensioned slab for diagonally reinforced coupling beams and from specimen FB33 for conventionally reinforced coupling beams. Backbone relations derived from test results (Naish 2010; Naish et al., 2013) are used to estimate the shear overstrength associated with the load-deformation behavior of the coupling beams. The shear overstrength (V/V_n) including the impact of slab can be accounted for by a factor of 1.1 for beams without slab, 1.3 for a reinforced concrete slab, and 1.4 for a post-tensioned (PT) slab. For the Archetypes in this study, the coupling beam shear strength is increased by a factor of 1.4 to account for the shear overstrength considering a PT slab. A section analysis is conducted for a sample coupling beam to confirm the overstrength associated with the presence of a PT slab providing axial force to the beam by the tensioned strands. For a sample 12 in. by 30 in coupling beam with 4#11 longitudinal top and bottom bars, the moment strength of a rectangular beam section without considering the slab is 794 k-ft, while the moment strengths of a T-beam section considering a PT slab with 150 psi of post-tensioning force are 1066 k-ft with the slab in compression and 993 k-ft with the slab in tension; the moment strength with the slab in compression differs by a factor of 1.34 as compared to the 1.4 factor used in this study for the ultimate shear strength of coupling beams with a PT slab as recommended by Naish (2010).

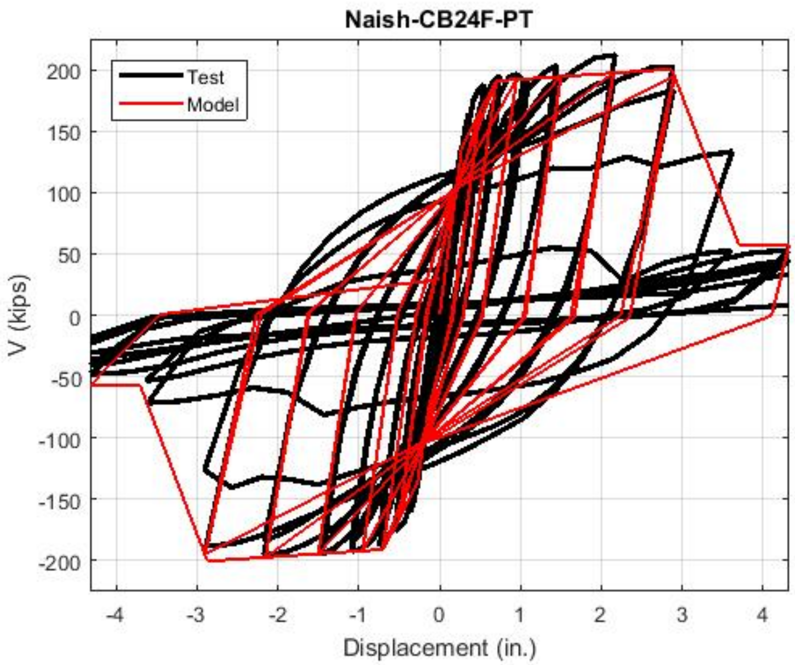

Specimen	k	FU	Point 1	Point 2	Point 3	Point 4	rForceP
CB24F (no slab)	0.11	1.1*FY	(0.001*L, FY)	(0.015*L, FU)	(0.07*L, 1.01*FU)	(0.1*L, 0.3*FU)	0.70
CB24F-PT (PT slab)	0.15	1.4*FY	(0.001*L, FY)	(0.01*L, FU)	(0.07*L, 1.05*FU)	(0.1*L, 0.3*FU)	0.55
FB33 (CR)	0.15	1.1*FY	(0.001*L, FY)	(0.015*L, FU)	(0.045*L, 1.01*FU)	(0.07*L, 0.3*FU)	0.35

*Note: OpenSees *Pinching4* model (*rDisP* = 0.05; *uForceP* = 0.01; *gK#*: 0.5,0.45,0.4,0.35,1.0)

Figure 3.8: Coupling beam modeling approach validation

3.1.4 Damping

The nonlinear model uses Rayleigh damping for the analyses per the recommendations of the PEER TBI (2017) guidelines §4.2.7 for MCE_R. The critical damping value used is a function of building height (H), i.e., $\zeta_{critical} = 0.36/\sqrt{H}$ with a trend of damping reducing for taller buildings (Figure 3.9). Periods of $0.2T_1$ and $1.5T_1$ (where T_1 is the fundamental period of the building from modal analysis) are used to compute the mass and stiffness dependent Rayleigh damping coefficients using current stiffness. A sample damping relation for the Archetype 12H-DR-3.0 is presented in Figure 3.10.

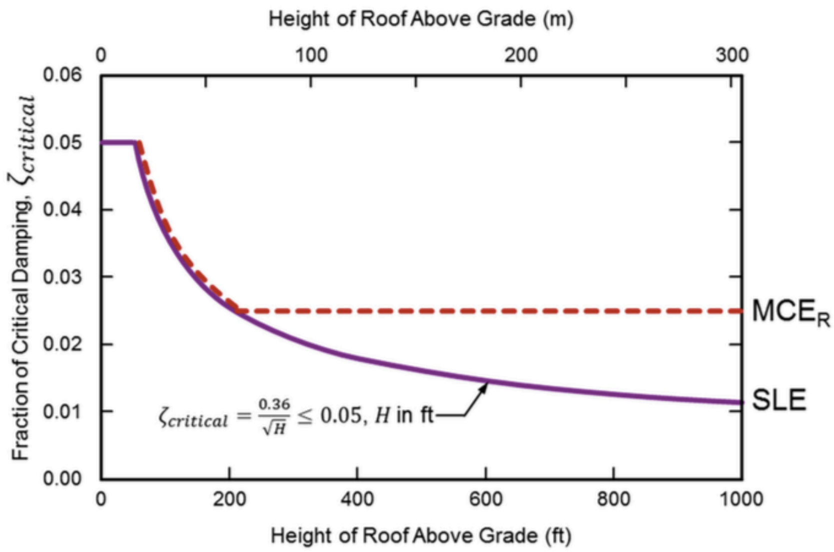

Figure 3.9: Equivalent viscous damping versus building height (PEER TBI, 2017)

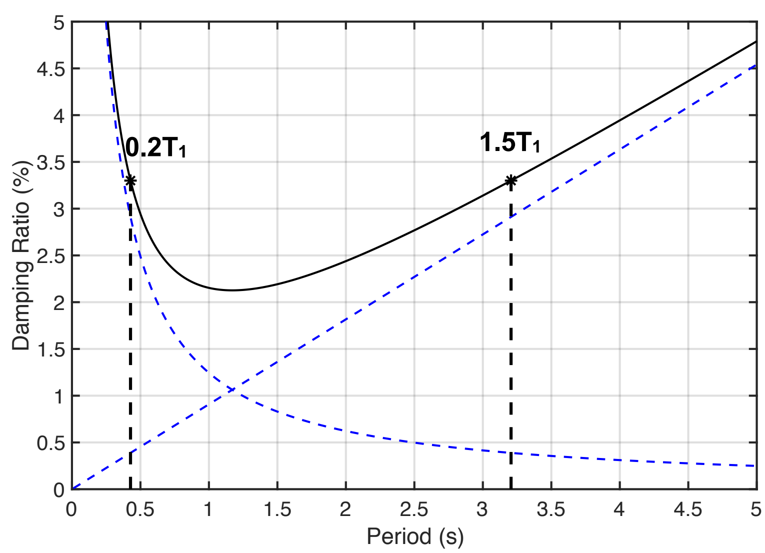

Figure 3.10: Rayleigh Damping for Archetype 12H-DR-3.0

3.2 Model Validation

In order to validate the modeling approach adopted for the coupled wall Archetypes, experimental data are used to compare results.

3.2.1 Model Validation - 1996 BRI 12-Story Coupled Wall Test

In the following section, a model validation is presented using experimental data from a quasi-static cyclic test of a one-third scale, twelve-story, reinforced concrete coupled wall system that was performed by the US-Japan Collaborative in 1996 (Sugaya et al., 2003). The Japanese team of researchers performed this test at the Building Research Institute (BRI) with goals to study the transfer of shear forces between the tension and compression wall piers of coupled shear walls. This test is unique in that load cells are attached to structural elements to track the axial load transfer between the coupling beams and the linked wall piers.

3.2.1.1 Description of the test specimen

The coupled T-walls system had twelve typical story heights measuring 1200 mm each for a total height of 14.4 meters. The test specimen consisted of 200 mm thick flanged T-walls each measuring 2000 m in length with 2000 mm wide flanges, linked at each floor level by 200 mm wide by 400 mm deep coupling beams spanning 1000 mm. Figure 3.11 demonstrates the elevation and plan view of the test specimen.

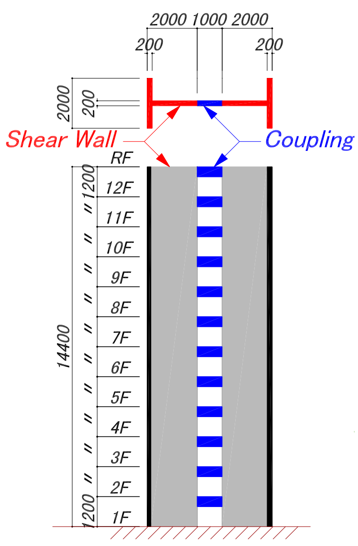

a) Elevation View

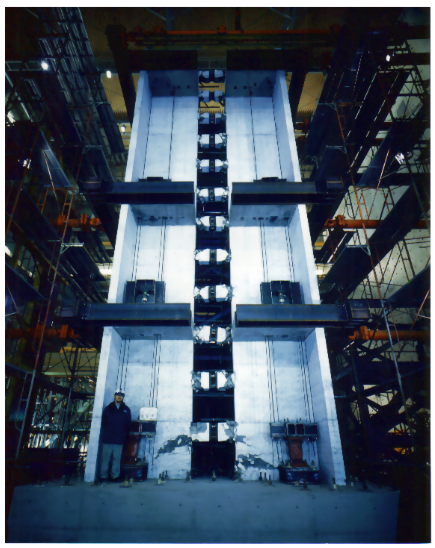

b) Deformed Shape of Test Specimen

Figure 3.11: Twelve-Story Test Specimen (Sugaya et al., 2003)

The T-walls consisted of typical longitudinal reinforcement of D6 bars spaced at 50mm (reinforcement ratio ρ_s of 0.64%) and horizontal reinforcement with D6 ties spaced at 200mm. The walls had additional longitudinal reinforcement and confinement in the compression zones that increased down the height of the building as summarized in Table 3-1. This confined zone was essential for the ability of the wall piers to resist the compressive forces resulting from the overturning moment. The coupling beams consisted of diagonal reinforcement that increased down the height of the building, i.e., two D-13 bars at the higher floor levels 8^{th}-Roof and two D-16 bars at the lower 2^{nd}-7^{th} floor levels. Each coupling beam was also reinforced with two D-10 longitudinal bars with shear reinforcement consisting of 2 legs of D6 ties spaced at 100mm. The reinforcement layout for the lower Level walls and beams are shown in Figure 3.12.

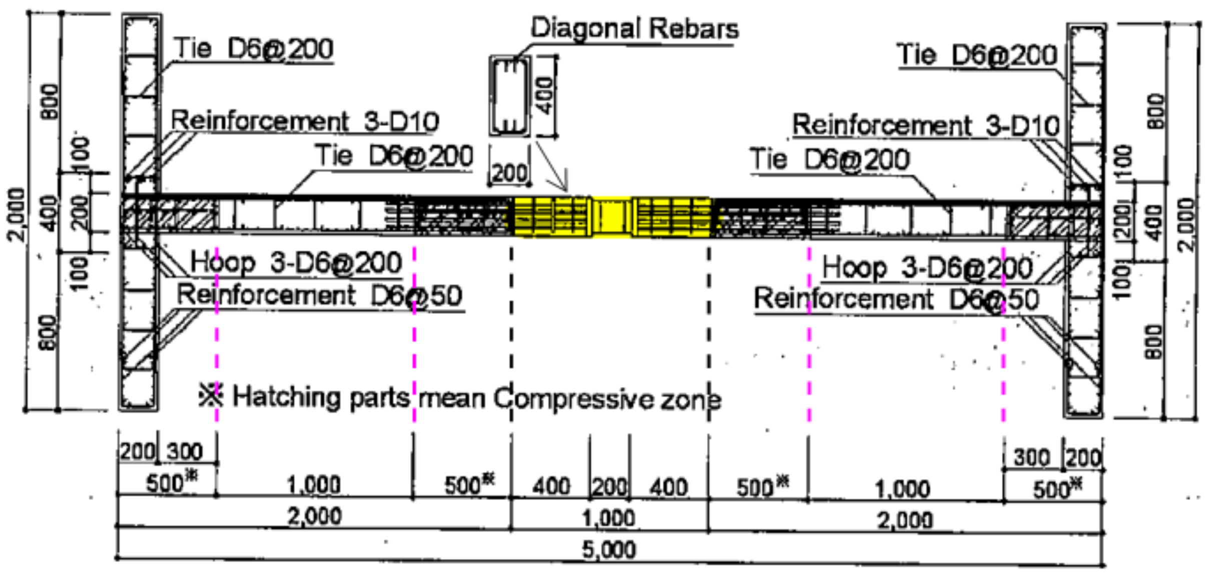

Figure 3.12: Wall Reinforcement (Sugaya et al., 2003)

Table 3-1: Reinforcement Arrangement of the Confined Wall Regions

Floor Level	**Length of Confined Zone**	**Main Rebar**	**Hoops**
10^{th} - 12^{th}	300 mm	14 – D13	D6 @ 50 mm
7^{th} - 9^{th}	400 mm	17 – D13	D6 @ 50 mm
4^{th} - 6^{th}	500 mm	20 – D13	D6 @ 50 mm
1^{st} - 3^{rd}	500 mm	20 – D13	D6 @ 40 mm

The material properties of the system vary by floor and reinforcement bar type. The reinforcement yield stress, f_y, ranges from 316 to 357 MPa, and the average Young's modulus,

E_s, for the steel reinforcement is about 177,504 MPa. The concrete compressive strength (f'_c) is highest at the first story and decreases up the building height depending on the concrete age at the time of the cylinder tests. Table 3.2 summarizes the steel and concrete material properties.

Table 3-2: Material Properties

Steel Reinforcement					**Concrete**		
Rebar	**f_y (ksi)**	**E_s (ksi)**	**$F_{ultimate}$ (ksi)**	**elongation (%)**	**Floor**	**f'_c (ksi)**	**E_c (ksi)**
D6	45.9	27025	80.9	22.2	12th	3.99	2,745
D10	51.8	24891	71.3	19.7	10-11th	3.86	2,688
D13	49.6	25745	68.8	21.7	7-9th	4.07	2,845
D16	50.9	25318	72.1	18.2	4-6th	4.23	2,788
					2-3rd	5.90	3,172
					1st	5.71	3,385

The coupled T-walls were subject to axial and lateral point loads at the 4th, 7th, and 12th floor levels. Axial loads were applied as a set of four point loads on each of the north and south walls by PC strands. Lateral loads were applied by hydraulic jacks and gradually increased by ratios of 1.0, 1.97, and 3.73 respectively at the 4th, 7th, and 12th floor levels. Horizontal load was simulated by repeated loading of alternately pushing and pulling the positive and negative hydraulic jacks. The locations at which loads are applied are presented in Figure 3.13, while the displacement history of the loading is summarized in Figure 3.14. Load transducers measured the axial force in the coupled wall system and the fluctuating shear force in the coupled walls. The coupling beam shear force, axial force, axial displacement, and rotation as well as wall displacements and reinforcing bar strains were also measured. At each of the 886 load steps, many channels of data are recorded.

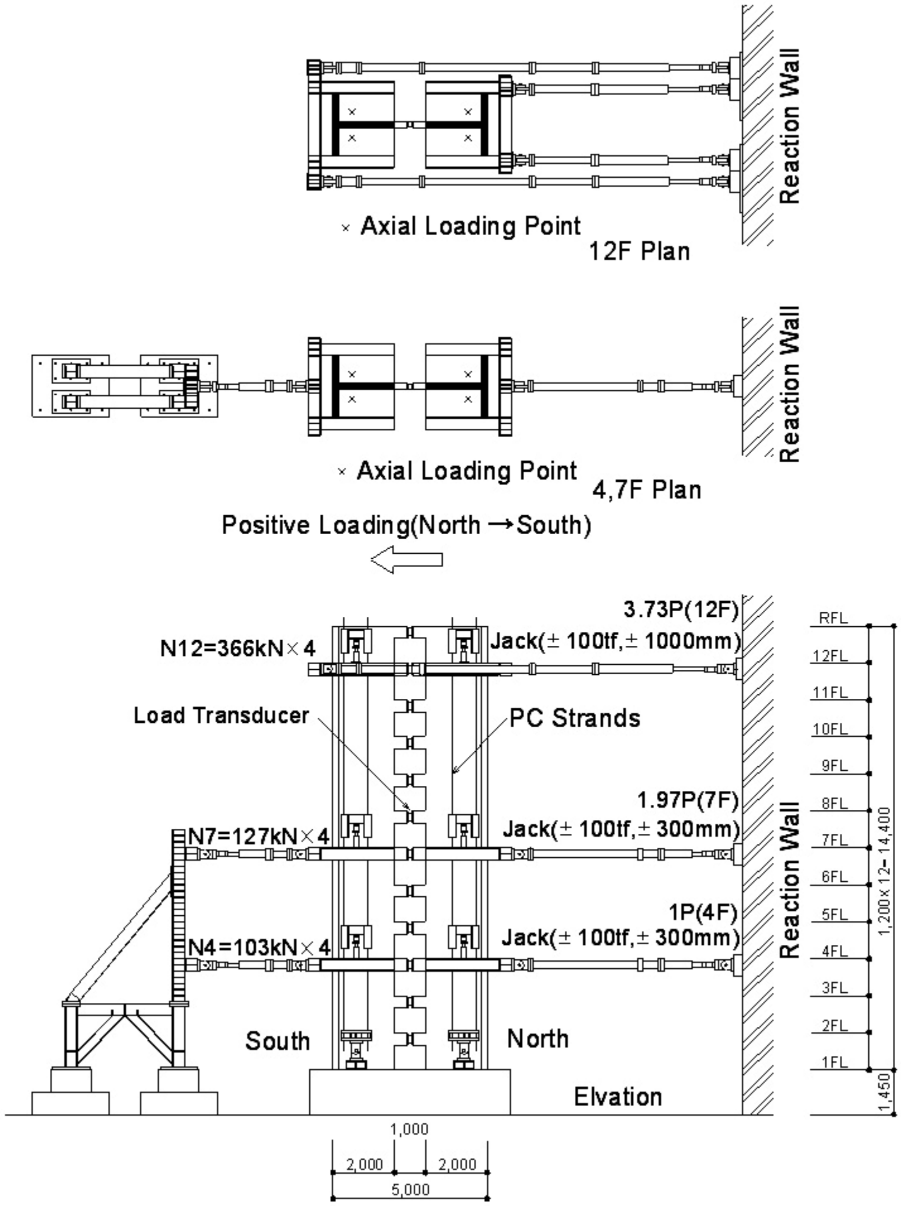

Figure 3.13: Loading of Test Specimen (Sugaya et al., 2003)

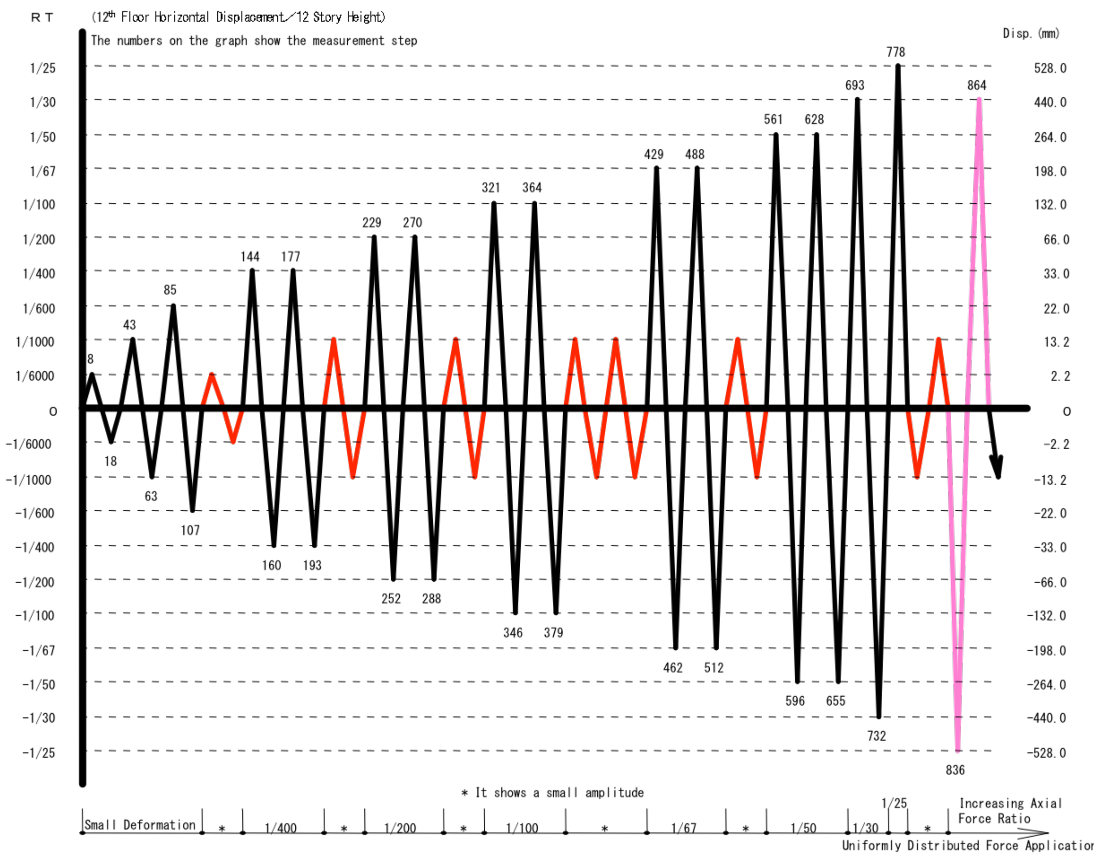

Figure 3.14: Loading History of Test Specimen (Sugaya et al., 2003)

Overall, the coupled T-shaped walls were subjected to lateral drifts of approximately 4% resulting in significant lateral strength loss (overall system failure). Buckling of the beam reinforcement and spalling of concrete occurred at lateral wall drifts of about 2%. As a result of cyclic plastic deformations, the coupling beams elongated and experienced increased compression load. The maximum base shear of 1440 kN occurred at a drift 1.5%, mostly resisted by the compression wall. Under this shear force, the coupling beams developed their maximum displacements. Beyond this point, excessive shear deterioration made the two wall piers behave as individual walls with nearly identical shear resistance. At 4% lateral drift, the compression toe of the tension wall had crushed.

Bending cracks were first observed for the coupling beams at the building drift of 0.02%, while cracks were first observed at the compression wall web and then at tension wall flange at 0.1% drift. Following those cracks, yielding at the main rebar of coupling beams began. Upon reaching a drift of 0.167%, the main rebar of the upper level coupling beams (roof to 5th floor) yielded. At 0.5% drift, yielding of the main rebar of the coupling beams was observed as well as for the main rebar at the tension ends of the compression wall. Upon reaching 1.0% drift, buckling of the main rebar occurred at the roof to 8th floor level coupling beams. At 1.5% drift buckling of the main rebar occurred along the 3rd to roof levels. Yielding of the longitudinal bars was observed for both the compression and tension walls. The maximum shear force reached was 1440 kN in the positive direction and 1370 kN in the negative direction. At 3.3% drift, the main rebar of the 2nd floor beam buckled, the main rebar of roof to 5th floor beams fractured, and concrete crushing occurred at the wall base (Sugaya et al, 2003).

While the coupled wall specimen was in the elastic range at low drifts, the shear force resistance of the two wall piers was equal at each level. As the deformation progressed, the shear force ratio of the compression wall to the tension wall increased at the 1st and 2nd stories up to the maximum ratio of 9:1 at the relative drift of 1.5% (Sugaya et al, 2003). The difference of shear force transfer between the compression and tension walls was more pronounced at the lower stories suggesting that the coupling beam axial force is larger at the lower levels versus the upper levels.

This fluctuation in shear force between the tension and compression wall piers is due to wall slip effects. When the flange of the T-shaped wall experiences compression, bending cracks develop at the web end of the wall pier; once the load reverses, the web end of the wall undergoes compression and the cracks close. Since the rebar at the wall web end cannot adequately carry the demand, the wall shear force moves to the stiffer compression wall.

The total sum of the axial forces of the 2nd floor to roof level coupling beams (recorded as 622 kN) was linked to the compression force at the lower stories (Sugaya et al, 2003). By examining the axial force vs. displacement relations of the coupling beams, it is evident that as the beam axial displacement increases, the beam compressive axial force increases. The fluctuation of the axial force at the same axial displacement represents a wedge action effect as the expansion of the coupling beams gradually increases with axial force. Moreover, from the relation between rotation drift angle and total axial force in the coupling beams, the residual axial force including the effect of slip is determined to be about 420 kN. From measuring the coupling beam axial force, the total value of the wall slip and residual axial force effects are approximated to be 263kN + 127 kN = 390 kN (Sugaya et al, 2003).

3.2.1.2 Model development

The experimental verification and development of a nonlinear OpenSees model of the twelve-story coupled T-walls test is presented herein. This study focuses on the response of the system in the direction of the main walls and coupling beams (in-plane, out-of-plane deformations are restrained). The modeling approaches implemented for different components, such as fiber wall elements and coupling beam hinge parameters, are described. Analytical results are compared to the recorded experimental results, such as base shear versus 12th floor displacement as well as wall and coupling beam forces.

All structural elements and material properties of the test specimen are modeled as described in section 3.1, and the nonlinear model is subject to the loading sequence of the test. The model mass and wall gravity loads (including member self-weights) have been specified at each floor level. From member self-weights, each floor has a typical weight of 10.1 kips plus the additional weights of 92.62 kips, 114.2 kips, and 329.12 kips applied at the 4th, 7th, and 12th floor respectively. No slab elements are modeled since the experiment did not include floor slabs, however equal degree of horizontal displacement is maintained at the nodes for the left and right wall piers. The boundary conditions of the test are represented through the base being fixed in translation and rotation. Geometric nonlinearity and P-delta effects are incorporated in the model. Rayleigh damping with an effective damping ratio of 2 percent has been assumed.

The wall piers have been modeled as fiber elements with defined material force-deformation relations. Each wall pier measuring 78.74 inches is discretized into twenty equal fibers measuring 3.937 inches in width. The shear wall properties are summarized in Table 3-3. Shear behavior has been modeled using an elastic shear modulus of 0.5G where $G = E/(2(1\text{-}v))$.

Table 3-3: Properties of the Shear Wall Elements in the Model

Level	t_w (in.)	B.E. length (in.)	$\rho_{v,BE}$ (%)	$\rho_{v,web}$ (%)	$\rho_{horiz.}$ (%)
1st	7.87	19.69	2.655	0.639	0.16
2-3rd	7.87	19.69	2.655	0.639	0.16
4-6th	7.87	19.69	2.655	0.639	0.16
7-9th	7.87	15.75	2.821	0.639	0.16
10-11th	7.87	11.81	3.097	0.639	0.16
12th	7.87	11.81	3.097	0.639	0.16

The steel reinforcement component properties were defined for each of the four rebar types (D6, D10, D13, D16 bars) using the OpenSees *SteelMPF* model. The concrete material properties were based on the material tests performed on concrete cylinders prior to the test with unconfined and confined concrete stress-strain relationships modeled as described in section 3.1.2. Concrete tensile strength was estimated as $3.7\sqrt{f_c'}$. The tri-linear concrete stress-strain relationships of the unconfined and confined concrete materials are summarized in Table 3-4.

Table 3-4: Stress-Strain Relationships defined in the Concrete Material Properties

	Unconfined Concrete			Confined Concrete			
Level	ε @ f_{max}	$f_{max}=f'_c$ (ksi)	ε_u	ε @ f_{max}	f_{max} (ksi)	ε_u	f_r (ksi)
1st	0.002	5.708	0.012	0.004	7.07	0.045	1.41
2-3rd	0.002	5.897	0.012	0.004	7.26	0.045	1.45
4-6th	0.002	4.229	0.012	0.005	5.36	0.038	1.07
7-9th	0.002	4.071	0.012	0.005	5.20	0.046	1.04
10-11th	0.002	3.863	0.012	0.005	5.00	0.059	1.00
12th	0.002	3.993	0.012	0.005	5.13	0.058	1.03

The coupling beams were modeled using an elastic beam section with concentrated inelastic shear-hinges at the center of each coupling beam as described in section 3.1.3. The elastic beam section was modeled as 7.87 inches (200 mm) wide by 15.75 inches (400 mm) deep with defined elastic modulus and shear modulus. The effective flexural stiffness was reduced to $0.175E_cI_g$ following the relation $0.07(l_n/h)$ using the beam aspect ratio l_n/h of 2.5. The beam shear strength (FY) was computed based on the ACI 318 equation for capacity of diagonal reinforcement as described in section 2.2.1. The coupling beam properties used in the model are summarized in Table 3-5.

Table 3-5: Coupling Beam Properties

Level	Dimensions	l_n (in.)	l_n/h	k = E_cI_{eff}/E_cI_g	A_{vd}	α	FY (kips)	FU=1.1*FY (kips)
2nd-7th	7.87"x15.75"	39.37	2.5	0.175	2-D16	18.9°	20.55	22.61
8th-Roof	7.87"x15.75"	39.37	2.5	0.175	2-D13	19.0°	13.29	14.62

Three different approaches were considered for modeling the shear hinge parameters of the BRI coupling beam specimen, and each set of backbone parameters was compared to experimental results as shown in Figure 3.15. At first, the modeling parameters for diagonally reinforced coupling beams from ASCE 41-17 Table 10-19 were considered given that the recommended plastic hinge rotations at strength loss (***a***) and at failure (***b***) are 0.030 and 0.050, respectively, while the recommended residual strength ratio is (***c***) is 0.8; however, the ASCE 41-17 backbone parameters underestimate the deformation at strength loss (dashed black line in Figure 3.15). Next, the hysteretic coupling beam behavior from specimen CB24F (without a slab) tested by Naish (2010) as presented in Figure 3.8 was assessed to model the beam shear hinge properties; however, the specimen tested by Naish have higher diagonal and transverse reinforcement ratios with improved confinement compared to the BRI coupling beam specimen, and therefore the backbone behavior (dotted purple line in Figure 3.15) is not as representative of the BRI specimen. Based on a review of a database of 56 diagonally reinforced concrete specimen tested between 1972 to present, there are limited tests of lighter reinforced diagonally reinforced coupling beam specimen that are comparable to the 1996 BRI beam test specimen, namely specimen CB-2 (Zhou et al., 2003) and a pair of individual coupling beams (specimen BMB and BLB) that were tested at the BRI facility just prior to the 12-story Coupled T-Walls test in order to verify the behavior of the center load cell placed in the midspan of the coupling beams (Sugaya et al., 2003). Overall (as shown in Figure 3.15) it is most appropriate to use the backbone relations measured during the BRI isolated coupling beam test of specimen BMB as the basis to model the shear hinge properties of the 12-story test coupling beams.

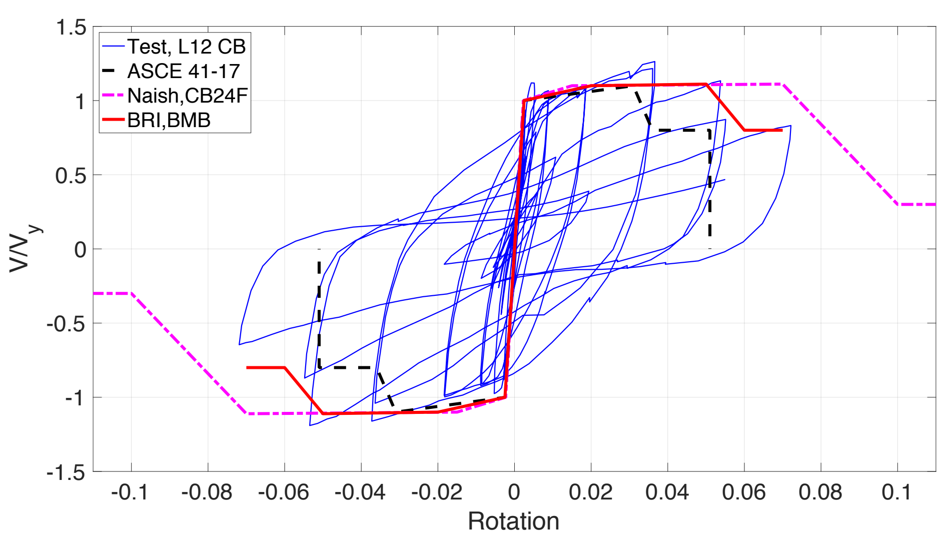

Figure 3.15: Coupling beam modeling parameters

The coupled wall system model is subject to applied gravity loads followed by a series of nonlinear static pushover analyses. The sequences of lateral pushover load cases were set up to simulate the displacement history that the walls were subjected to during the actual test. The lateral load pattern consisted of nodal loads that incrementally increase in the positive and negative directions at the 12th, 7th, and 4th levels in ratios of 1, 1.97, and 3.73 respectively. After application of gravity forces, static or cyclic pushover analyses were run in sequence to match the test loading history.

3.2.1.3 Model validation results

Comparisons between experimental and analytical results for the 12-story coupled T-walls specimen are presented considering global base shear versus 12th floor drift (Figure 3.16 and Figure 3.17) and local coupling beam force deformation response (Figure 3.17). It is observed from Figure 3.15 that the model initial stiffness matches well with the test thus verifying the accuracy of the input parameters.

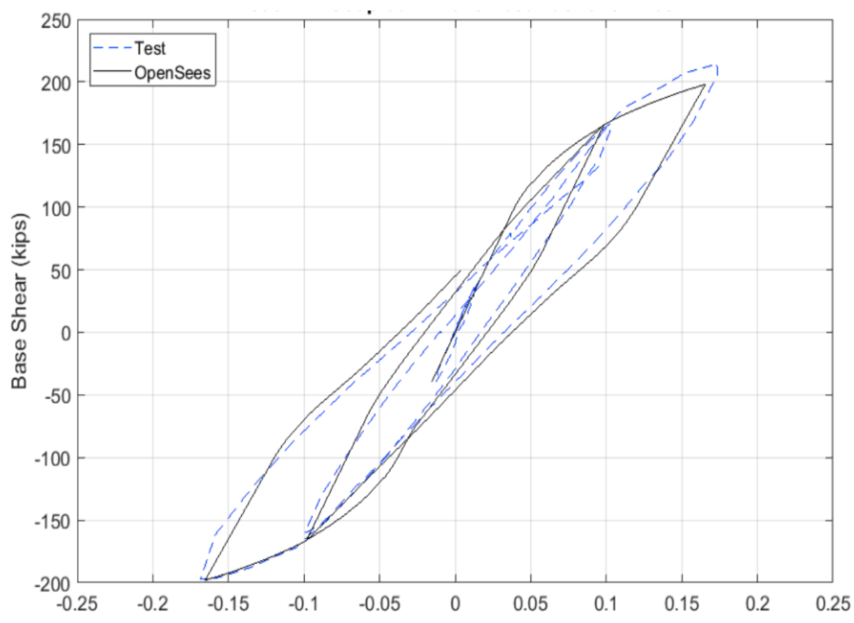

Figure 3.16: BRI Coupled Walls Test - Initial Pushover Results

The model's predicted overall pushover response reasonably matches the global response from the experiment (see Figure 3.17) except that the hysteretic pinching behavior can be improved. In order for the model to appropriately capture the coupling beam force-deformation response (see Figure 3.18), the shear strength (FY) should include the strength due to the capacity of the diagonal bars (i.e., $FY = 2A_{vd}f_y\sin\alpha$) as well as the strength from the developed longitudinal bars; the shear strength (*FY*) is computed as the shear corresponding to the coupling beam moment strength (M_n) from moment-curvature analysis, i.e., $FY = 2M_n/l_n$. The coupling beam response as illustrated in Figure 3.18 reasonably matches test results up to the point of strength loss, however the model overestimates the coupling beam deformations after strength loss due to the hysteretic properties of the OpenSees *Pinching4* material model.

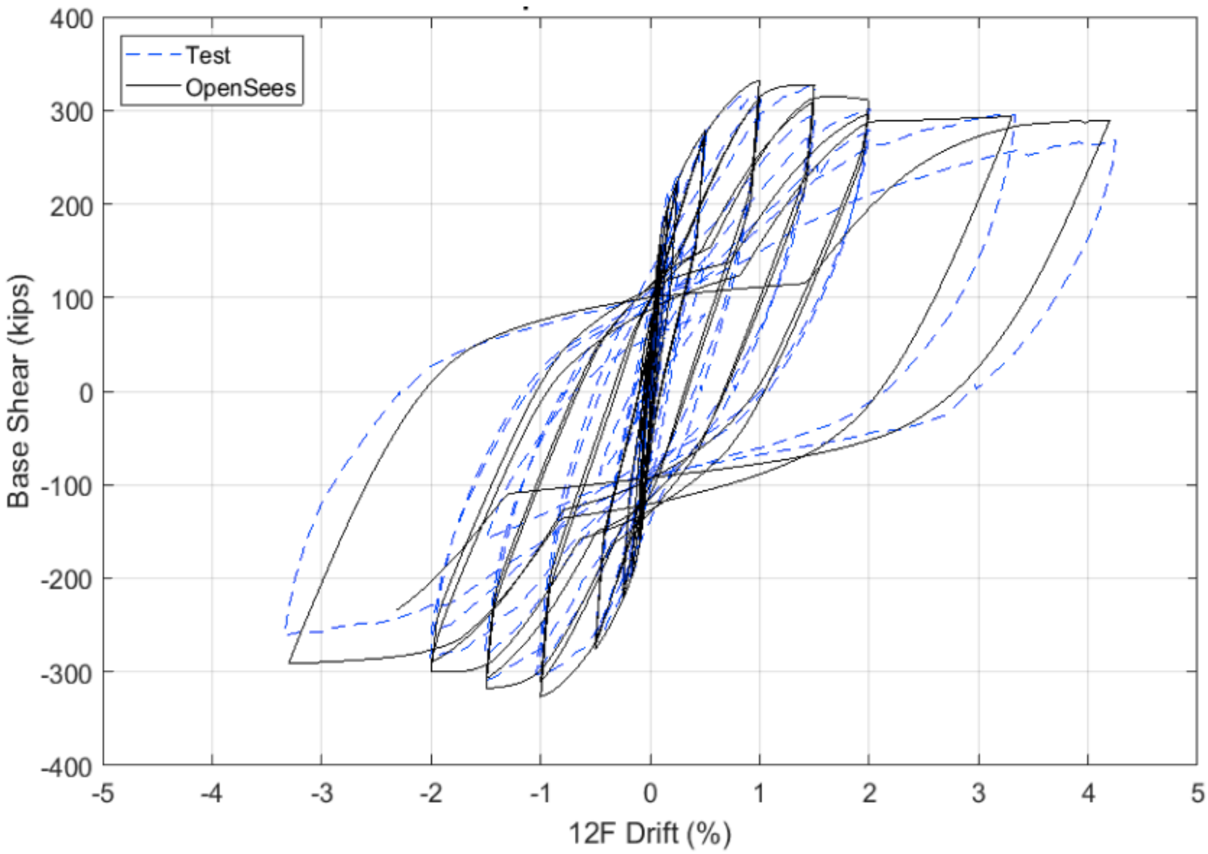

Figure 3.17: BRI Coupled Walls Test - Experimental vs. Analytical Pushover Results

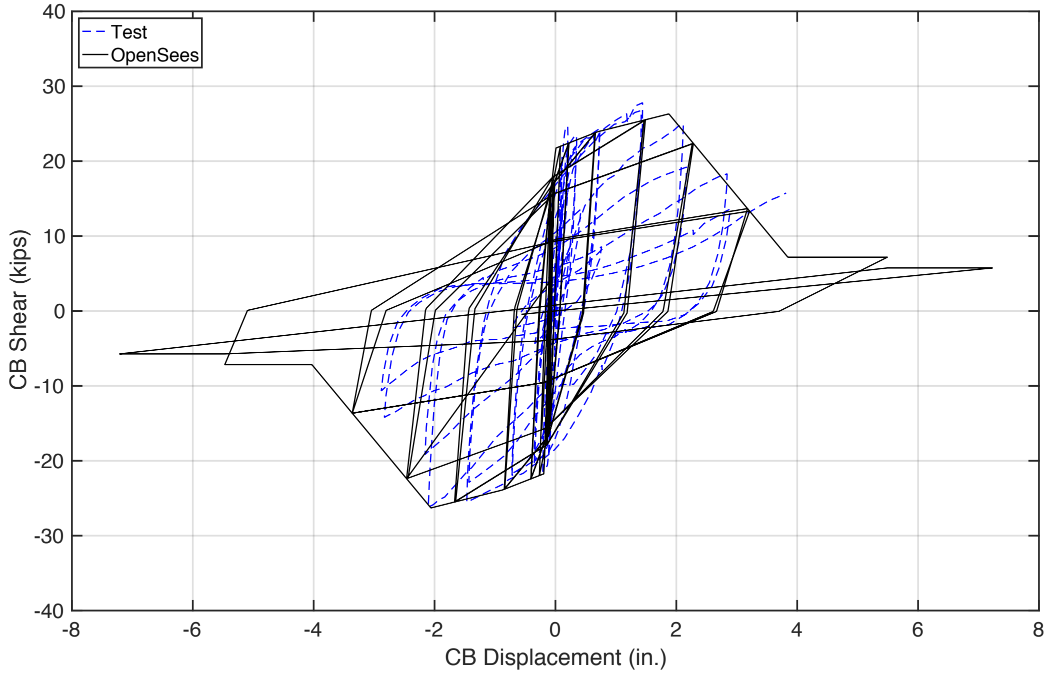

a) 5th Floor Coupling Beam Load-Deformation

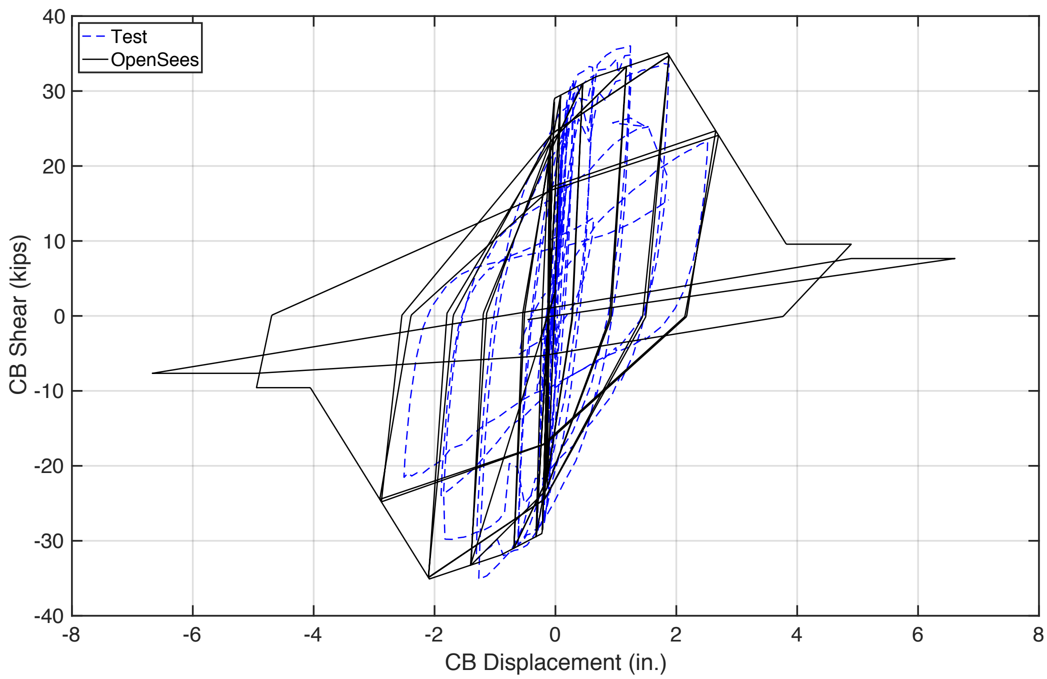

b) 12th Floor Coupling Beam Load-Deformation

Figure 3.18: BRI Coupled Walls Test - Experimental vs. Analytical Coupling Beam Results

3.2.2 Model Validation – 1974 Test by Santhakumar

This section summarizes a study done by Kolozvari et al. (2018) that validates the OpenSees model with shear-flexure interaction effects (SFI-MVLEM) described in section 3.1. The validation study uses data from the ¼ scale 7-story RC coupled wall specimen with diagonally reinforced coupling beams tested by Paulay and Santhakumar at the University of Canterbury (Santhakumar, 1974).

3.2.2.1 Description of the test specimen

The test specimen consisted of wall piers with an overall height to length ratio of 9.0 and measuring 610 mm (24 in.) long and 102 mm (4 in.) thick as shown in Figure 3.19a. The concrete compressive strength was 30 MPa (4.4 ksi), and the yield strength of reinforcement was 304.7 MPa (44.2 ksi) for the wall boundary vertical reinforcement and 343.4 MPa (49.8 ksi) for the wall web reinforcement. The wall piers were connected by 381 mm (15 in.) long coupling beams with an aspect ratio l_n/h of 1.25 and measured 76.2 mm (3 in.) wide by 304.8 mm (12 in.) deep. The beam diagonal reinforcement consisted of two D10 bars with reinforcement yield strength of 314.7 MPa (45.6 ksi). Details of the test and the behavior of the specimen are provided in the referenced dissertation by Santhakumar.

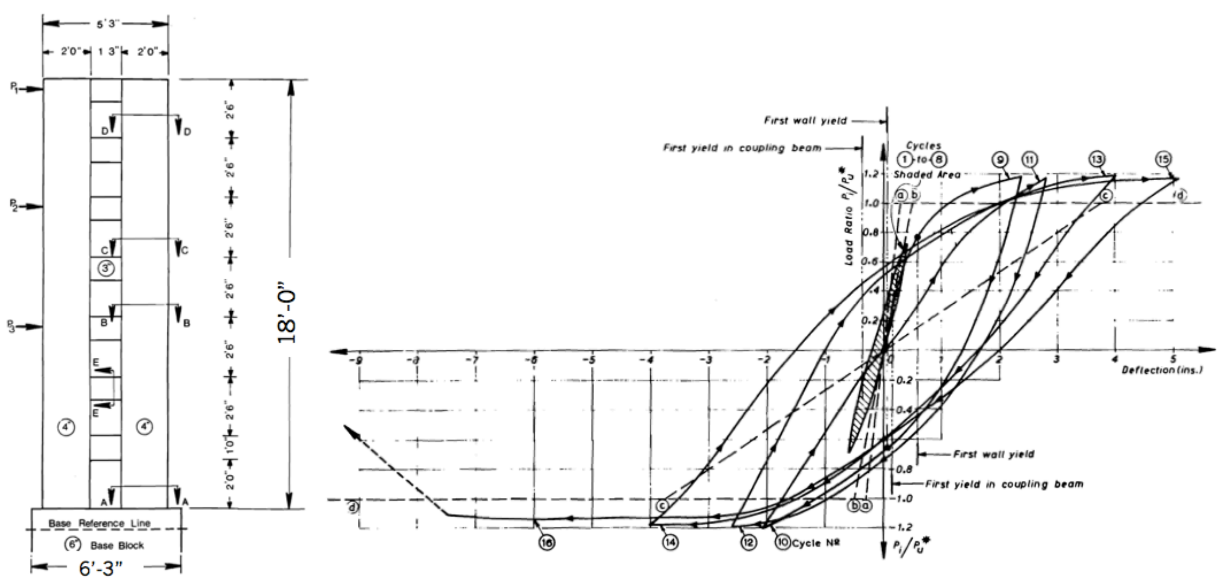

a) Elevation view b) Specimen behavior

Figure 3.19: Seven-Story Coupled Wall Test (Santhakumar,1974)

The specimen was subjected to reversed cyclic loading in the horizontal direction and tested under a constant axial load of about 6 percent of the pier axial load carrying capacity (***$A_g f'_c$***).

Failure was observed at a drift of about 3.5% (cycle 16) as presented in the global load-deformation response in Figure 3.19b with the compression wall (left pier) buckling out of plane due to an initial imperfection in the wall caused by a misalignment in the concrete formwork. The diagonally reinforced coupling beams endured large deformation demands and maintained adequate strength, stiffness, and energy dissipation while limited damage consisted of minor spalling and diagonal cracking; the coupling beams did not suffer from shear sliding or pinching behavior in the hysteresis loops.

3.2.2.2 Model validation results

Comparisons of experimental and analytical responses presented in Figure 3.20 confirm that the model can reasonably capture the global base shear vs. top displacement behavior as well as the coupling beam rotations and wall curvatures. Overall, model results match the wall strength and stiffness very well as shown in Figure 3.20a, except that the model overestimates the system unloading stiffness resulting in modestly larger area of hysteretic loops. The predicted coupling beam rotations illustrated in Figure 3.20b reasonably match the experimental measurements at the three considered drift levels with analytical results only overestimating the measured response by less than about 10 to 20%. Wall curvature predictions presented in Figure 3.20c for the three drift levels over the wall height and within the plastic hinge region also agree well with experimental results except at the drift level of 2.3% where the model spread of plasticity is not well captured. The model's predicted diagonal cracking patterns also reasonably match the distribution and orientation of experimentally observed diagonal cracks which suggest shear-dominant behavior of the wall piers.

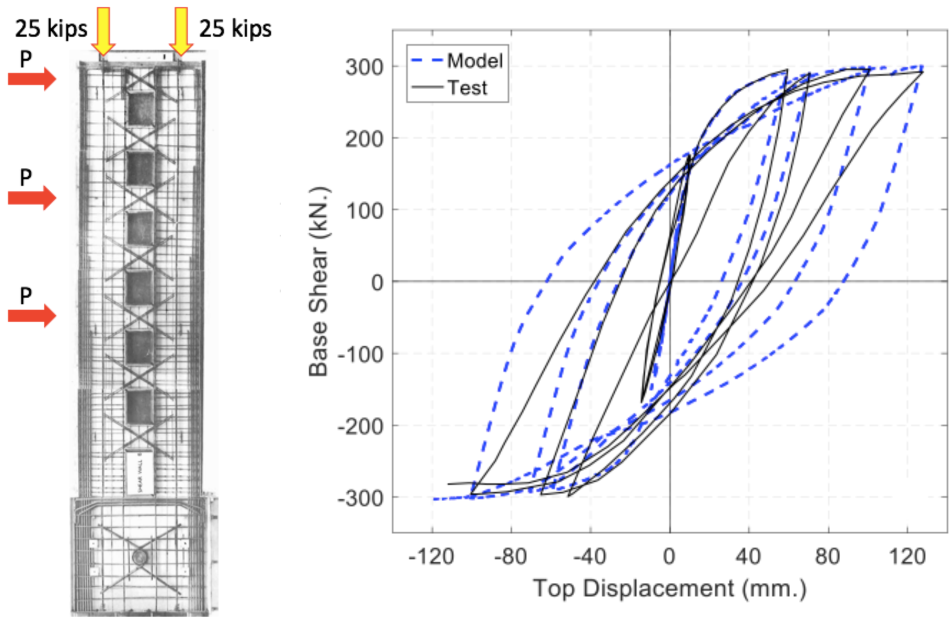

a) base shear vs. top displacement

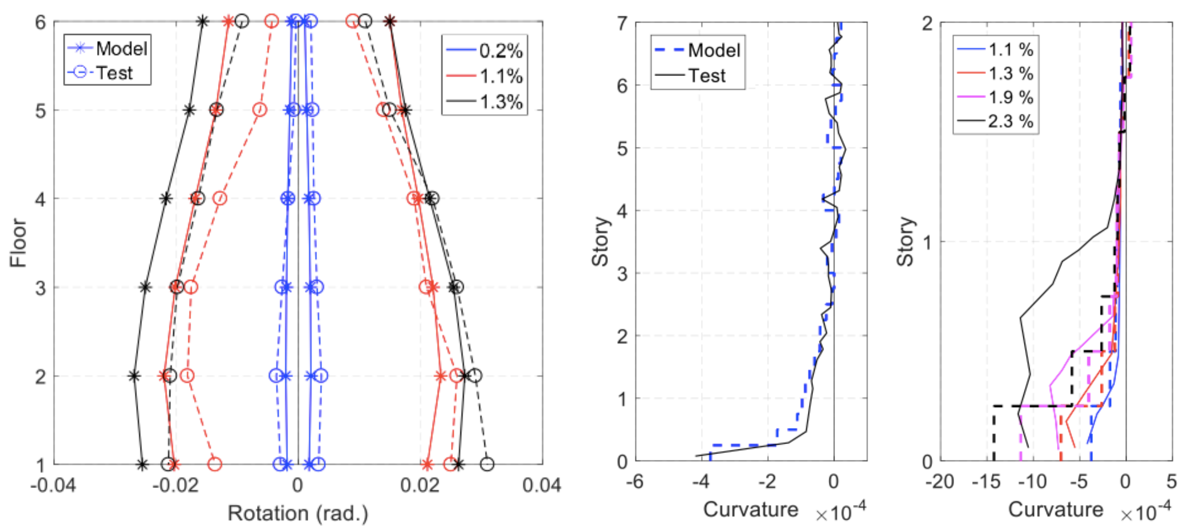

b) coupling beam rotations c) wall curvature

Figure 3.20: Model validation using Santhakumar test specimen (Kolozvari et al., 2018): a) base shear vs. top displacement, b) coupling beam rotations, c) wall curvature

3.3 Summary of nonlinear modeling approach

The modeling approach used for the overall building system was described. A two-dimensional modeling approach of the lateral system was adopted. Approaches used to consider damping and $P\text{-}\Delta$ effects were described.

A simple modeling approach based on using a linear beam element and a nonlinear shear spring was adopted to model the diagonally- and conventionally-reinforced coupling beams. The impact of floor slabs and axial stress due to post-tensioning reinforcement on coupling beam strength was considered in the beam shear strength and hysteretic behavior. The modeling approach adopted for coupling beams was validated by showing that the modeling approach very reasonably captured tests results reported in the literature.

Wall sections were modeled using fiber elements with uniaxial material relations for unconfined and confined concrete, and longitudinal reinforcement. The OpenSees *Concrete02* model was used for concrete because of the desire to use a computationally efficient model due to the large number of analyses needed for the FEMA P695 study. The OpenSees *SteelMPF* model was used to simulate the behavior of steel reinforcement. Shear response was simulated using a linear elastic hinge with an effective stiffness of $0.5G$.

The modeling approach was validated using a 12-story test of a coupled wall conducted at the Building Research Institute in Japan and using a specimen tested by Santhakumar. The comparison in model and test results indicated both the wall and coupling beam modeling approaches reasonably capture the reported test results.

Chapter 4 - Failure Modes

4.1 Description of failure modes

Three main failure modes are considered and assessed through post-processing of results (non-simulated), i.e., 1) flexural, 2) shear, and 3) axial failure. Details of the failure modes are presented in the following subsections. The governing failure mode is determined for each Archetype subjected to ground acceleration response histories as the failure mode that occurs first. Using the failure analysis results, the median collapse intensity is determined using the ground motion scaling factor that results in just more than half of the 44 records described in Chapter 5 reaching failure.

4.1.1 Flexural failure via Drift Capacity Model

Flexural failure is defined using the drift (rotation) capacity model proposed by Abdullah and Wallace (2019). This new approach was developed using recent research findings by studying a large database of over 1000 concrete wall tests that have either failed due to concrete crushing, bar buckling and/or fracture, or lateral instability of the flexural compression zone at the wall boundary. The database includes detailed information such as wall cross-section, material properties, configuration of transverse reinforcement, and backbone relations from experimental results. The backbone information from tests is used to assess trends for the total displacement or rotation at which strength degrades 20% from the peak strength. An expression is derived for wall lateral drift capacity at significant strength loss by studying the impact of design parameters from a comprehensive filtered database with a low coefficient of variation (COV = 0.15) that includes 164 tests of well-detailed walls (depicted in

Figure 4.1) that generally satisfy the requirements of ACI 318-14 for special structural walls. The drift capacity model is then used to derive plastic hinge total rotation and total curvature models, with plastic hinge length defined in the tests as $l_w/2$, as these models are generally more appropriate to use for nonlinear models of taller buildings. The assumed plastic hinge length of $l_w/2$ is a reasonable estimate for structural walls (Wallace and Moehle, 2012; Segura and Wallace, 2018).

The drift capacity model presented in Figure 4.2 is a function of the wall length, width of compression zone (wall thickness), neutral axis depth, and shear stress. For a given Archetype, this model employs the analysis results to track the wall neutral axis depth and shear stress in order to define a drift or rotation/curvature capacity at which a significant drop in strength occurs. The wall elements in the OpenSees models are discretized using two elements per story to match closely with the assumed plastic hinge length of $l_W/2$ to be consistent with concrete material regularization as well as with the total wall curvature model at strength loss.

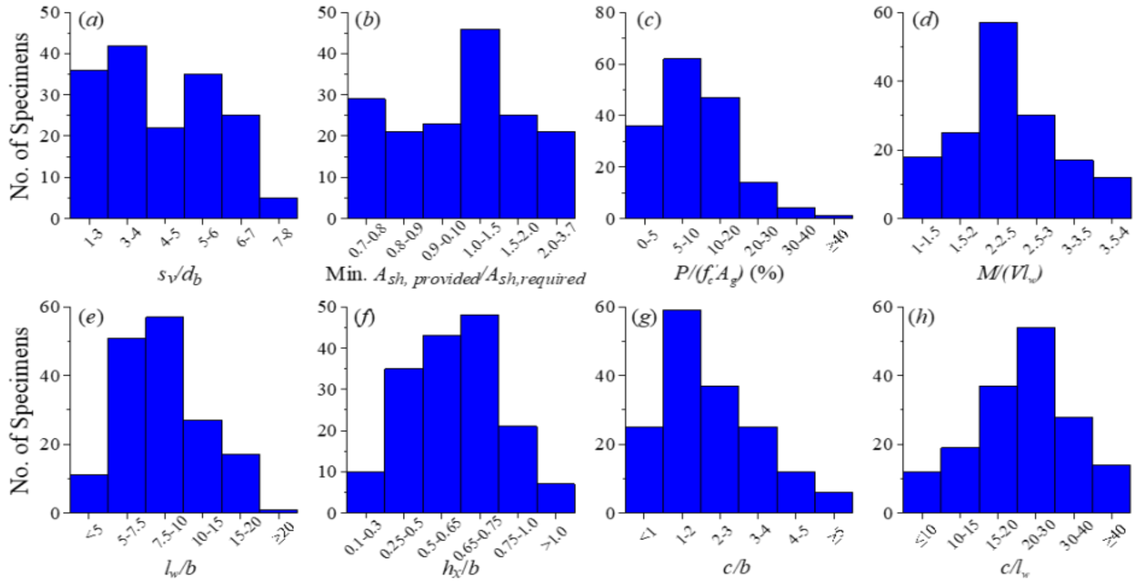

Figure 4.1: Histogram of 164 Tests in the Drift capacity model (Abdullah and Wallace, 2019)
(Note: Units are in mm; 1mm= 0.0394 in.)

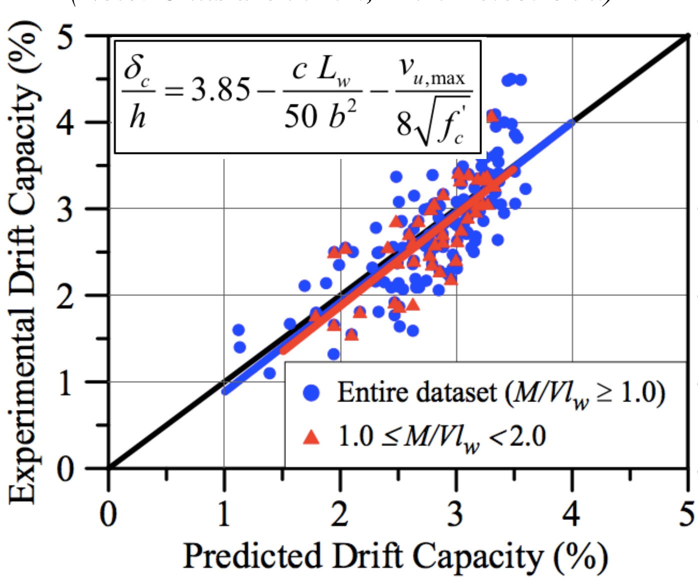

Figure 4.2: Drift capacity model

In prior studies (NIST, 2010), axial collapse has been defined to occur at a roof drift of 5 percent based on limited studies of axial collapse (Wallace et al, 2008) and judgement. Therefore, using the drift (or curvature) capacity model as a failure criterion is a conservative approach since it is a model that predicts the onset of strength loss and not necessarily collapse.

Use of this approach is computationally efficient and acceptable if the objectives of the study are satisfied; otherwise, a more comprehensive definition of collapse is required, as discussed in Section 4.1.3.

4.1.2 Shear Failure

Evaluation of shear failure is done using the first approach, and sensitivity studies are done (see Section 6.4) using the second approach to compare results. For the MVLEM with uncoupled shear response (linear shear stiffness), shear failure is defined using the model in the LATBSDC guide Appendix A (2017) presented in Figure 4.3a, which is derived from experimental data obtained from walls that experienced shear and flexure-shear failure. This model relates wall axial strains (or curvature) with the shear force capacity in the wall. Wall axial tensile strains at the boundary and shear force demands obtained from the dynamic analysis of building Archetypes are processed and compared to the failure envelope proposed by the model. Failure is reached when the shear demand for a given curvature demand from the analysis exceeds the envelope line as illustrated in Figure 4.3b for a sample wall pier of the 12-story Archetype 12H-DR-3.0 .

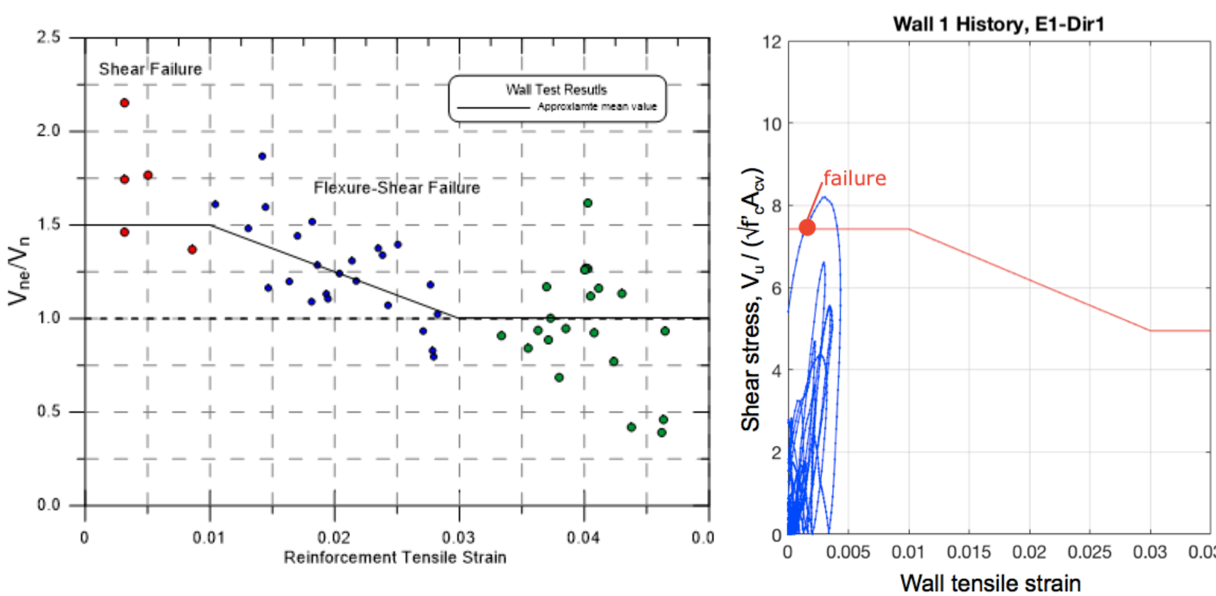

a) Shear failure model (LATBSDC, 2017) b) Illustration of reaching failure envelope

Figure 4.3: Modeling of shear failure with “uncoupled” wall models

4.1.3 Axial Failure

Wall axial failure is defined using the lateral drift capacity model proposed by Wallace et al. (2008) which defines the lateral drift capacity at axial failure using an assumed critical shear crack angle and a shear friction model as shown in Figure 4.4. The initial model for the limit state of axial collapse is based on the column model proposed by Elwood and Moehle (2003, 2005), and modified for application to walls (Wallace et al., 2008). The model is based on equilibrium for an assumed shear friction relation, assuming the critical crack plane extends along the main diagonal of the wall pier (or over a single story). Axial failure results along the critical crack plane when the shear demand exceeds the shear friction capacity.

The relationship between predicted drift ratio corresponding to axial failure and axial stress ratios are plotted in Figure 4.4b for typical geometry, materials, and reinforcement, and compared with several pier tests (Wallace et al., 2008) having axial load ratios of 5% and 10%. The blue dashed lines (two relations on the right) represent the potential variation in the predicted lateral drift at axial load failure based on the assumed shear friction relations. The red broken line (furthest to the left) represents a modified model prediction to account for the test conditions (lack of hooks on horizontal web reinforcement). The model and test results are in reasonable agreement, including the insensitivity of the results for axial load ratio greater than ~3%, although sensitivity of the results to the assumed shear friction relation was observed. The findings to date warrant more in-depth study to assess the lateral drift capacity for walls/piers with improved details, higher axial load, and variable quantities of longitudinal reinforcement.

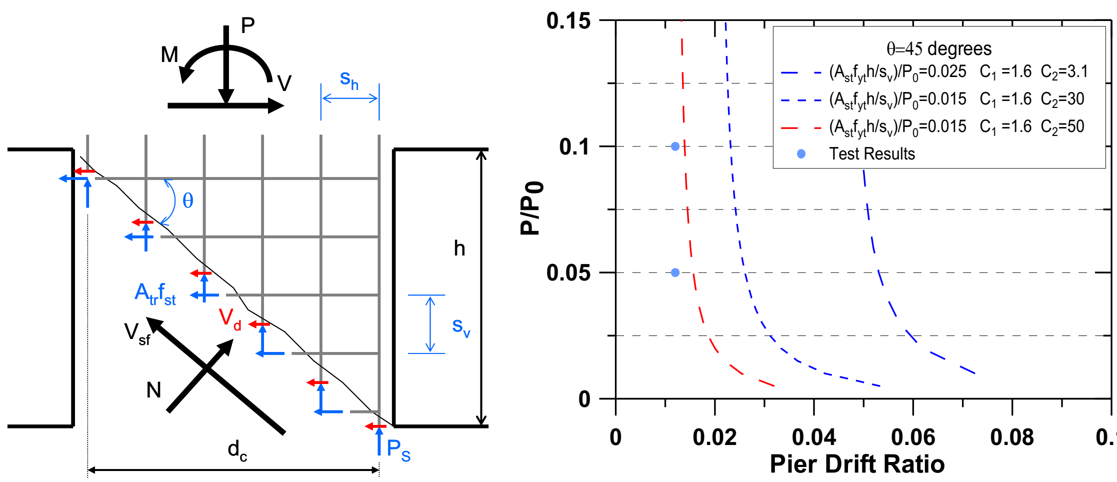

(a) Free-body diagram (b) Model and test results

Figure 4.4: Axial load capacity model for a wall pier after diagonal cracking.

As a note for future studies, the SFI-MVLEM model described in Section 3.1 can be used to gain insight on the relationship between shear and axial load to predict axial failure. As observed in tests conducted by Orakcal *et al* (2009), initiation of shear sliding along a diagonal plane typically led to (nearly) immediate loss of axial load carrying capacity; the developed SFI-MVLEM provides an ideal framework to couple sliding and axial failure without the need to develop a shear friction versus drift relation (e.g., loss of axial load could be related to the magnitude of sliding obtained, a parameter that is already tracked in the existing implementation).

The model developed by Wallace *et al.* (2008) is implemented and validated against recent test data (e.g., Tran and Wallace, 2012; including three additional tests that have been completed) to assess an appropriate shear friction relation, and ultimately assess model capabilities over a broad range of test conditions. This model has been validated by computing the axial failure drift for tests conducted by Tran and Wallace (Figure 4.5) that were pushed to 3% drift. Results show that axial failure was neither experienced nor predicted by the model.

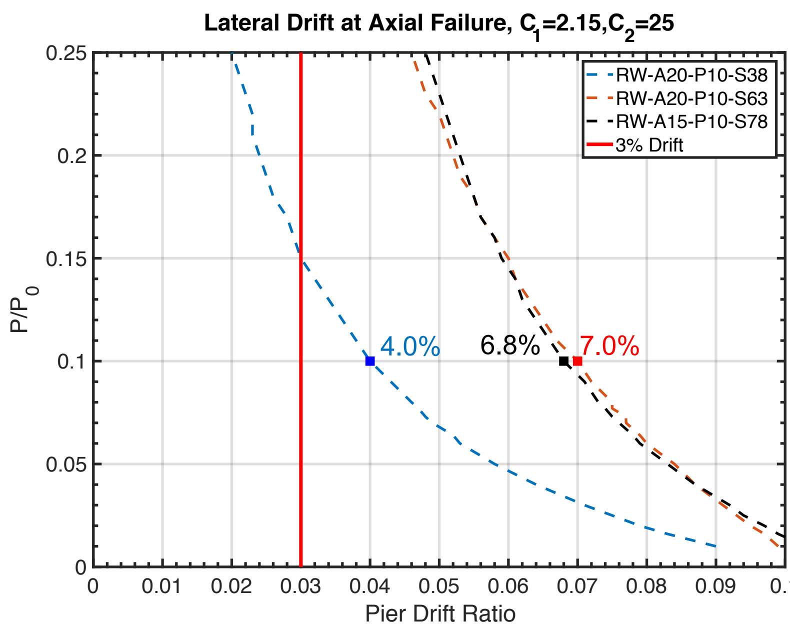

Figure 4.5: Validation of the axial failure prediction model (specimen by Tran, 2012)

The drift at which axial failure is predicted is computed for several of the Archetypes, namely the 8-, 12-, 18-, 24-, and 30- story Archetypes with coupling beam aspect ratio $l_n/h = 3.0$. However, as shown by the high predicted roof drifts (around 5.0%) in Figure 4.6, neither of the Archetypes are prone to experience axial failure since the computed axial failure drifts are not low enough for axial failure to govern.

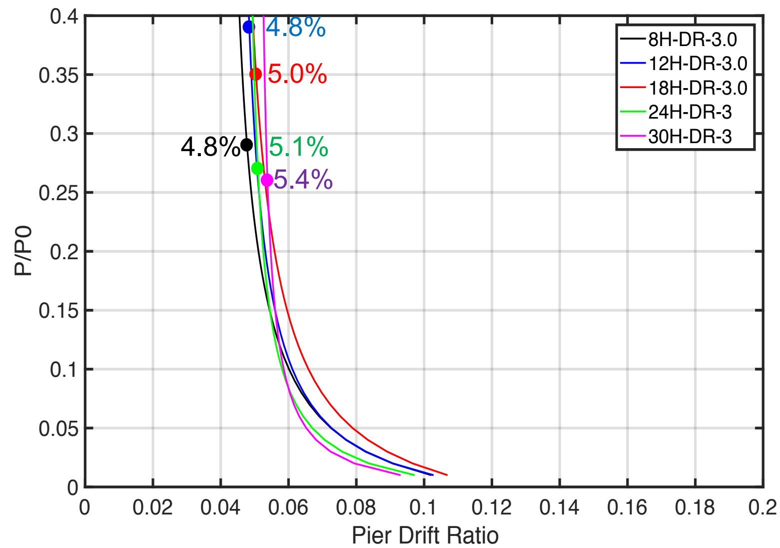

Figure 4.6: Drift at Axial Failure for a Subset of Archetypes

It is important to note that during incremental dynamic analyses of the Archetype buildings, either the flexural failure model or the shear failure model described in the previous sections always resulted to be the governing failure mode before axial failure occurring at a higher drift would be predicted. Moreover, although the axial failure model has been calibrated using a few test specimen, there are very limited experiments of RC walls that have been tested to collapse, and not many shake-table tests are available to better validate the model. Therefore, the axial failure model was not employed in the collapse assessment procedure used in this study.

4.2 Assessment of Failure Modes

The governing failure mode is determined for each Archetype subjected to ground acceleration response histories as the failure mode that occurs first. Using the failure analysis results, the median collapse intensity is determined using the ground motion scaling factor that results in just more than half of the records reaching a failure flag.

A sample failure mode assessment is presented in Figure 4.7 using the IDA results of the 12H-DR-3.0 Archetype for one ground motion record. In this example, flexural failure is predicted at a time step of 3775 and roof drift of 2.85% by tracking when the roof drift response history first reaches the failure envelope computed using the drift capacity model which fluctuates as a function of the neutral axis depth and shear demand of the outermost compressive fiber of the bottom wall element; however, there is no shear failure predicted as the history of shear response at the base of the wall piers does not reach the shear failure envelope. Moreover, axial failure is not predicted at these drift levels and is typically not the governing failure mode for any of the Archetypes.

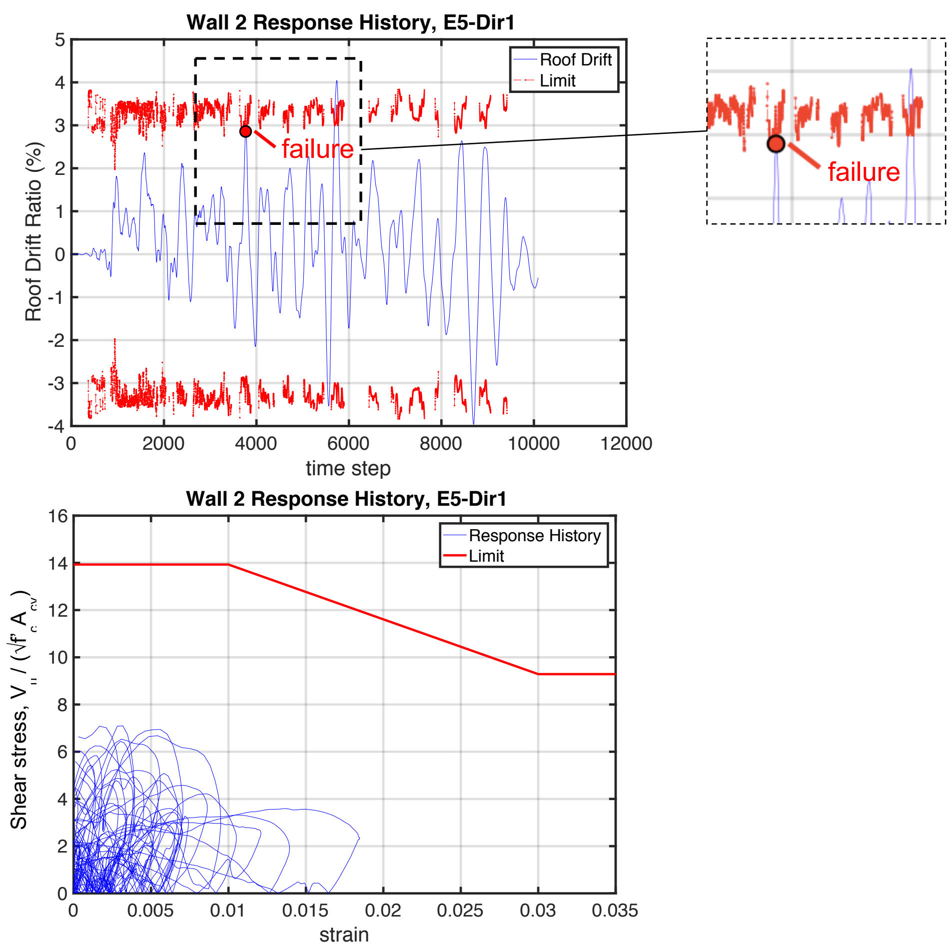

Figure 4.7: Assessment of Failure Modes for Archetype 12H-DR-3.0

4.3 Summary

Criteria to define flexure, shear, and axial failures have been summarized in this section. The Conceptual relations are presented to described how each failure criterion is assessed through post-processing of analysis results. For flexure, a drift (or curvature) capacity model is used that defines strength loss as collapse. This model is adopted as a conservative approach to assess if the project objectives can be achieved. Shear failure is defined using a model where shear strength (capacity) is related to the average curvature demand over an element (plastic hinge length). As nonlinear curvature increases, shear strength degrades from $1.5V_n$ to $1.0V_n$ defined by ACI 318-19. Although an axial failure model is defined, and some model validation results are presented, results presented in Chapter 5 will be used to show that use of the axial failure model is not necessary to achieve the project objectives.

Chapter 5 - Nonlinear Structural Analyses

5.1 Analysis Procedure

Nonlinear static pushover (NSP) analyses and incremental dynamic analyses (IDA) are performed in accordance with FEMA P695 for each Archetype using the structural analysis software Open Systems for Earthquake Engineering Simulation (*OpenSees*). Gravity loads for the analyses are based on the load combination 1.05*D*+0.25*L*, where *D* and *L* are the nominal dead and live loads of the structure, respectively. Pushover analyses are used to compute the system overstrength factor ($\boldsymbol{\Omega_0}$) and the period-based ductility (μ_T), while incremental dynamic analyses are used to assess collapse by incrementally increasing the intensity of the 22 pairs of scaled far-field ground motions of FEMA P695 Appendix A until just less than half of the records reach the established failure flags.

Nonlinear static pushover analyses are conducted using a distribution of lateral forces over the building height that is directly proportional to the fundamental mode shape of the building per FEMA P695 Section 6.3. For each Archetype, the overstrength factor ($\boldsymbol{\Omega_0}$) is calculated as the ratio of the maximum base shear strength from pushover analysis (V_{max}) to the design base shear ($\boldsymbol{V_b}$). The period-based ductility (μ_T) is obtained by dividing the ultimate roof displacement ($\boldsymbol{\delta_u}$) by the effective yield displacement ($\delta_{y,eff}$). The effective yield displacement is a function of the ratio of the maximum base shear normalized by the building weight (W) as well as the design period ($T = C_u T_a$) and the fundamental period of the building using eigenvalue analysis (T_1). The ultimate roof displacement is computed at the onset of 20% strength loss as predicted by the drift capacity model described in section 4.1.1, or at the onset of shear failure, whichever occurs first. The static pushover parameters are summarized as:

$$\Omega_0 = V_{max}/V_b \tag{5-1}$$

$$\mu_T = \delta_u/\delta_{y,eff} \tag{5-2}$$

$$\delta_{y,eff} = C_0 \frac{V_{max}}{W}\left(\frac{g}{4\pi^2}\right)(max\{T, T_1\})^2 \tag{5-3}$$

where

$$C_0 = \phi_{1,r} \frac{\sum_1^N m_x \phi_{1,x}}{\sum_1^N m_x \phi_{1,x}^2} \tag{5-4}$$

Nonlinear incremental dynamic analyses (IDA) are conducted to compute the collapse capacity of the Archetypes by proportionally increasing the intensity of the 44 ground motion records until the collapse of the Archetype building is reached as represented by the model. For the analyses, the ATC-63 Far-Field ground motions are used, which includes twenty-two pairs of horizontal ground motions. These far-field ground motions are selected from the PEER NGA database from sites located greater than or equal to 10 km from fault rupture having peak ground accelerations greater than 0.2g, peak ground velocities greater than 15 cm/sec, and magnitudes greater than M6.5. The accelerations are adjusted with the normalization factors prescribed in FEMA P695 Table A-4D to remove unwanted variability between records. The 44 ground motions (22 records, each with 2 horizontal components) are summarized in Table 5-1, and their response spectra are shown in Figure 5.1. Per ATC-63, the vertical direction of earthquake shaking is not considered important for collapse evaluation and is thus neglected for IDA. For this study, each of the horizontal pairs is applied to the 2D model; therefore, 44 runs are considered for each ground motion intensity.

Table 5-1: Summary of the Far-Field Record Set (FEMA P695 Table A-4A)

ID No.	Earthquake			Recording Station	
	M	Year	Name	Name	Owner
1	6.7	1994	Northridge	Beverly Hills - Mulhol	USC
2	6.7	1994	Northridge	Canyon Country-WLC	USC
3	7.1	1999	Duzce, Turkey	Bolu	ERD
4	7.1	1999	Hector Mine	Hector	SCSN
5	6.5	1979	Imperial Valley	Delta	UNAMUCSD
6	6.5	1979	Imperial Valley	El Centro Array #11	USGS
7	6.9	1995	Kobe, Japan	Nishi-Akashi	CUE
8	6.9	1995	Kobe, Japan	Shin-Osaka	CUE
9	7.5	1999	Kocaeli, Turkey	Duzce	ERD
10	7.5	1999	Kocaeli, Turkey	Arcelik	KOERI
11	7.3	1992	Landers	Yermo Fire Station	CDMG
12	7.3	1992	Landers	Coolwater	SCE
13	6.9	1989	Loma Prieta	Capitola	CDMG
14	6.9	1989	Loma Prieta	Gilroy Array #3	CDMG
15	7.4	1990	Manjil, Iran	Abbar	BHRC
16	6.5	1987	Superstition Hills	El Centro Imp. Co.	CDMG
17	6.5	1987	Superstition Hills	Poe Road (temp)	USGS
18	7.0	1992	Cape Mendocino	Rio Dell Overpass	CDMG
19	7.6	1999	Chi-Chi, Taiwan	CHY101	CWB
20	7.6	1999	Chi-Chi, Taiwan	TCU045	CWB
21	6.6	1971	San Fernando	LA - Hollywood Stor	CDMG
22	6.5	1976	Friuli, Italy	Tolmezzo	--

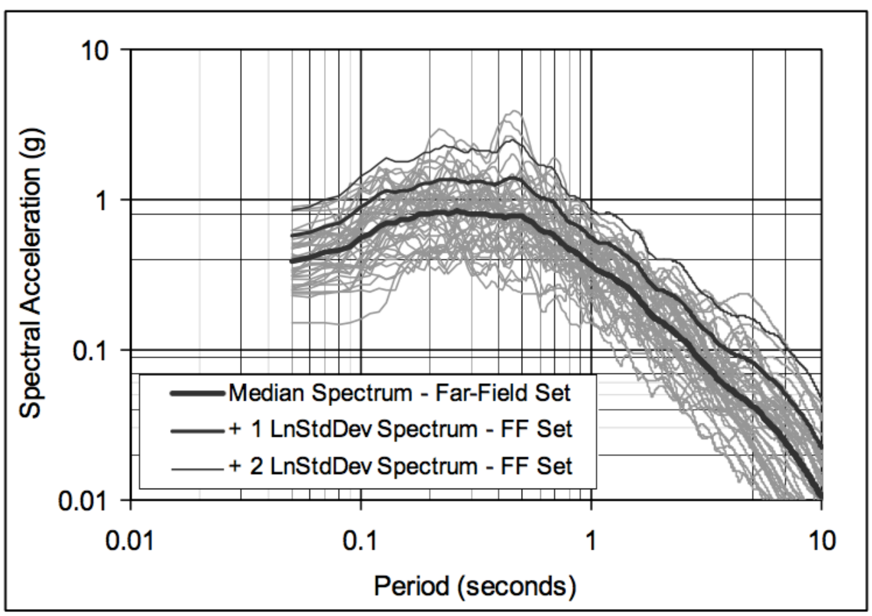

Figure 5.1: Response Spectra of ATC-63 Far Field Ground Motions (FEMA P695 Figure A-3)

Results from the incremental dynamic analyses are used to obtain the median collapse capacity intensity (S_{CT}) and the collapse margin ratio (CMR) for each Archetype. The median collapse intensity (S_{CT}) is established by determining the 5%-damped spectral acceleration at which half of the ground motions cause the structure to collapse using the project failure criteria, i.e., with the drift capacity model or the shear failure model for this study. The collapse margin ratio is then computed to characterize the collapse safety of the Archetype as the ratio of the median collapse spectral intensity S_{CT} to S_{MT}, where S_{MT} is the intensity of the Maximum Considered Earthquake (MCE) obtained from the response spectrum of MCE ground motions at the fundamental period (T) of the building.

$$CMR = S_{CT}/S_{MT} \tag{5-5}$$

$$ACMR = SSF \times CMR \tag{5-6}$$

The collapse margin ratio is adjusted by the period and ductility dependent spectral shape factors (SSFs) prescribed in FEMA P695 §7.2.2 (Table 5-2) in order to account for the effects of the frequency content (spectral shape) of the ground motion record set.

Table 5-2: Spectral shape factor (SSF) for Archetypes designed for SDC D_{max}

(FEMA P695, Table 7-1b)

T (sec.)	Period-Based Ductility, μ_T							
	1.0	1.1	1.5	2	3	4	6	≥ 8
≤ 0.5	1.00	1.05	1.1	1.13	1.18	1.22	1.28	1.33
0.6	1.00	1.05	1.11	1.14	1.2	1.24	1.3	1.36
0.7	1.00	1.06	1.11	1.15	1.21	1.25	1.32	1.38
0.8	1.00	1.06	1.12	1.16	1.22	1.27	1.35	1.41
0.9	1.00	1.06	1.13	1.17	1.24	1.29	1.37	1.44
1.0	1.00	1.07	1.13	1.18	1.25	1.31	1.39	1.46
1.1	1.00	1.07	1.14	1.19	1.27	1.32	1.41	1.49
1.2	1.00	1.07	1.15	1.2	1.28	1.34	1.44	1.52
1.3	1.00	1.08	1.16	1.21	1.29	1.36	1.46	1.55
1.4	1.00	1.08	1.16	1.22	1.31	1.38	1.49	1.58
≥ 1.5	1.00	1.08	1.17	1.23	1.32	1.4	1.51	1.61

In order to account for uncertainty that can contribute to variability in collapse capacity, four sources of uncertainty are considered in the collapse assessment process. The total system uncertainty is based on uncertainties associated with ground motions (β_{RTR}), design requirements (β_{DR}), test data (β_{TD}), and modeling uncertainty (β_{MDL}), and is computed as:

$$\beta_{TOT} = \sqrt{\beta_{RTR}^2 + \beta_{DR}^2 + \beta_{TD}^2 + \beta_{MDL}^2} \tag{5-7}$$

The record-to-record uncertainty is set to $\beta_{RTR} = 0.4$ as specified in FEMA P695 §7.3.1 for the far-field ground motion record set. The "Good" quality ratings chosen in this project are based on consideration of thorough design requirements, comprehensive test databases, and improved modeling capabilities. Although use of lower uncertainty values can be justified based on having more comprehensive design and analysis requirements compared to what was available during previous research efforts, "Good" quality ratings are still chosen in this project, as was done in the NIST (2010) study, with $\beta_{DR} = 0.2$, $\beta_{TD} = 0.2$, and $\beta_{MDL} = 0.2$ resulting in a total system collapse uncertainty (β_{TOT}) of about 0.525.

Given a total system uncertainty, the acceptable collapse margin ratios at 20% collapse probability ($ACMR_{20\%}$) and at 10% collapse probability ($ACMR_{10\%}$) are determined per FEMA P695 §7.4. In this project, $ACMR_{20\%}$ and $ACMR_{10\%}$ values corresponding to $\beta_{TOT} = 0.525$ are 1.56 for each individual Archetype within a performance group and 1.96 on average across a performance group, respectively. Table 5-3 presents the collapse probabilities at total system collapse uncertainty values of 0.525 and 0.500 for comparison purposes.

Table 5-3: Acceptable ACMR Values (FEMA P695, Table 7-3)

Total System Collapse Uncertainty	Collapse Probability				
	5%	10% ($ACMR_{10\%}$)	15%	20% ($ACMR_{20\%}$)	25%
0.500	2.28	**1.90**	1.68	**1.52**	1.40
0.525	2.37	**1.96**	1.72	**1.56**	1.42

Once results from IDAs are obtained and the acceptable ACMR values are established, each Archetype is assessed for conformance with the FEMA P695 acceptability criteria by comparing the adjusted collapse margin ratio (ACMR) to the acceptable collapse margin ratios listed in FEMA Table 7-3 based on the system collapse uncertainty (β_{TOT}). For a given Archetype, if the building ACMR is greater than the Acceptable ACMR at 20% collapse probability ($ACMR_{20\%}$), then the Archetype passes the performance criteria. The average of the ACMRs of Archetypes in a given performance group must also be compared to the Acceptable ACMR at 10% collapse probability ($ACMR_{10\%}$) to assess whether the performance group as a whole passes the FEMA P695 performance criteria. A summary of the collapse assessment results for the Archetypes in this project are presented in Table 5-8.

5.2 Results of initial Archetype designs

During preliminary assessment, analyses were conducted for a subset of Archetypes that were designed conforming to ACI 318-14 provisions without considering the increased wall shear demands accounting for shear amplification. Flexural failure using the drift capacity model and shear failure were both assessed. Although the preliminary Archetypes met the drift capacity design check described in section 2.2.2, they experienced too many shear failures at low median collapse intensities and had ACMRs that did not satisfy the FEMA P695 acceptability criteria.

The failure flags for a select number of preliminary analyses are summarized in Table 5-4 by tracking the step at which the first failure mode occurs, whether it is the drift capacity flexural failure or shear failure. It is evident that Archetypes designed per ACI 318-14 shear provisions experience shear failures resulting in low median collapse intensities and ACMRs. For example, when the 8-story Archetype 8H-DR-3.0 is subjected to MCE level shaking (at a ground motion scaling factor (SF) of 2.45), 31 out of 44 records fail, 27 due to shear failure and 4 due to flexural failure; even at a lower ground motion scaling factor of 2.20, 18 instances of shear failure occur along with 2 flexural failures resulting in a low median collapse intensity S_{CT} = 1.22. The 12-story Archetype 12H-DR-3.0 similarly experiences too many shear failure flags with 24 records failing in shear and 2 records failing in flexure at a ground motion scaling factor of 2.0, and has a resulting low S_{CT} = 0.68 that leads to not conforming to the FEMA P695 Acceptability criteria; the number of records that reach failure is even higher at MCE level shaking (at SF=2.59) with Archetype 12H-DR-3.0 experiencing 33 shear failures and 7 drift capacity failures.

Figure 5.2 and Figure 5.3 each show a sample collapse margin ratio (CMR) plot from IDA results in which the median collapse spectral intensity (S_{CT}) is lower than the MCE spectral intensity (S_{MT}) resulting in an unacceptably low ACMR. Other Archetypes experienced similar unacceptable ACMRs due to high occurrences of shear failures.

Table 5-4: Failure Results for Preliminary Archetypes (time step at failure)[1]

EQ	8H-DR-3.0				12H-DR-3.0				18H-DR-3.0	
	SF = 2.20		SF = 2.45		SF = 2.00		SF = 2.59		SF = 1.73	
	Flexure	Shear	Flexure	Shear	Flexure	Shear	Flexure	Shear	Flexure	Shear
1	-	-	-	905	1016	957	1017	745	-	-
2	-	569	-	568	-	-	-	546	-	841
3	-	1165	-	1166	-	-	-	1224	-	1221
4	-	-	-	-	-	-	-	-	-	-
5	-	-	5619	961	5534	933	5524	932	-	-
6	-	-	2007	-	-	-	3077	1753	-	-
7	-	830	-	830	-	836	-	810	-	880
8	-	-	-	-	-	-	1624	1318	-	-
9	-	-	-	-	2986	-	2974	-	-	-
10	-	-	-	-	-	-	-	-	-	-
11	-	-	-	-	-	918	1007	919	-	980
12	-	-	-	-	-	-	-	5720	-	-
13	-	1279	-	1277	-	1032	-	1009	-	1309
14	-	1044	-	1045	-	-	-	1387	-	-
15	-	-	-	-	-	670	-	669	-	-
16	-	-	-	2792	-	-	2739	-	-	-
17	-	723	-	723	796	726	789	725	-	728
18	-	-	-	380	-	379	-	366	-	446
19	-	-	-	-	-	-	8153	-	-	-
20	-	9070	-	9036	-	9032	-	9027	-	-
21	-	809	866	809	1055	456	894	294	-	536
22	-	1026	-	1024	-	955	-	916	-	919
23	-	558	-	535	-	1024	-	930	-	-
24	-	592	-	591	-	589	-	586	-	592
25	-	1187	-	1186	-	1185	-	1183	-	1156
26	-	-	-	698	-	-	-	736	-	627
27	3199	-	3183	1142	-	1023	3141	1022	-	-
28	-	-	-	1858	-	2158	-	2152	-	2155
29	-	864	-	862	-	895	-	895	-	932
30	-	-	-	1446	-	1446	-	1446	-	-
31	-	-	1783	-	-	1904	1677	1896	-	1818
32	-	-	-	-	-	-	3629	-	3743	-
33	-	-	-	-	-	-	-	-	-	-
34	-	5261	6262	5159	-	5140	6262	5133	-	5463
35	-	1395	-	1394	-	1882	-	1750	-	1664
36	-	-	1178	-	-	-	1052	-	-	-
37	-	-	-	-	-	-	-	598	-	637
38	2959	-	2935	-	-	-	-	-	-	-
39	-	-	-	621	-	629	681	630	-	925
40	-	348	-	328	-	-	-	353	-	350
41	-	-	-	-	8325	-	8305	-	8469	7890
42	-	9082	-	9082	-	9081	-	9038	-	9034
43	-	-	-	-	-	-	-	380	-	654
44	-	888	-	888	-	886	-	886	-	890
Failures:	2 Flexure, 18 Shear		4 Flexure, 27 Shear		2 Flexure, 24 Shear		7 Flexure, 33 Shear		2 Flexure, 23 Shear	

[1] Values in red indicate the failure flag that was reached first.

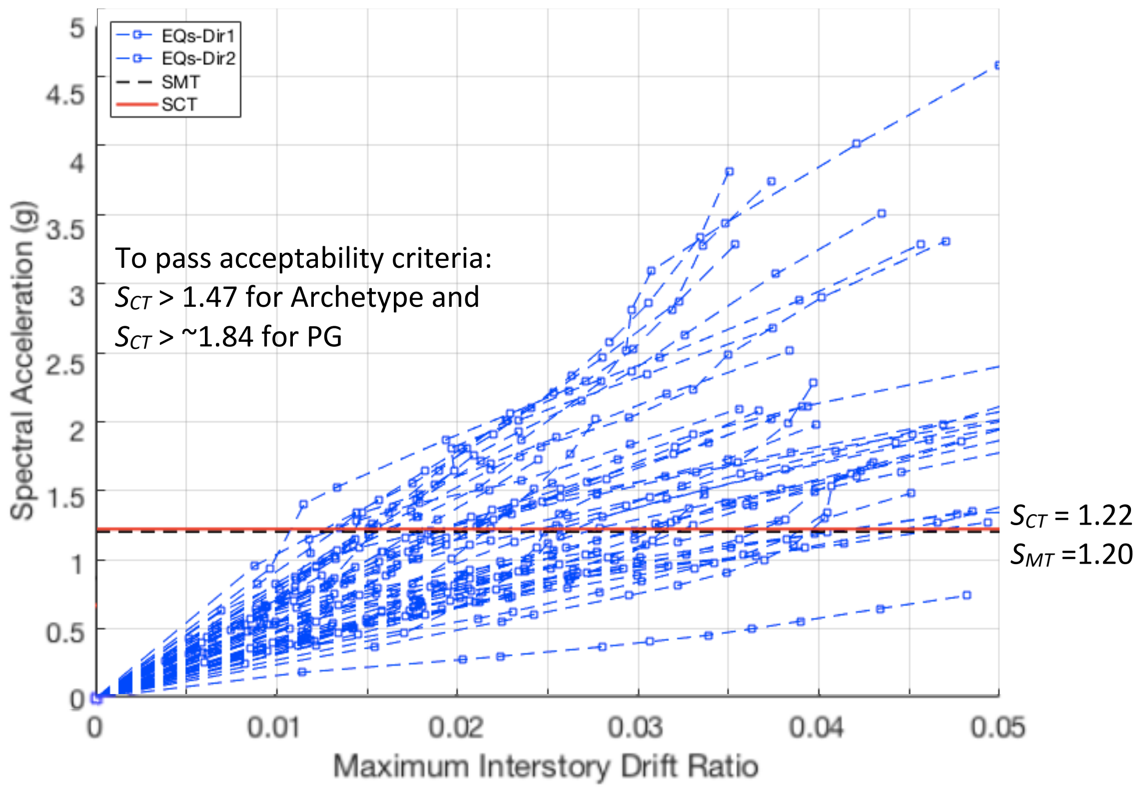

Figure 5.2: CMR Plot for Preliminary Archetype 8H-DR-3.0 designed per ACI 318-14

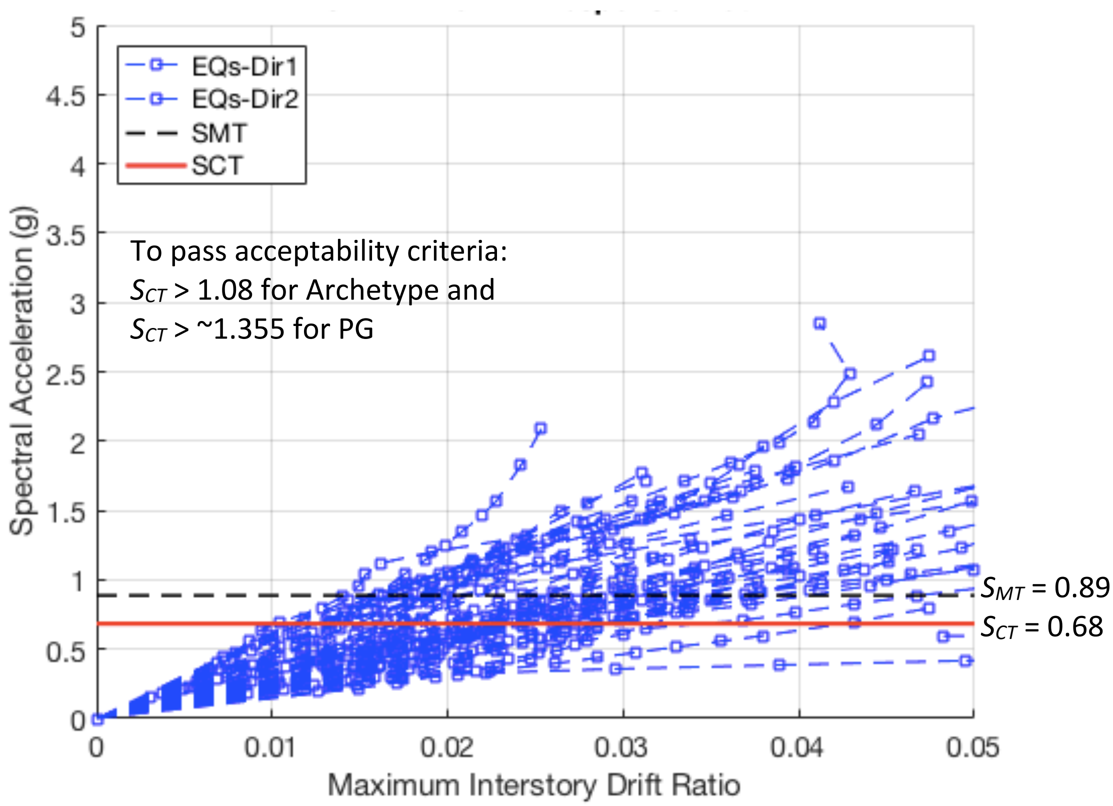

Figure 5.3: CMR Plot for Preliminary Archetype 12H-DR-3.0 designed per ACI 318-14

As the height of the Archetypes increase, the system overstrength and design period (C_uT_a) per ASCE 7 increase resulting in an acceptable Archetype ACMR greater than $ACMR_{20}$. However, even though the ACMRs of the preliminary Archetypes satisfy the 20% probability of collapse criteria, the mean of the ACMRs for the entire performance group do not satisfy the 10% probability of collapse criteria, thus still requiring the taller Archetypes to be redesigned with increased shear capacity. For example, the 18-story 18H-DR-3.0 Archetype experiences failure in over half of the records (23 shear failures and 2 drift capacity failures) at a ground motion scaling factor of 2.20 (Table 5-4); this results in S_{CT} = 0.672, CMR = 1.03, and ACMR = 1.58, which is just above the acceptable value of $ACMR_{20}$ = 1.56; however, in order for the performance group to satisfy the 10% probability of collapse acceptability criteria, the 18-story Archetypes need to have an S_{CT} greater than 0.82 with fewer than 22 records failing at a ground motion SF of 2.4.

5.2.1 Summary

A summary of the collapse assessment results for the preliminary Archetypes are presented in Table 5-5 highlighting the need to revise the Archetype designs for conformance with the FEMA P695 acceptability criteria. For these preliminary Archetypes, although the drift level associated with the axial failure model had not yet been reached, (which was typically around 5% lateral drift as illustrated in Figure 4.6), the project team and the advisory panel opted for a more conservative design approach to revise the Archetypes to meet amplified shear demands as presented in Section 2c since the axial failure model has only been validated based on relatively few tests of isolated cantilever walls.

Table 5-5: IDA and Collapse Assessment Results for a Subset of Preliminary Archetypes

Archetype ID	Preliminary Designs Conforming to ACI 318-14 Shear Provisions								
	Ω_0	μ_T	S_{MT} [T]	S_{CT} [T]	CMR	SSF	ACMR	Arch. Pass?	PG Pass?
8H-DR-3	2.04	4.17	1.20	1.22	1.02	1.25	1.27	Fail	Fail
12H-DR-3	1.65	3.07	0.89	0.68	0.77	1.25	0.96	Fail	Fail
18H-DR-3	1.77	6.92	0.65	0.67	1.03	1.53	1.58	Pass	Fail
24H-DR-3	1.79	> 8	0.53	0.59	1.12	1.61	1.80	Pass	Fail
30H-DR-3	1.81	7.46	0.45	0.51	1.13	1.63	1.84	Pass	Fail

5.3 Analysis Results of Final Archetype Designs

The nonlinear pushover analysis and IDA results of the final Archetype designs are presented in this section. As described in section 2.3 of this report, the preliminary Archetypes were redesigned to meet amplified shear demands with additional wall shear reinforcement and increased wall thickness at the lower levels. The increased overstrength and collapse margin ratios of the final revised Archetypes are described herein.

5.3.1 Pushover analysis results

Results from the nonlinear pushover analyses are presented in Table 5-8 as well as by the pushover curves in Figure 5.4 for the Archetypes considered in this project. On each pushover curve, the roof drift at which the drift capacity model predicts flexural failure is indicated by a specified point which typically occurs close to the onset of strength loss predicted by the nonlinear model. Analysis results confirm that Archetypes with diagonally reinforced (DR) coupling beams have a higher base shear overstrength and perform better than Archetypes with conventionally reinforced (CR) coupling beams. The Archetypes with DR coupling beams tend to experience the onset of strength loss at larger roof drifts between 3 to 3.5 percent as predicted by the drift capacity model due to flexural failure at the base of the wall piers. However, the Archetypes with conventionally reinforced coupling beams experience an earlier more abrupt degradation in base shear strength at lower roof drifts ranging from 2 to 3 percent due to the strength loss associated with coupling beams.

For assessment of the system overstrength per FEMA P695 section 7.6, the proposed overstrength factor is taken as the upper bound value from the mean of the performance groups, rounded to the next half unit interval. For the Archetypes considered in this study, the average overstrength factors among the performance groups vary from 1.3 to 2.2. As a result, an overstrength factor $\boldsymbol{\Omega_0}$ = 2.5 is proposed for RC Ductile Coupled Wall systems.

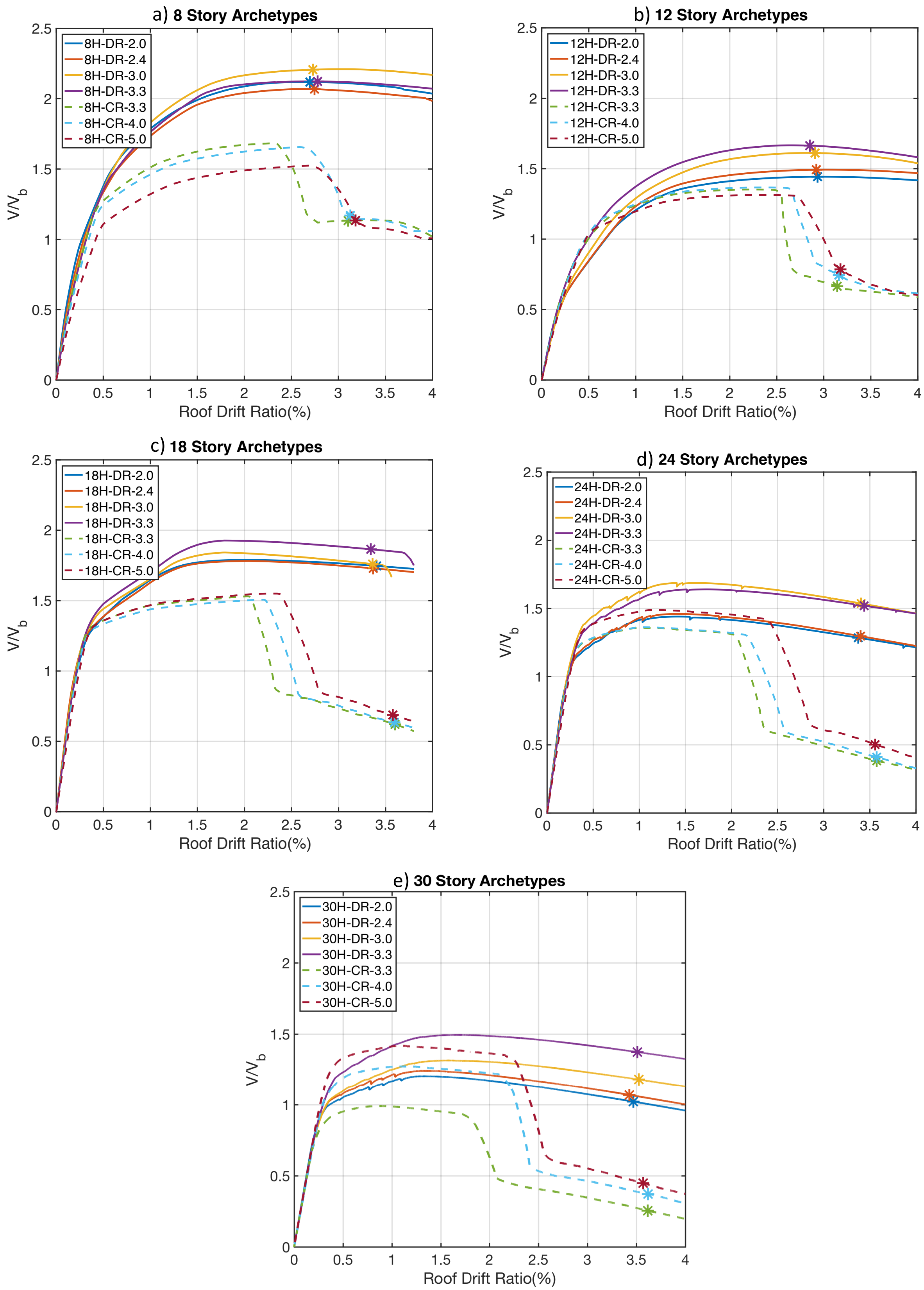

Figure 5.4: Pushover Curves for various Archetypes

Sample pushover results for the Archetype 8H-DR-3.0 are presented in Figure 5.5 at the specified roof drifts including the drift at which the drift capacity model predicts failure. At the failure drift of 2.77% for this Archetype, the maximum wall shear stresses are below $6\sqrt{f_c'}A_{cv}$ and coupling beam rotations are below 0.045. The strain profile along the wall height presented in Figure 5.5(c) indicates that the nonlinear tension strains in longitudinal reinforcement are concentrated at the wall base, as intended in the design, and that tensile strains exceed yield at locations where longitudinal reinforcement is terminated over the wall height. For taller wall buildings, it is generally not practical to limit yielding to only the critical section at the wall base, especially for the tension pier, as noted in Figure 5.5c for Wall 1. The system overstrength computed using the ratio of the maximum shear to the design base shear is 2.25. Similar results determining the system overstrength and member stresses are obtained for all other Archetypes.

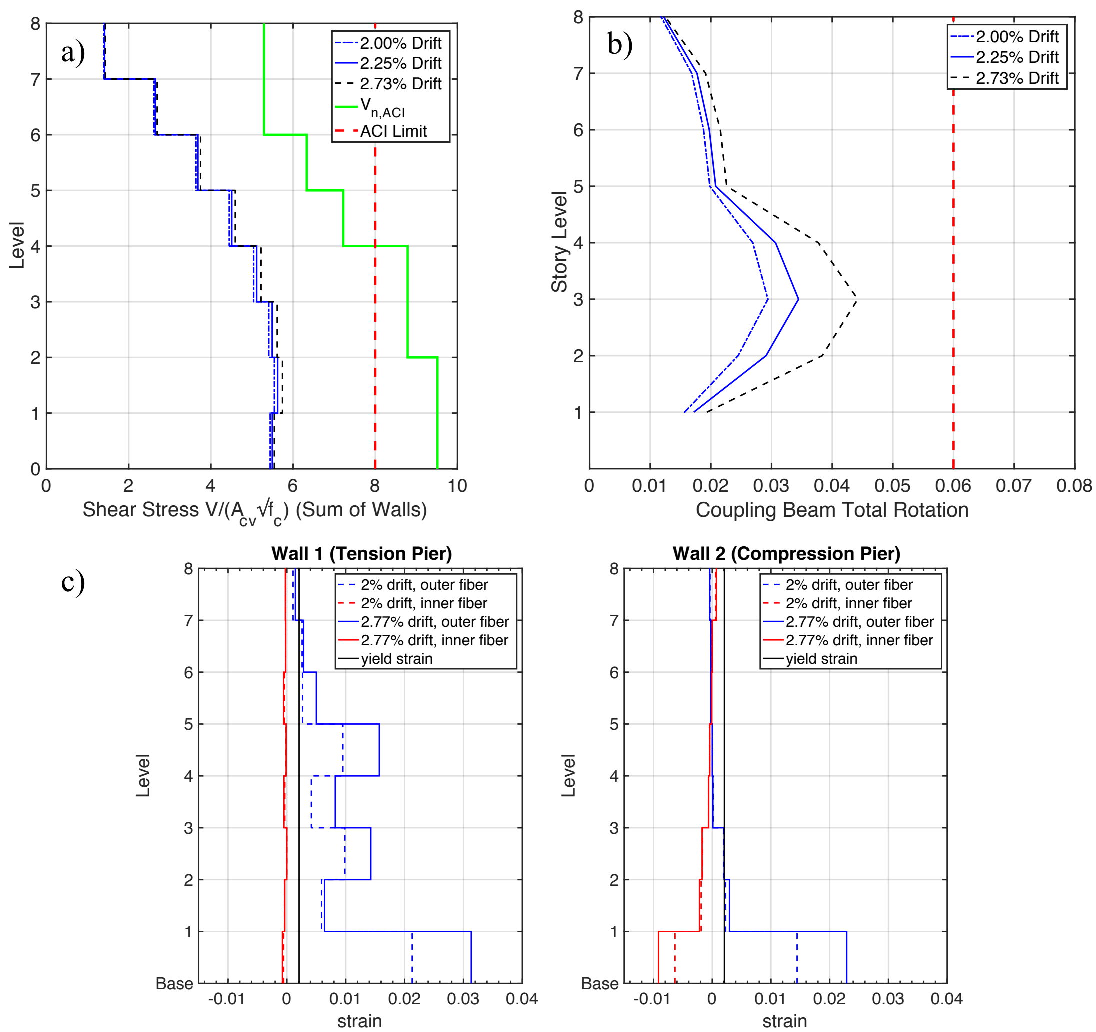

Figure 5.5: Sample Pushover Results for Archetype 8H-DR-3.0:
a) wall shear stress, b) coupling beam rotation, c) wall strain profile

Sample pushover results of wall and coupling beam shears (Figure 5.6) for the Archetype 8H-CR-4.0 present the typical strength loss that occurs for Archetypes with conventionally-reinforced coupling beams versus diagonally-reinforced coupling beams. In the example of 8H-CR-4.0, it is evident that the lateral strength loss of the system occurs as a result of the coupling beam strength loss at a time step corresponding to a roof drift of about 2.9%, whereas the drift capacity model predicts flexural failure of the compression wall pier at a drift of 3.2%.

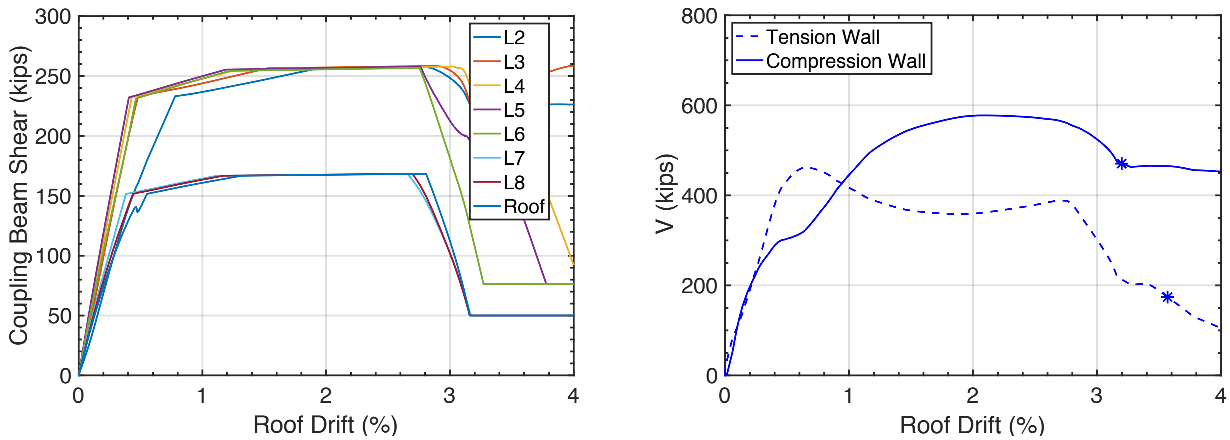

Figure 5.6: Sample Pushover Results for Archetype 8H-CR-4.0

5.3.2 IDA results

Following the pushover analyses, IDAs are conducted for each Archetype by incrementally scaling up the ground motions until just fewer than half of the records reach collapse according to one or more of the failure models described in Chapter 4. The results of the incremental dynamic analyses are summarized in Table 5-8.

In comparison to the preliminary designs, the revised final Archetypes experience fewer shear failures, have higher median collapse intensities and ACMRs, and meet the FEMA P695 acceptability criteria. For example, when the revised Archetype 8H-DR-3.0 is subjected to ground motion shaking at SF of 3.9, only two records experience shear failure and 17 records experience flexural failure the records fail (21 flexural failures) resulting in an improved ACMR = 2.08 which meets the $ACMR_{20}$ and $ACMR_{10}$ acceptability limits. The 12-story Archetype 12H-DR-3.0 also experiences far fewer shear failures at the ground motion SF of 4.1 with only 2 of 44 records failing in shear and 19 records failing the drift capacity failure criteria, thus resulting in a higher S_{CT} = 1.39 and ACMR = 2.14 and passing the FEMA P695 Acceptability criteria. Similarly, the taller Archetype buildings experience fewer shear failures, higher S_{CT} values, and acceptable ACMRs.

To demonstrate collapse, an illustrative IDA plot for a sample Archetype is presented in Figure 5.7 indicating the ground motion spectral accelerations at increasing maximum drifts. For a certain Archetype model, each point on the IDA plot corresponds to the nonlinear dynamic analysis results subject to a single ground motion at a specific intensity level, and each line represents results for one ground motion for all increasing intensities. The IDA plot of Archetype 8H-DR-3 shown in Figure 5.7 indicates the median collapse intensity, S_{CT} = 1.95 and the collapse margin ratio, CMR = 1.62.

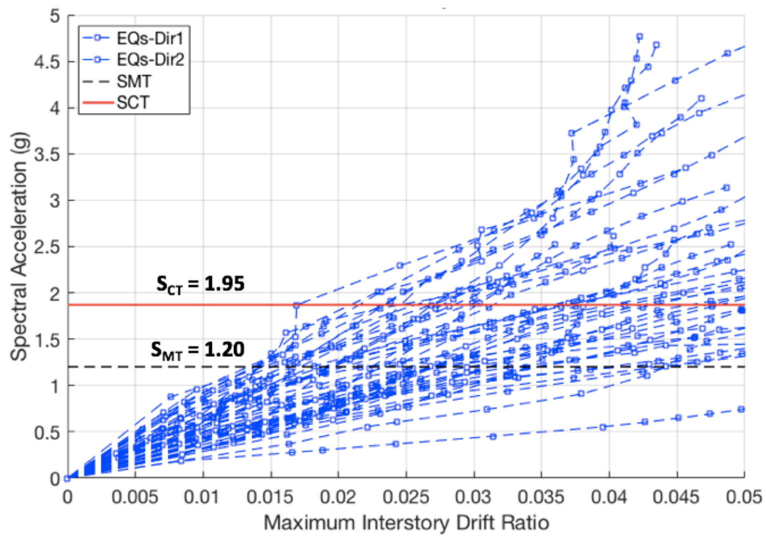

Figure 5.7: CMR Plot for Archetype 8H-DR-3

Response history analysis results are presented in Figure 5.8 for Archetype 12H-DR-3.0 subject to ground motions at the scaling factor corresponding to the median collapse intensity (at "collapse"). Peak analysis results from the 44 records show that the mean peak wall pier shear stresses along the building height are less than the mean shear strength of 1.5 times $10\sqrt{f_c'}A_{cv}$, and the shear profile presented in Figure 5.8(a) highlights the need to design for amplified shear demands (V_e) where linear methods of ASCE 7 are used for design. Wall moments generally increase down the wall height as shown in Figure 5.8(b). The values presented in Figure 5.8(c) suggest that mean wall rotations are less than about 0.009 but reach yield considering an estimated value (i.e., $0.003/l_w \times 60" = 0.0016$) for yield rotation.

IDA results in Figure 5.8(d) present the concentration of compressive strains at the wall base, while Figure 5.9 presents the distribution of peak wall tensile and compressive strains from the 44 records at collapse. The peak tensile strains determined at "collapse" are typically less than 0.025 suggesting the unlikelihood of rebar buckling or fracture which is commonly considered at strains of about 0.05 (NIST, 2010). The peak compressive strains are less than the limit of 0.01, commonly considered to indicate the initiation of concrete crushing failure (Segura and Wallace, 2018b). The observed peak compressive strains below the value of 0.01 are typically acceptable for well-confined concrete considering that flexural compression failure is predicted in this study using the drift capacity model as described in section 4.1.1.

As presented in Figure 5.8(e) and Figure 5.8(f) respectively, the mean nonlinear maximum drifts are less than 3.5%, and the mean coupling beam rotations do not exceed 0.06. Similar results for story drifts, wall shear stresses, wall strains, and coupling beam rotations are observed for the other Archetypes.

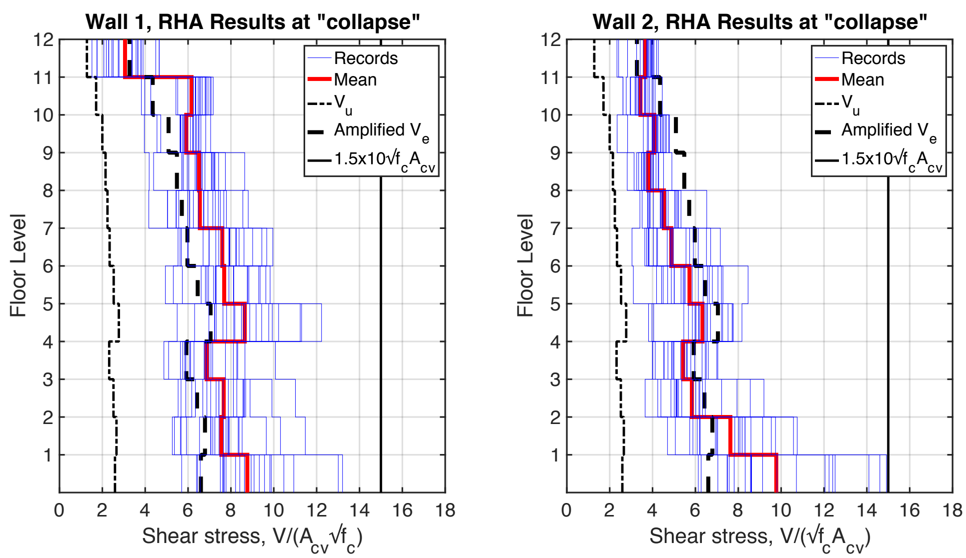

a) wall shear stress

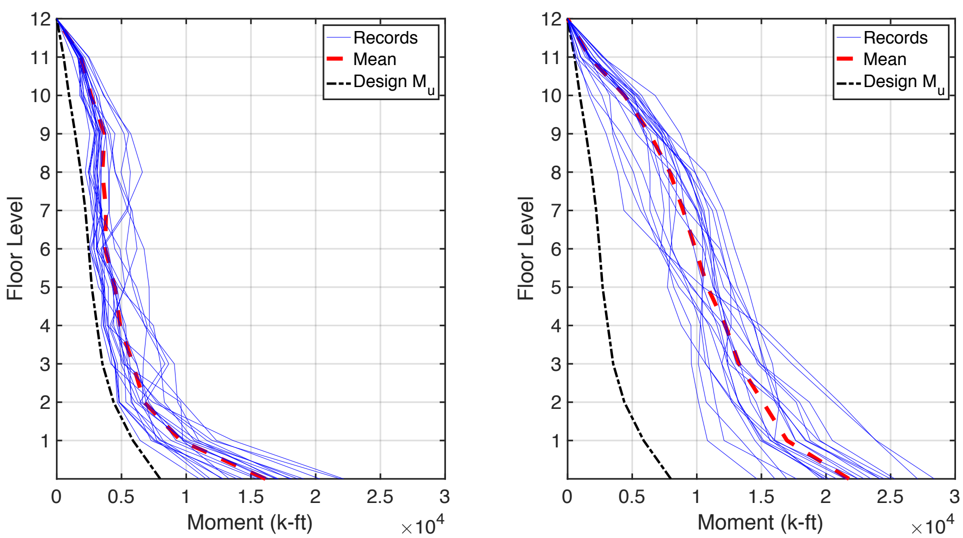

b) wall moment profile

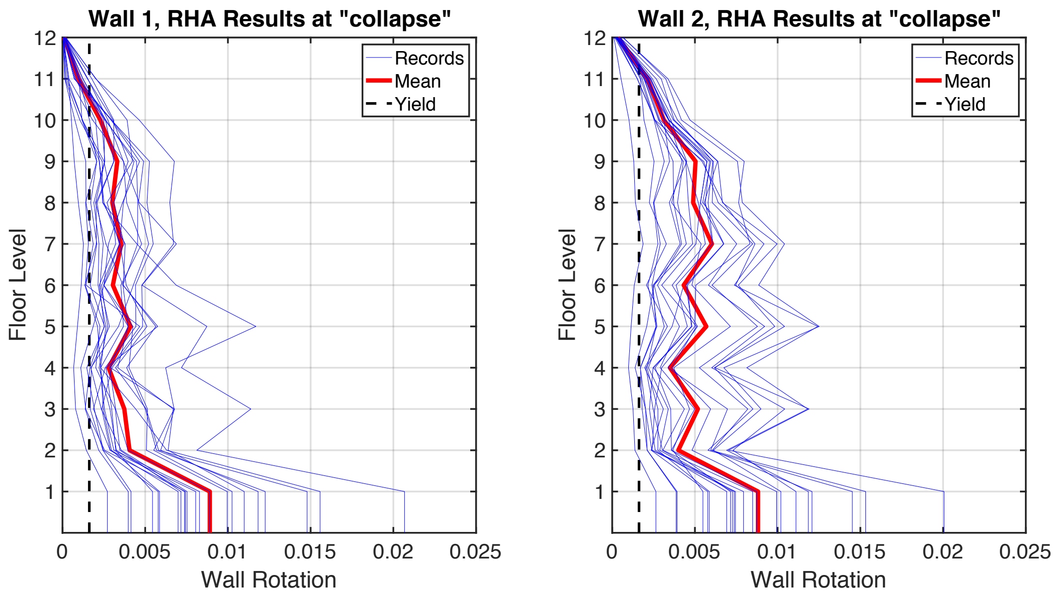

c) wall rotations

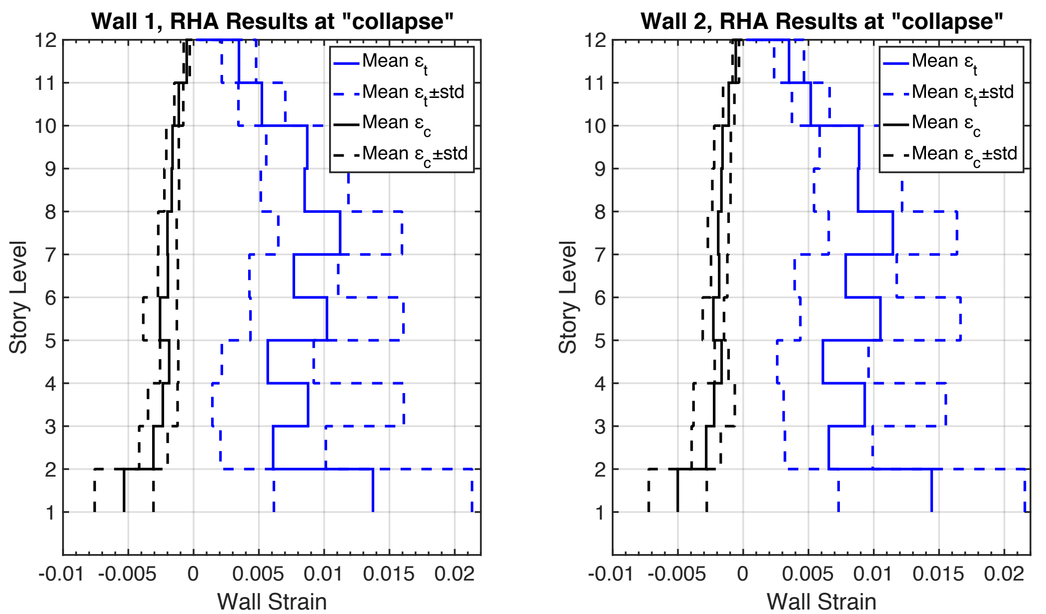

d) wall strains

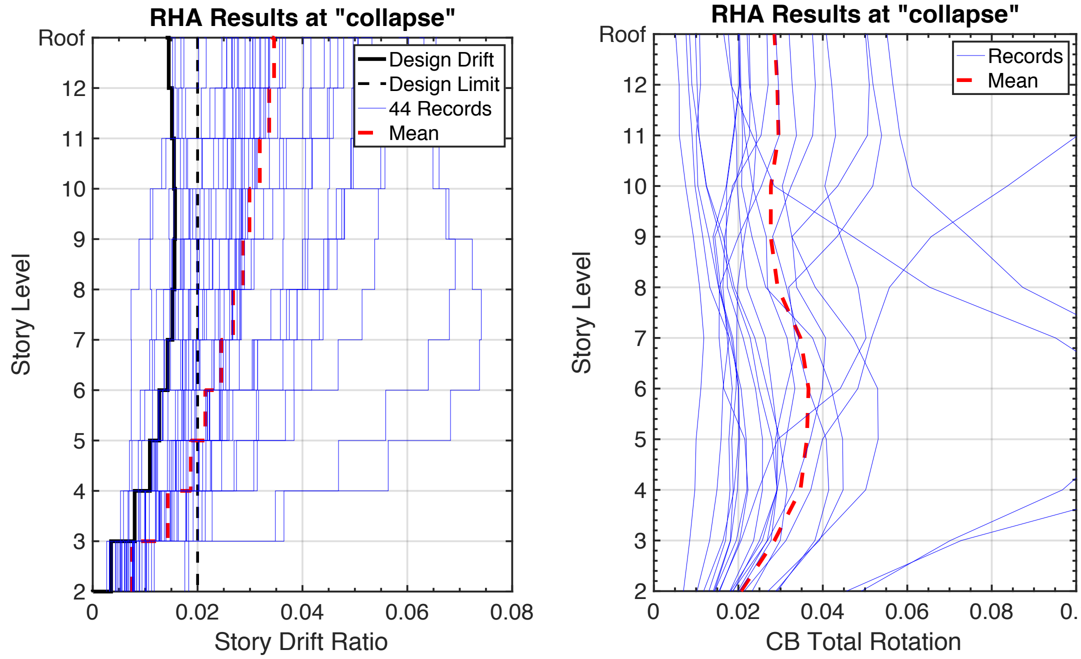

e) story drift f) coupling beam rotations

Figure 5.8: Sample Wall Analysis Results for Archetype 12H-DR-3.0 at collapse: a) wall shear stress ; b) wall moment profile; c) wall strains; d) wall rotations; e) story drift; f) coupling beam rotations

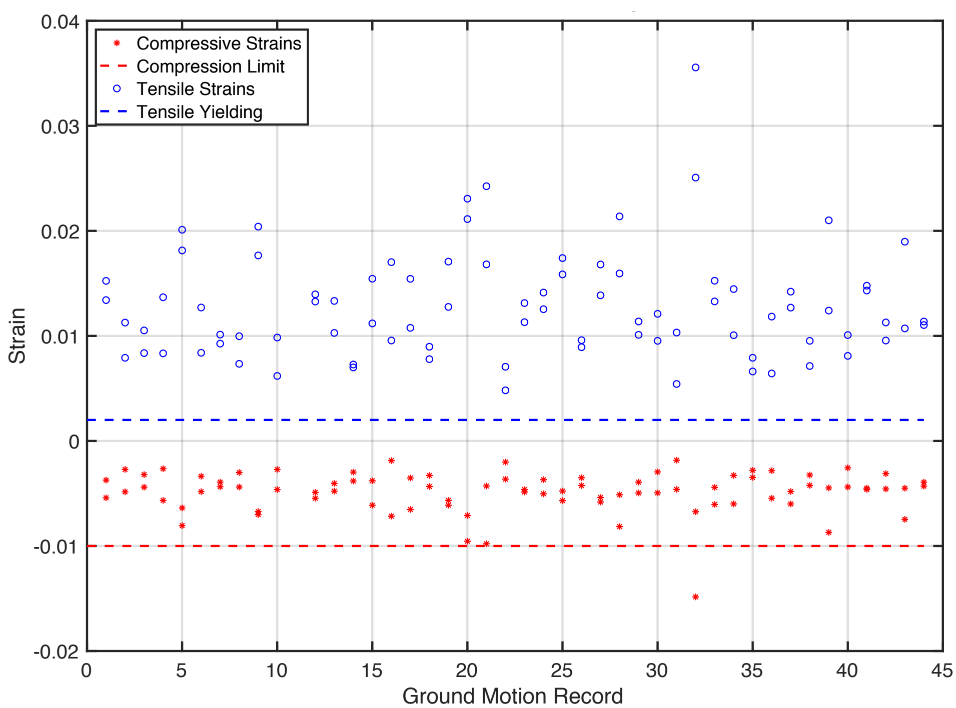

Figure 5.9: Peak wall strains for Archetype 12H-DR-3.0 at collapse

Drift responses at DE and MCE level shaking are presented in Figure 5.10 for one short (8-story) and in Figure 5.11 for one tall (30-story) Archetype. The results indicate that the mean peak story drifts from the 44 records at DE level shaking do not exceed the ASCE 7 design allowable drift of 2 percent, and that the taller Archetypes experience higher drifts as expected.

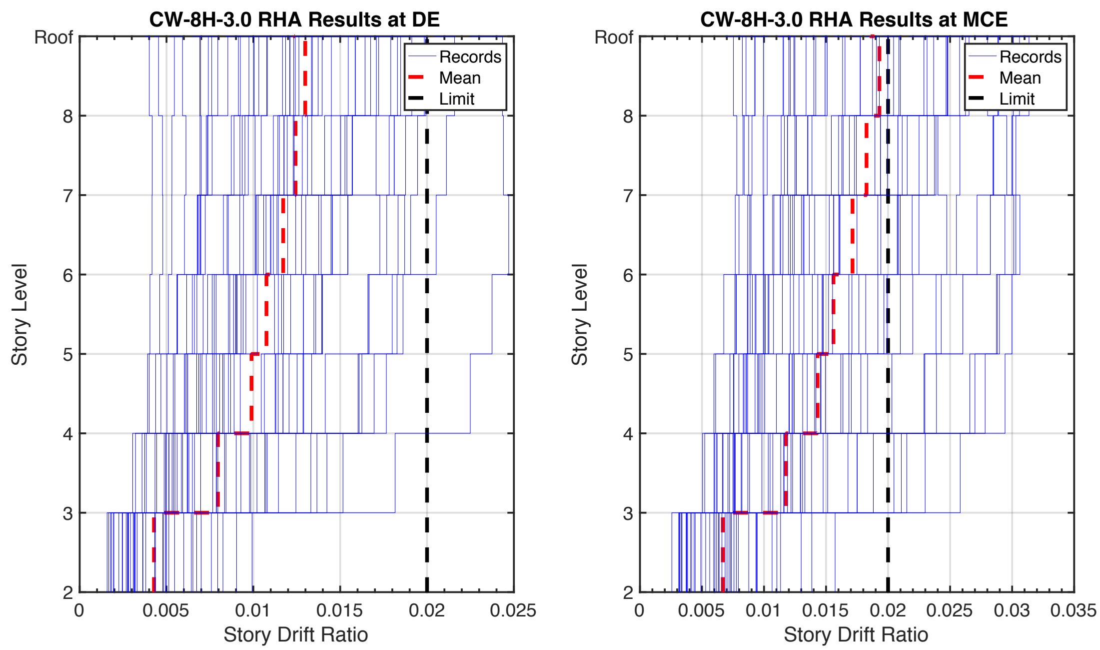

Figure 5.10: Drift Response Plot for Archetype 8H-DR-3.0

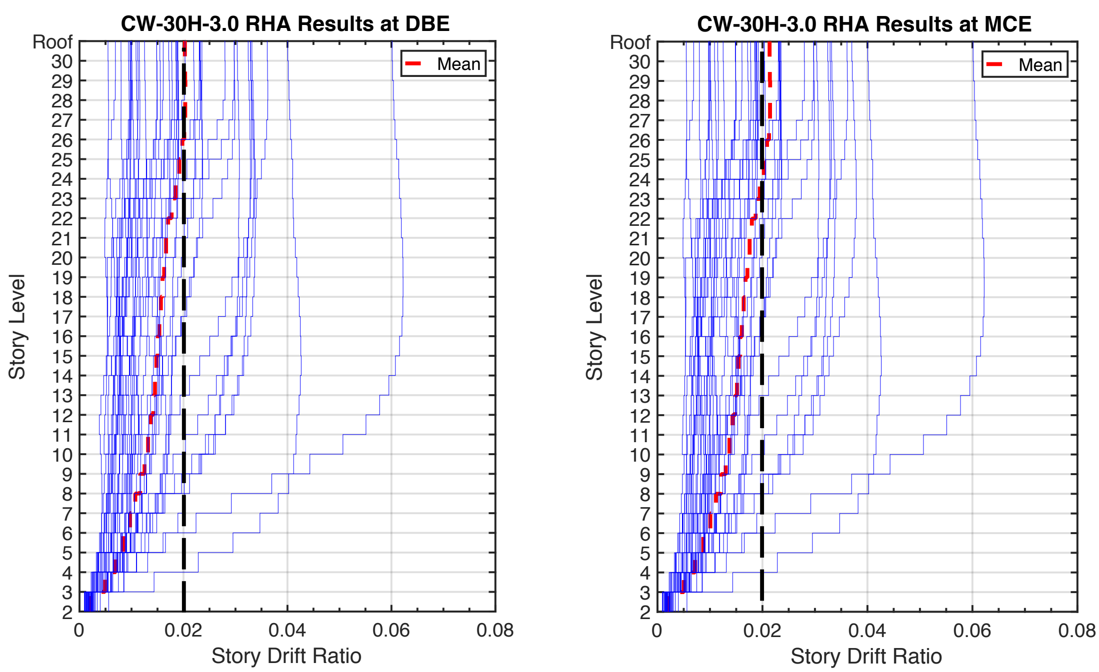

Figure 5.11: Drift Response Plot for Archetype 30H-DR-3.0

5.3.2.1 IDA Results at DE Level Shaking

Story shears are presented in Figure 5.12 for a coupled wall comparing the values from the ELF, RSA, RSA design amplified shear demand (V_e), and NLRHA results for DE level shaking. In general, ELF wall shear and moment demands exceed RSA demands along the building height. The NLRHA values shown include the mean of the maximum story shears from the 44 ground motions as well as mean ± standard deviation values. The story shears represent the sum of the individual shears of the coupled wall piers. The NLRHA results highlight the effects of wall shear amplification as nonlinear shear demands range about 2 to 4 times the design shear demands at the lower levels.

Story drifts are presented in Figure 5.13 including the drifts at the center of mass from the RSA designs using $\boldsymbol{C_d} = \boldsymbol{R} = 8$, the 2% drift limit, and the mean as well as mean ± standard deviation of the nonlinear story drift results from 44 ground motions scaled to the DE level shaking. Mean nonlinear story drifts match closely with design drifts for the shorter 6, 8, and 12-story coupled wall Archetypes. However, the design story drifts for the taller 24- and 30-story Archetypes exceed the average drift values determined from NLRHA.

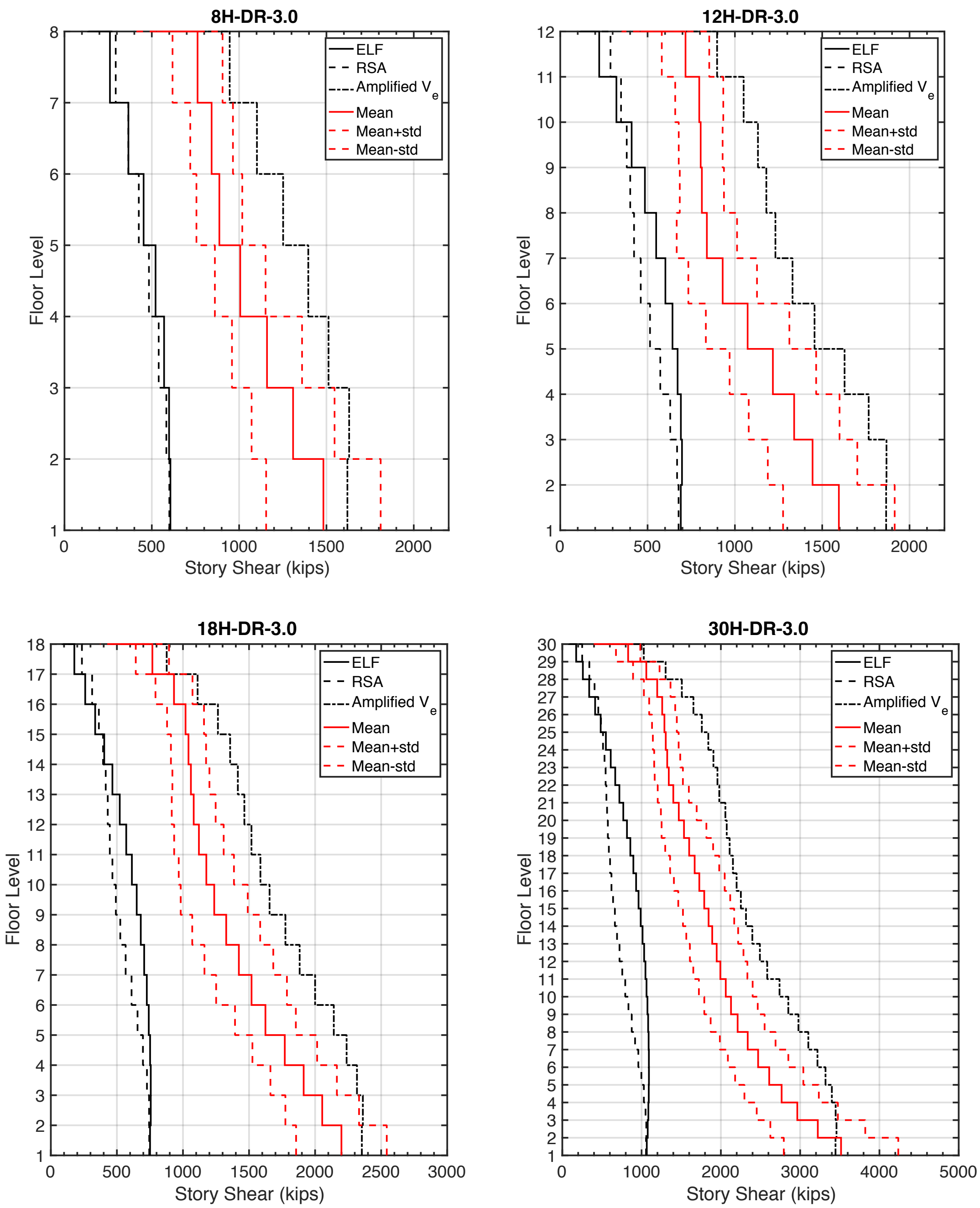

Figure 5.12: Story Shears at DE Level Shaking

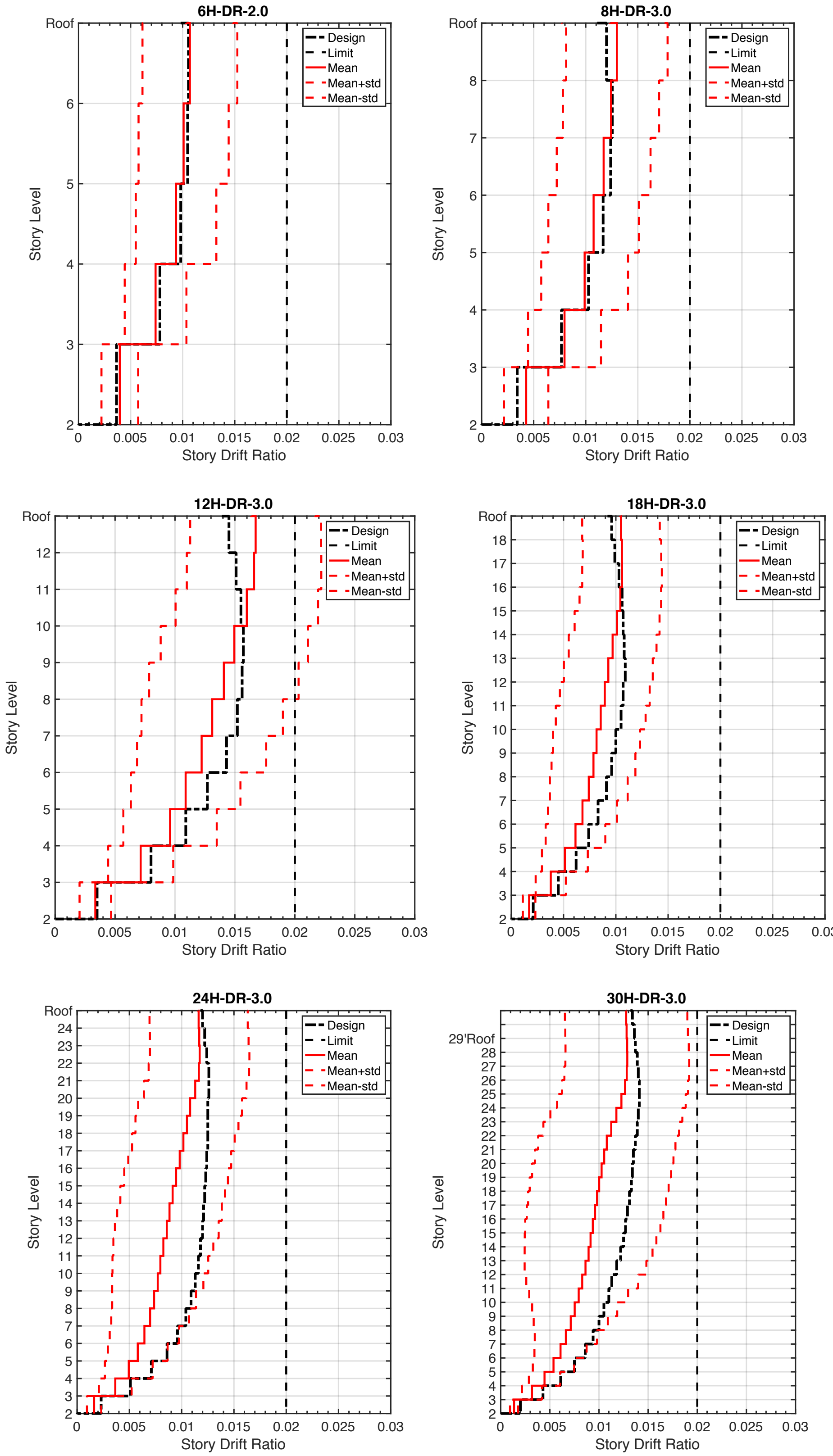

Figure 5.13: Story Drifts at DE Level Shaking

5.4 Assessment of the Deflection Amplification Factor, C_d

FEMA P695 describes the deflection amplification factor C_d as a ratio of the acceptable value of R of the system with consideration of the effective damping. The ratio of C_d to R can be assessed from analysis results using the roof drift corresponding to design base shear (δ_E/R) and the assumed roof drift of the yielded system corresponding to design earthquake (DE) ground motions (δ). Figure 5.14 presents the illustration of the seismic performance factors per FEMA.

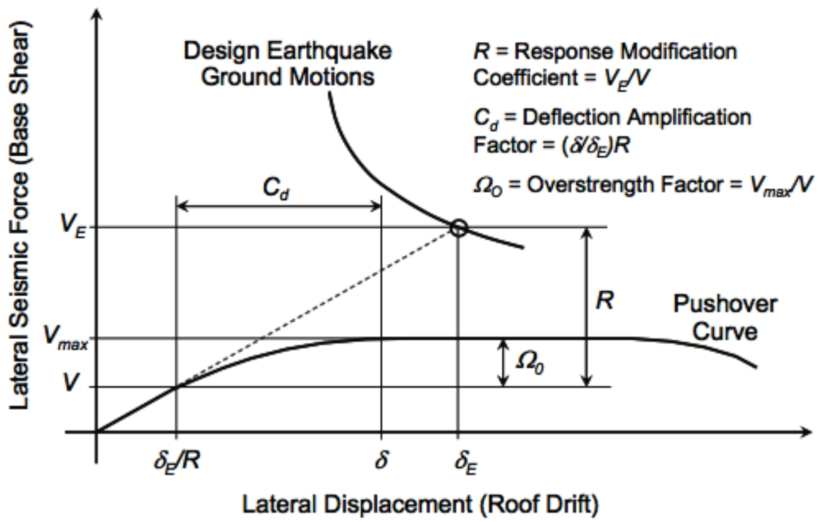

Figure 5.14: Illustration of seismic performance factors, FEMA P695 Figure 1-1

The C_d factor for RC Ductile Coupled Walls has been assessed using the ratio of a median value of nonlinear inelastic roof drifts (δ) from 44 records at DE level shaking to the design level drifts (δ_E/R). Table 5-6 summarizes the drifts and resulting C_d values for a subset of Archetypes. The computed C_d values for these Archetypes result in a median value of C_d = 8.8 (coefficient of variation = 0.13).

Table 5-6: Assessment of C_d based on drifts from a subset of Archetypes

Archetype	# stories	H_{tot} (ft.)	**Design (δ_E/R)**/H_{tot} (%)	**Median RHA δ** / H_{tot} (%)	**C_d δ / (δ_E/R)**
30H-DR-3	30	300	0.145	1.14	**7.9**
18H-DR-3	18	180	0.111	1.22	**10.9**
12H-DR-3	12	120	0.161	1.58	**9.8**
8H-DR-3	8	80	0.127	1.14	**9.0**
6H-DR-2	6	60	0.109	0.94	**8.6**
6H-CR-5	6	60	0.130	1.05	**8.1**

The RC Coupled Wall Archetypes have been designed per FEMA P695 guidelines to equate $\boldsymbol{C_d}$ to the $\boldsymbol{R}$ factor based on the equal displacement assumption (i.e., "Newmark rule") for systems with effective damping values approximately equal to 5% and structures with fundamental periods greater than T_S. However, systems with significantly higher levels of damping (e.g., systems with viscous dampers) would have significantly smaller displacements than those with 5%-damped elastic response; in those cases, an appropriate value of $\boldsymbol{C_d}$ can be determined as a fraction of the R factor, $\boldsymbol{C_d} = \boldsymbol{R}/B$, per the modification methods of Chapter 18 of ASCE 7. The numerical coefficient B per ASCE 7-16 Table C18.7-1 is summarized in Table 5-7.

Table 5-7: Damping Coefficient B per ASCE 7-16 Table C18.7-1

Effective Damping, β (%)	Table 17.5-1 of ASCE/SEI 7 (2010), AASHTO (2010), CBC (2013), seismically isolated structures)	Table 18.6-1 of ASCE/SEI 7 (2010) (structures with damping systems)	FEMA 440 (2005)	Eurocode 8 (2005)
2	0.8	0.8	0.8	0.8
5	1.0	1.0	1.0	1.0
10	1.2	1.2	1.2	1.2
20	1.5	1.5	1.5	1.6
30	1.7	1.8	1.8	1.9
40	1.9	2.1	2.1	2.1
50	2.0	2.4	2.4	2.3

The RC Ductile Coupled Wall Archetypes have been analyzed using equivalent viscous damping values ranging from 2.5% for the taller 30 and 24-story buildings to 4.6% for the shorter 8 and 6-story buildings following the recommendations of the PEER TBI (2017) guidelines §4.2.7 as described in Section 3.1.4 of this report. Since the RC Ductile Coupled Wall Archetypes have been analyzed with slightly lower levels of damping than 5%, the resulting drifts are slightly higher than if 5% damping had been used. For the subset of Archetypes listed in Table 1, scaling the nonlinear RHA roof drift values by the corresponding interpolated values of the numerical coefficient B, results in a median $\boldsymbol{C_d}$ value of 8.4. Therefore, a deflection amplification factor of $\boldsymbol{C_d} = 8$ can be reasonably proposed for RC Ductile Coupled Walls.

It is important to note that the proposal of $\boldsymbol{C_d} = 8$ is based on design drift values that are obtained using a wall flexural effective stiffness $I_{eff} = 0.75I_g$ based on input from our advisory panel for effective stiffness values commonly used in practice for RC coupled walls. This effective stiffness assumption results in lower design drifts than if, for example, $I_{eff} = 0.5I_g$ were used in design. However, since the Archetypes have been designed for amplified shear demands (and conform to the drift capacity check) per the new provisions of ACI 318-19, the designs are not drift-governed and the wall piers are thicker and stiffer than if designed per ACI 318-14. The maximum design drifts observed at the center of mass among any of our Archetypes is less than 1.6% when using $I_{eff} = 0.75I_g$ and less than 2% when using $I_{eff} = 0.5I_g$ (per ACI 318-14, Section 6.6.3.1.2, this value is permitted to compute drifts).

If any of our coupled wall Archetypes were designed with wall $I_{eff} = 0.5I_g$, instead of $0.75I_g$, they would still meet the 2% design drift limit due to shear amplification considerations governing the design. The design forces would also remain unchanged using wall $I_{eff} = 0.5I_g$ since the ASCE 7 code upper limit period $T_u = C_uT_a$ and minimum C_s considerations govern the base shear demand for all Archetypes. Moreover, the wall pier designs would remain unchanged because the minimum wall area (length and thickness) that have been optimized for these Archetypes are governed by shear amplification and the requirement that walls sharing a common shear force not exceed a shear stress of $8\sqrt{f_c'}A_{cv}$. However, it is possible that other building designs would not meet the code allowable drift using $I_{eff} = 0.5I_g$, and would require added stiffness to meet drift limits.

Overall, based on the results of the FEMA P695 study on RC Ductile Coupled walls, the deflection amplification factor being proposed in the ASCE 7 code change ballot is $\boldsymbol{C_d} = 8$.

5.5 Shear at Peak Drift

Nonlinear analysis results for MCE level shaking were studied for a subset of Archetypes to compare the wall shear at peak drift to the peak shear experienced in the response history. The goal was to assess the level of shear demand associated with the peak drift demand since the drift capacity model is based on using peak values for drift and shear. For each analysis the corresponding values of wall shears were recorded at the top 30 drift values throughout the response history as presented in Figure 5.15 for a sample 6-story Archetype subject to one MCE level shaking. Maximum drifts typically occurred in one or two peak cycles for many of the ground motion records; therefore, the statistics generated for mean shear to peak drift are not necessarily meaningful (Figure 5.15). The ratio of wall shears at peak drifts ($V_{@dmax}$) to the peak shear (V_{max}) were assessed for eleven Archetypes of varying building height as shown in the distribution plot in Figure 5.16. Overall, the median ratios of $V_{@dmax}$ to V_{max} from the 44 records reduce as building height increases with median ratios ranging from about 0.5 for a 2-story building to about 0.2 for a 30-story building. However, since the maximum ratios of $V_{@dmax}$ to V_{max} from the 44 records are about 0.92 on average, it is not overly conservative to assume that peak wall shears occur simultaneously with peak drift.

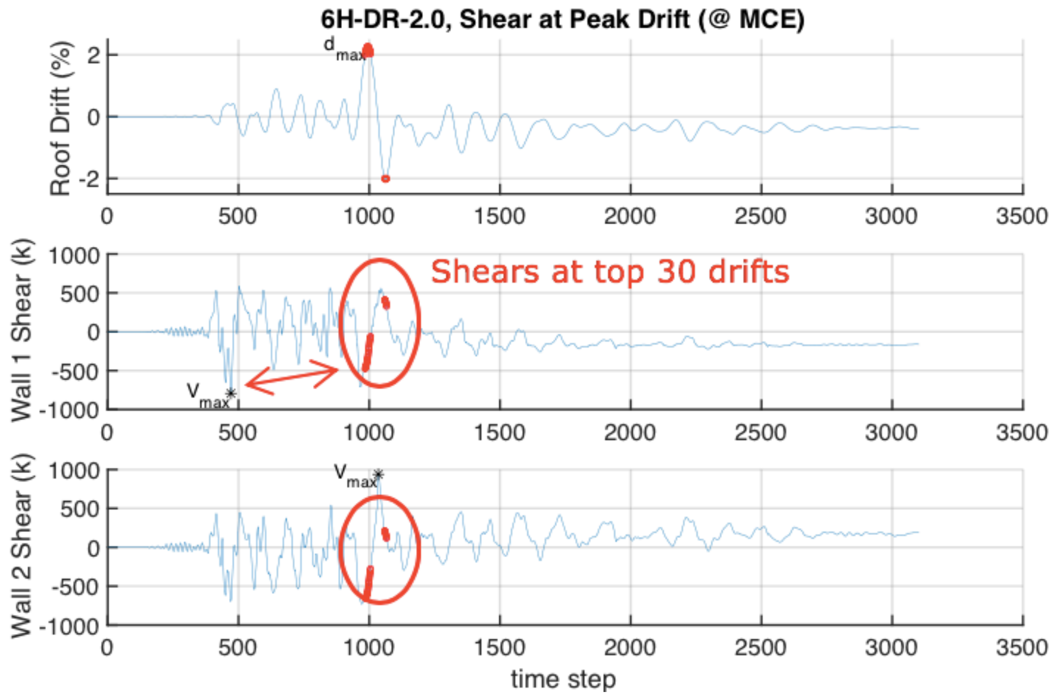

Figure 5.15: Shear at Peak Drift for Archetype 6H-DR-2.0

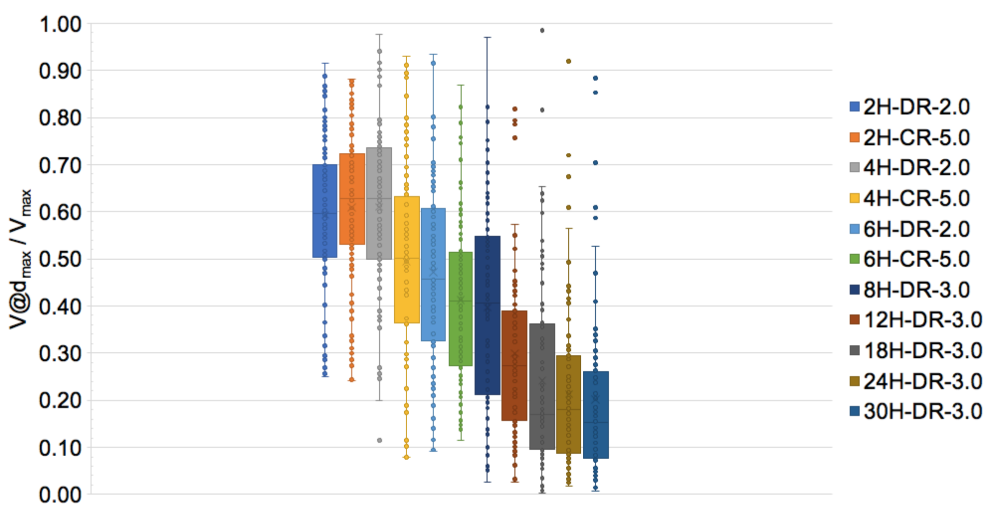

Figure 5.16: Ratio of $V_{@dmax}$ to Peak Shear for a subset of Archetypes

5.6 Summary of Analysis Results

A summary of the analysis results for all Archetypes is presented in Table 5-8. The results show that all 6 to 30 story Archetypes pass the FEMA P695 collapse acceptability criteria in efforts to help validate the use of $\boldsymbol{R} = 8$ for ductile coupled wall systems that are designed in conformance with the ASCE 7-16 and ACI 318-19 provisions.

It is noted that the ACMRs for the 6-, 8-, and 12-story Archetypes are very close to the acceptable ACMRs. This is a result of associated collapse with initiation of significant strength loss (deformation associated with a 20% drop from peak strength), which typically resulted in a drift capacity of around 3%. In prior studies, alternative definitions of collapse have been used based on consensus opinions. For example, in the NIST (2010) study, strength loss was modeled and collapse was defined as reaching a roof drift ratio of 5%. In this study, acceptable ACMRs were achieved despite using a conservative definition of collapse for flexural failures based on the drift capacity model. The actual probability of collapse is considerably smaller than suggested by comparing the computed ACMRs for a given Performance Group with the acceptable ACMR. It is noted that consideration of wall shear amplification also was critical to achieving acceptable ACMRs.

Table 5-8: Summary of Collapse Results for Ductile RC Coupled Wall Archetypes

Archetype ID	Pushover Results		IDA Results			Acceptability			
	Static Ω	μ_T	S_{MT} [T]	S_{CT} [T]	CMR	SSF	ACMR	Accept. ACMR	Pass /Fail
6H-DR-2.0	2.28	7.54	1.49	2.68	1.80	1.35	2.42	1.56	Pass
8H-DR-2.0	2.11	5.43	1.20	1.90	1.58	1.29	2.04		Pass
8H-DR-2.4	2.09	6.06		1.95	1.62	1.32	2.13		Pass
8H-DR-3.0	2.25	5.26		1.95	1.62	1.29	2.08		Pass
8H-DR-3.3	2.12	5.60		1.95	1.62	1.30	2.10		Pass
Mean:	**2.17**	**5.98**				**Mean:**	**2.16**	**1.96**	**Pass**
6H-CR-5.0	1.73	7.97	1.49	2.55	1.71	1.36	2.32	1.56	Pass
8H-CR-3.3	1.63	8.03	1.20	1.85	1.54	1.38	2.23		Pass
8H-CR-4.0	1.59	7.93		1.85	1.54	1.38	2.29		Pass
8H-CR-5.0	1.45	7.57		1.85	1.54	1.37	2.22		Pass
Mean:	**1.60**	**7.87**				**Mean:**	**2.27**	**1.96**	**Pass**
12H-DR-2.0	1.36	6.65	0.89	1.33	1.50	1.41	2.12	1.56	Pass
12H-DR-2.4	1.40	6.07		1.33	1.50	1.39	2.08		Pass
12H-DR-3.0	1.54	5.50		1.39	1.57	1.36	2.14		Pass
12H-DR-3.3	1.59	6.15		1.39	1.57	1.39	2.18		Pass
Mean:	**1.47**	**6.09**				**Mean:**	**2.13**	**1.96**	**Pass**
12H-CR-3.3	1.35	8.06	0.89	1.22	1.38	1.46	2.01	1.56	Pass
12H-CR-4.0	1.36	7.76		1.29	1.46	1.46	2.13		Pass
12H-CR-5.0	1.31	7.71		1.29	1.46	1.46	2.12		Pass
Mean:	**1.34**	**7.84**				**Mean:**	**2.09**	**1.96**	**Pass**
18H-DR-2.0	2.06	6.24	0.65	0.97	1.48	1.49	2.21	1.56	Pass
18H-DR-2.4	2.01	5.35		0.97	1.48	1.44	2.14		Pass
18H-DR-3.0	1.98	5.11		1.02	1.55	1.43	2.21		Pass
18H-DR-3.3	2.04	4.40		1.02	1.55	1.38	2.15		Pass
Mean:	**2.02**	5.28				**Mean:**	**2.18**	**1.96**	**Pass**
18H-CR-3.3	1.59	6.09	0.65	0.91	1.39	1.48	2.06	1.56	Pass
18H-CR-4.0	1.58	5.85		0.97	1.48	1.47	2.18		Pass
18H-CR-5.0	1.65	5.42		0.97	1.48	1.44	2.14		Pass
Mean:	**1.61**	5.79				**Mean:**	**2.13**	**1.96**	**Pass**
24H-DR-2.0	1.63	11.94	0.53	0.76	1.443	1.61	2.32	1.56	Pass
24H-DR-2.4	1.65	9.70		0.76	1.443	1.61	2.32		Pass
24H-DR-3.0	1.80	7.10		0.77	1.455	1.57	2.28		Pass
24H-DR-3.3	1.83	7.07		0.77	1.455	1.57	2.28		Pass
Mean:	**1.73**	8.95				**Mean:**	**2.30**	**1.96**	**Pass**
24H-CR-3.3	1.390	10.04	0.53	0.75	1.43	1.61	2.30	1.56	Pass
24H-CR-4.0	1.391	9.40		0.75	1.43	1.61	2.30		Pass
24H-CR-5.0	1.513	8.16		0.76	1.44	1.61	2.32		Pass
Mean:	**1.43**	9.20				**Mean:**	**2.31**	**1.96**	**Pass**
30H-DR-2.0	1.21	14.61	0.45	0.79	1.77	1.61	2.85	1.56	Pass
30H-DR-2.4	1.25	13.66		0.79	1.77	1.61	2.85		Pass
30H-DR-3.0	1.43	10.30		0.82	1.84	1.61	2.96		Pass
30H-DR-3.3	1.62	8.32		0.82	1.84	1.61	2.96		Pass
Mean:	**1.38**	11.72				**Mean:**	**2.91**	**1.96**	**Pass**
30H-CR-3.3	1.24	14.44	0.45	0.76	1.70	1.61	2.74	1.56	Pass
30H-CR-4.0	1.29	10.13		0.76	1.70	1.61	2.74		Pass
30H-CR-5.0	1.44	10.03		0.75	1.68	1.61	2.71		Pass
Mean:	**1.32**	11.53				**Mean:**	**2.73**	**1.96**	**Pass**

Chapter 6 - Additional Studies

Chapter 6 summarizes the findings from additional studies to address various additional items related to the study presented in the first five chapters.

6.1 D_{min} Archetypes

A select number of Archetypes have been designed for the seismic hazard level of D_{min} having spectral design values for S_{DS} and S_{D1} of 0.50g and 0.20g, respectively. This effort confirms that the D_{min} designs do not govern the collapse assessment by validating that their resulting collapse margin ratios exceed those of the D_{max} Archetype designs. A 12-story Archetype and a 24-story Archetype are assessed having coupling beam aspect ratio $l_n/h = 3$. The D_{min} Archetypes are based on the same design approach and basic floor plan layout as the D_{max} Archetypes except for having thinner and shorter wall piers due to reduced seismic demands.

Although seismic loading from high hazards (i.e., D_{max}) typically govern over wind loading, tall buildings subject to lower seismic hazard levels (i.e., D_{min}) may be governed by wind load considerations. FEMA P695 section 4.2.4 states that overstrength from non-seismic loading, that would not apply to all buildings everywhere (e.g., hurricane wind forces), should not be considered in the development of Archetype designs; only the 10 psf minimum wind load requirements of ASCE 7 (that are required for all structures) need be considered for the designs. Section 5.2.6 of FEMA P695 also states that, although it is not required to design Archetypes for wind loads, the lowest basic wind speed of ASCE 7 can be used for wind demands in cases where minimum values of wind load exceed seismic load. Based on input from the advisory panel, the lowest wind demand for checking member strengths for a typical design is the 700-year MRI 90mph wind speed from the ASCE 7-16 wind maps, and the lowest wind demand for checking drifts is the 10-year MRI 72 mph wind speed per ASCE 7-16 Figure CC.2-1. For the Archetypes considered in this study, member forces from the lowest wind demands of ASCE 7-16 were either less than or not significantly greater than the D_{min} seismic force demands; therefore, overstrength due to wind loading was not applied in the designs. However, the design of the D_{min} 24-story Archetype was established considering that story drifts due to wind loading not exceed a wind drift limit of h/400 (0.25 percent).

6.1.1 12-Story D_{min} Archetype Design

Design details of the 12-Story D_{min} Archetype with coupling beam aspect ratio l_n/h = 3.0 (12H-DR-3.0-D_{min}) are presented in this section. The design is governed by seismic forces (versus wind) and consists of planar wall piers that are 6 feet long and 12 in. thick and coupling beams that are 12 in. wide x 30 in. deep. The design concrete compression strength f'_c is 6 ksi. The fundamental period (T_1) of the building is 3.53 seconds, and the period for design (T) is the minimum of T_1 and C_uT_a = 1.088 seconds. With a seismic weight of 17,811 kips and governing seismic coefficient $C_s = (S_{D1}/T)/(R/I_e) = 0.023$, the base shear V_b is 411 kips. The maximum seismic story drifts presented in Figure 6.1 are less than the allowable drift of 2.0%, and no extreme torsional irregularity exists ($\Delta_{max}/\Delta_{avg} < 1.4$).

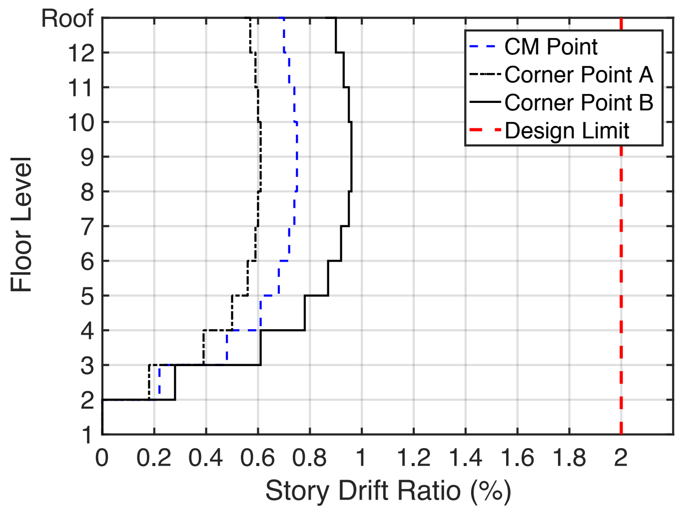

Figure 6.1: Archetype 12H-DR-3.0-D_{min} Story Drifts

Wall amplified shear stresses range from $2.3\sqrt{f'_c(psi)}$ at the upper levels to $4.6\sqrt{f'_c(psi)}$ at the lower levels. The peak axial stress at the wall base is $0.22A_gf'_c$ under the governing gravity load combination 1.2D+1.6L and $0.33A_gf'_c$ when seismic load effects are included under the governing load combination $(1.2+0.2S_{DS})$D+0.5L+1.0E. The governing net tension force is about $-0.23A_sf_y$ for the piers near the base of the wall. The design is governed by limiting the peak axial stress of the wall piers under the governing seismic load combination to about $0.3A_gf'_c$ following input from the advisory panel.

The wall shear reinforcement ratio (ρ_t) is designed to meet amplified shear demands (V_e) per the ACI 318-19 §18.10.3 code change proposal using 2 legs of #4 bars and ranges from 0.56% at the wall base to 0.28% at the upper levels, exceeding the ACI 318 code minimum reinforcement ratio of 0.25%. The contribution of shear strength from horizontal web reinforcement (V_s) is below the ACI 318 limit of $8\sqrt{f'_c}A_{cv}$ without having to increase the wall thickness any further.

The wall boundary longitudinal reinforcement (A_{sb}) is designed to have adequate strength just slightly greater than the factored demands. The detail for one wall pier at Level 1 showing the outer boundary (BE_1) and inner boundary (BE_2) longitudinal reinforcement as well as the corresponding *P-M* interaction surface is presented in Figure 6.2. *P-M* interaction section analysis is done at every level to compute the flexural strength and determine the maximum neutral axis depth of the wall.

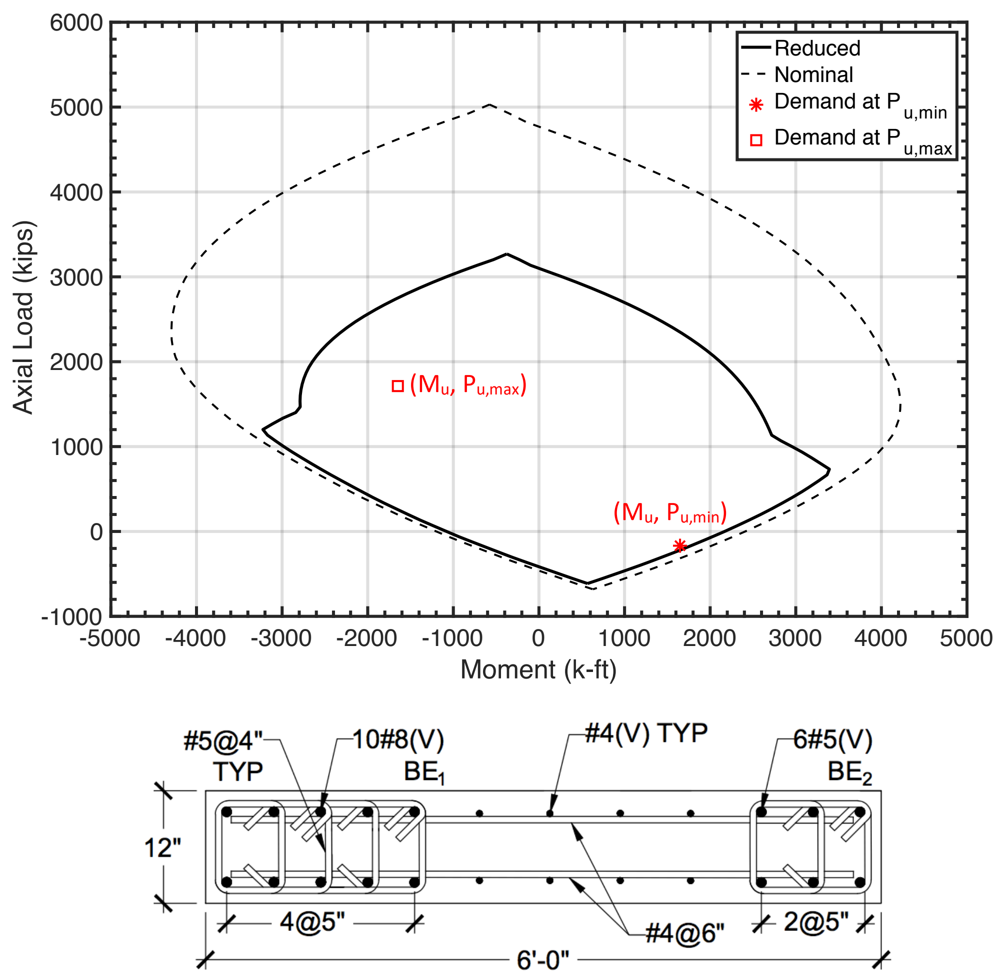

Figure 6.2: Archetype 12H-DR-3.0-D$_{min}$ Level 1 Wall *P-M* Interaction

The displacement-based approach of ACI 318 §18.10.6.2 is used to determine whether special boundary elements are required. At the wall base, since the maximum neutral axis depth c = 33 in. exceeds the limit $\ell_w/(600(1.5\delta_u/h_w))$ = 9.6 in., special boundary elements are required.

The length of the special boundary element (SBE) is 26 in., computed according to §18.10.6.4(a) as the maximum of $\{c\text{-}0.1\ell_w, c/2\}$. The SBE extends from the critical section at the base of the wall to the top of the first story, a height of 10 feet (i.e., $h_{SBE} \geq \max\{\ell_w, M/(3V)\} = 6$ ft). Boundary transverse reinforcement for the SBE consists of #5 ties spaced at 4 in. on center per ACI 318 §18.10.6.4(e) and (f). Moreover, where the boundary longitudinal reinforcement ratios above the SBE exceed the limit of $400/f_y$, ordinary boundary elements conforming to ACI 318 §18.10.6.5(a) are required at levels 2 through 8.

The 12-story D_{min} Archetype has a design drift capacity of 3.5 percent as computed per equation (2-4b) in Section 2.2 of this report.

The coupling beam and wall reinforcement details are summarized in

Table 6-1. Maximum coupling beam shear stresses range from 2 to 4 $\sqrt{f'_c(psi)}$ and do not exceed the code limit stress of $8.5\sqrt{f'_c(psi)}$. The degree of coupling is about 70 percent as computed using the seismic axial force couple due to overturning (T), the moment arm (l) between the center of the tension and compression piers, and the seismic moments M_1 and M_2 at the base of each wall pier:

$$DOC = \frac{Tl}{Tl + M_1 + M_2} = \frac{714\ kips\ (6' + 7.5')}{714\ k\ (6' + 7.5') + 3270\ k - ft} = 0.7$$

Table 6-1: Archetype12H-DR-3.0-D_{min} Design Summary

Level	Wall Shear Design			Wall Flexure Design				Coupling Beam Design		
	Wall f_v $V_e/(\sqrt{f'_c}A_v)$	Wall ρ_t (%)	Shear D/C	Outer A_{sb}	Middle A_{sb}	Inner A_{sb}	Flexure D/C	Diagonal Bars	Shear D/C	$V_u/(\sqrt{f'_c}\ A_g) < \varphi*10$
12	2.33	0.28	0.75	4#4	8#4	4#4	0.43	4#7	0.72	1.7
11	2.53	0.28	0.81	4#4	8#4	4#4	0.71	4#7	0.87	2.1
10	2.75	0.28	0.88	4#4	12#4	4#4	0.70	4#7	1.00	2.4
9	2.88	0.28	0.92	4#4	12#4	4#4	0.92	4#8	0.83	2.6
8	3.07	0.28	0.99	4#5	12#4	4#4	0.86	4#8	0.90	2.8
7	3.25	0.33	0.95	4#5	12#4	4#4	0.98	4#8	0.97	3.0
6	3.44	0.33	1.00	8#5	10#4	6#4	0.79	4#9	0.83	3.2
5	3.63	0.42	0.93	8#5	10#4	6#4	0.92	4#9	0.89	3.5
4	3.84	0.42	0.98	8#6	10#4	6#5	0.78	4#9	0.93	3.6
3	4.18	0.56	0.88	8#6	10#4	6#5	0.96	4#9	0.95	3.7
2	4.61	0.56	0.97	10#8	8#4	6#5	0.65	4#9	0.90	3.5
1	4.33	0.56	0.92	10#8	8#4	6#5	0.91	4#9	0.66	2.6

6.1.2 24-Story D_{min} Archetype Design

Design details of the 24-Story D_{min} Archetype with coupling beam aspect ratio l_n/h = 3.0 (24H-DR-3.0-D_{min}) are presented in this section. The design consists of flanged wall piers that are 8 feet in length with wall pier thickness that is 14 in. thick at the lower six levels and 12 in. thick at the upper eighteen levels. The concrete compression strength f'_c is 8 ksi. Although a design with 12 in. thick wall piers all along the building height had seismic story drifts less than 1% and wind story drifts less than 0.25%, the wall thickness at the lower six levels had to be increased from 12 in. to 14 in. to keep the wall nominal shear strength (V_n) below the $10\sqrt{f'_c}A_{cv}$ ACI 318 limit.

The fundamental mode of the building is torsional, with a period of 7.05 seconds, whereas the fundamental translational period is 4.80 seconds. The period for design (T) per ASCE 7-16 is the minimum of T_1 and C_uT_a = 1.829 seconds. With a seismic weight of 35,835 kips and the governing seismic coefficient is $C_s = 0.044S_{DS}I_e = 0.022$, the base shear V_b is 786 kips. The maximum story drifts are less than the maximum allowable value of 2.0%, and no extreme torsional irregularity exists ($\Delta_{max}/\Delta_{avg} < 1.4$).

The wall pier and coupling beam designs are summarized in Table 6-2. The coupling beams and flanged walls are designed as previously described in Section 2.2 including bi-directional effects and the impact of accidental torsion. The wall piers require special boundary elements throughout the entire wall length at the first story because the neutral axis depth far exceeds the limit $l_w/(600(1.5\delta_u/h_w))$. Boundary transverse reinforcement for the SBE consists of #5 ties spaced at 4 in. on center per ACI 318 §18.10.6.4(e) and (f). Moreover, at levels 1-9 where the longitudinal reinforcement ratio exceed the limit of $400/f_y$, confined ordinary boundary elements are required with transverse reinforcement conforming to ACI 318 §18.10.6.5.

The 24-story D_{min} Archetype has a design drift capacity of 2.9 percent as computed per equation (2-4b) in Section 2.2 of this report. Maximum coupling beam shear stresses range from 2 to $4.5\sqrt{f'_c(psi)}$ and do not exceed the code limit stress of $8.5\sqrt{f'_c(psi)}$. The degree of coupling is about 70 percent, computed using the seismic tensile force due to overturning (T) and the moments M_1 and M_2 at the base of each wall pier:

$$DOC = \frac{T(8' + 7.5')}{T(8' + 7.5') + M1 + M2} = \frac{1796\,kips\,(8' + 7.5')}{1796\,k\,(8' + 7.5') + 10644\,k - ft} = 0.72$$

Table 6-2: Archetype 24H-DR-3.0-D_{min} Design Summary

Level	Wall Shear Design			Wall Flexure Design		Coupling Beam Design		
	Wall f_v $V_e/(\sqrt{f'_c}A_v)$	Wall ρ_t (%)	Shear D/C	A_{sb}	Flexure D/C	Diagonal Bars	Shear D/C	$V_u/(\sqrt{f'_c}\,A_g) < \varphi*10$
24	2.49	0.28	0.86	2#4@12"	0.46	4#7	0.91	1.9
23	3.13	0.33	0.99	2#4@12"	0.56	4#8	0.79	2.1
22	3.85	0.57	0.88	2#4@12"	0.75	4#8	0.89	2.4
21	4.26	0.57	0.97	2#4@12"	0.98	4#8	0.98	2.6
20	4.46	0.73	0.86	2#5@12"	0.87	4#9	0.83	2.8
19	4.56	0.73	0.88	2#5@12"	0.99	4#9	0.88	3.0
18	4.70	0.73	0.91	2#6@12"	0.81	4#9	0.91	3.1
17	4.87	0.73	0.94	2#6@12"	0.84	4#9	0.95	3.2
16	5.04	0.73	0.97	2#6@12"	0.86	4#9	0.99	3.4
15	5.25	0.81	0.94	2#6@12"	0.89	4#10	0.82	3.5
14	5.38	0.81	0.96	2#6@12"	0.92	4#10	0.85	3.6
13	5.52	0.81	0.99	2#6@12"	0.94	4#10	0.88	3.8
12	5.72	0.92	0.94	2#6@12"	0.94	4#10	0.92	3.9
11	5.96	0.92	0.98	2#6@12"	0.95	4#10	0.96	4.1
10	6.23	1.00	0.95	2#6@12"	0.98	4#10	0.99	4.2
9	6.44	1.00	0.99	2#7@12"	0.83	4#11	0.84	4.4
8	6.61	1.11	0.93	2#7@12"	0.89	4#11	0.85	4.4
7	6.78	1.11	0.96	2#7@12"	0.97	4#11	0.85	4.5
6	6.10	1.07	0.89	2#7@9"	0.83	4#11	0.97	4.3
5	6.37	1.07	0.92	2#7@9"	0.91	4#11	0.95	4.3
4	6.66	1.07	0.97	2#9@9"	0.68	4#11	0.91	4.1
3	6.83	1.07	0.99	2#9@9"	0.83	4#11	0.84	3.7
2	6.89	1.07	1.00	2#11@9"	0.71	4#11	0.69	3.1
1	6.42	1.07	0.93	2#11@9"	0.93	4#11	0.45	2.0

6.1.3 Analysis Results of D_{min} Archetypes

Analysis results of the D_{min} Archetypes are presented in Table 6-3 confirming that the D_{max} Archetypes govern the collapse assessment since they have much lower ACMRs than the D_{min} Archetypes. The sample CMR plot for the 12-story Archetype in Figure 6.3 also demonstrates that the median collapse intensity (S_{CT}) is almost three times the spectral intensity at MCE (S_{MT}), and the ACMR that is twice that of the D_{max} Archetype.

Table 6-3: Pushover analysis and IDA results of D_{min} Archetypes

Archetype ID	Pushover Results		IDA Results			Acceptability			
	Static Ω	μ_T	S_{MT} [T]	S_{CT} [T]	CMR	SSF	ACMR	Accept. $ACMR_{10}$	Pass /Fail
12H-3.0-D_{max}	1.61	5.46	0.89	1.33	1.50	1.36	2.03	1.96	Pass
12H-3.0-D_{min}	1.32	9.36	0.28	0.76	2.76	1.46	**4.02**		Pass
24H-3.0-D_{max}	1.69	8.35	0.53	0.75	1.42	1.61	2.29	1.96	Pass
24H-3.0-D_{min}	1.37	9.14	0.16	0.53	3.31	1.57	**5.20**		Pass

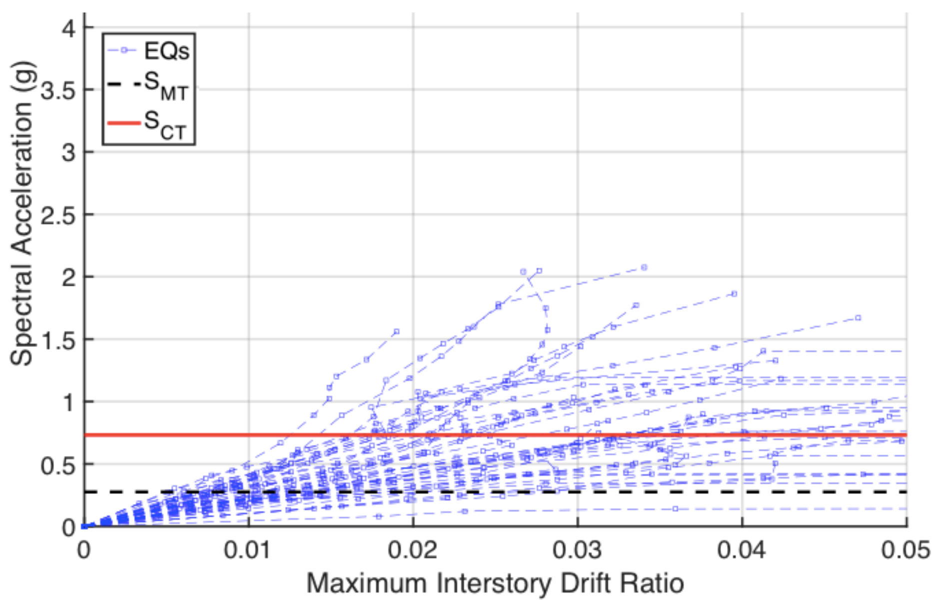

Figure 6.3: Archetype 12H-DR-3.0-D_{min} CMR Plot

6.2 Uncoupled Shear Wall System

Given the new design requirements for special structural walls approved for ACI 318-19, and the prior FEMA P695 study on isolated cantilever walls (NIST, 2010), a limited study was undertaken to compare ACMRs from the current study with similar archetypes but with cantilever walls. The 12-story coupled wall Archetype with coupling beam aspect ratio $l_n/h = 3.0$ (12H-DR-3.0) designed for seismicity D_{max} is revised to a cantilever uncoupled shear wall lateral system of comparable height and plan configuration by removing the coupling beams as shown in the plan view of Figure 6.4 (a). The uncoupled wall system is then analyzed with a nonlinear OpenSees model similar to that of the coupled wall model, except with just one wall pier connected to a P-delta column as shown in Figure 6.4 (b).

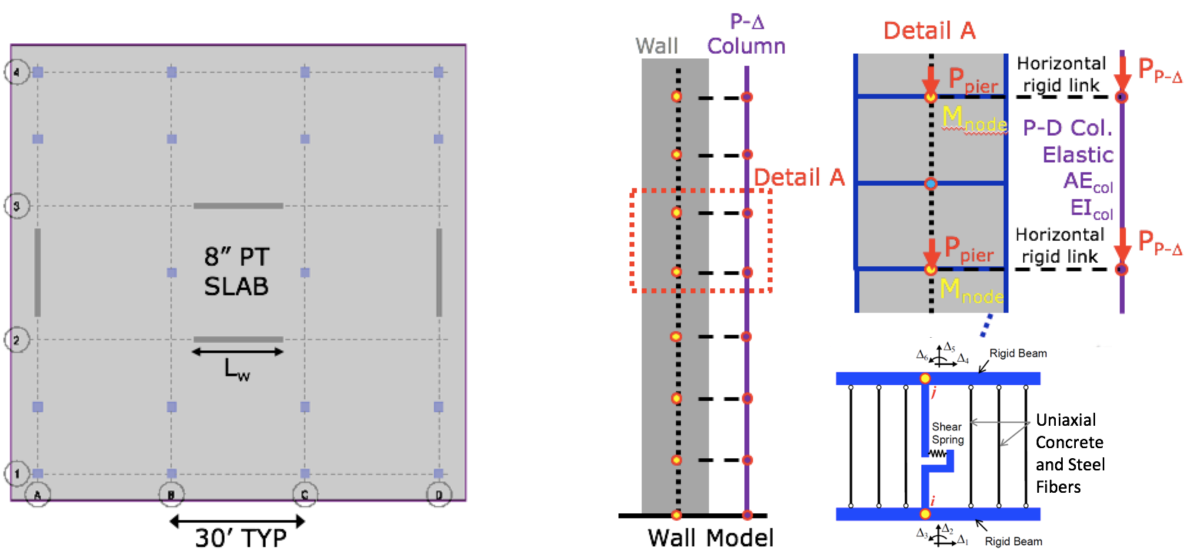

(a) Plan View of Archetype Building **(b) Elevation View of Wall Model**

Figure 6.4: 12-Story Uncoupled Wall Archetype

The uncoupled wall Archetype is designed using $\boldsymbol{R} = 6$ and $\boldsymbol{C_d} = 5$ (versus using $\boldsymbol{R} = \boldsymbol{C_d} = 8$ for the coupled wall system) subject to the same code provisions as the coupled wall Archetypes including the drift capacity check and designing the wall horizontal reinforcement for amplified shear demands. The most efficient wall length and thickness dimensions are selected in efforts to develop a design that would govern the collapse assessment. Both an ELF and a RSA design were considered with 23 ft long wall piers for the ELF design and a shorter wall length of 20 ft for the RSA design due to reduced RSA drift demands. Both the ELF and RSA Archetypes have maximum design wall neutral axis depths of about 30% of the wall length and relatively high amplified wall shear demands close to the ACI 318 shear stress limits. The drift capacities computed per equation (2-4b) in Section 2.2 of the report are 2.37% and 2.27% for the ELF and RSA designs, respectively. Details of the ELF and RSA designs are presented in Table 6-4.

Table 6-4: Design Summary of 12-Story Uncoupled Wall Archetype

ELF Design

Level	t_w (in.)	Wall Shear Design				Wall Flexure Design		
		Wall f_v $V_u/(\sqrt{f'_c}A_v)$	Wall f_v $V_e/(\sqrt{f'_c}A_v)$	Wall ρ_t (%)	Shear D/C	Boundary A_{sb}	Middle A_{sb}	Flexure D/C
12	12	0.62	1.57	0.28	0.28	6#4	40#4	0.22
11	12	1.21	3.09	0.28	0.28	6#4	40#4	0.57
10	12	1.74	4.44	0.74	0.74	10#5	44#5	0.64
9	12	2.20	5.62	0.74	0.74	10#5	44#5	0.98
8	12	2.60	6.64	1.03	1.03	12#9	46#6	0.74
7	12	2.94	7.50	1.03	1.03	12#9	46#6	0.98
6	14	2.76	7.03	1.03	1.03	18#10	50#7	0.81
5	14	2.94	7.50	1.03	1.03	18#10	50#7	0.99
4	18	2.40	6.11	0.83	0.83	36#10	38#7	0.83
3	18	2.47	6.29	0.83	0.83	36#10	38#7	0.96
2	18	2.50	6.37	0.83	0.83	36#11	38#10	0.85
1	18	2.50	6.36	0.83	0.83	36#11	38#10	0.95

RSA Design

Level	t_w (in.)	Wall Shear Design				Wall Flexure Design		
		Wall f_v $V_u/(\sqrt{f'_c}A_v)$	Wall f_v $V_e/(\sqrt{f'_c}A_v)$	Wall ρ_t (%)	Shear D/C	Boundary A_{sb}	Middle A_{sb}	Flexure D/C
12	12	1.06	2.70	0.52	0.60	10#4	38#4	0.32
11	12	1.69	4.30	0.52	0.96	10#4	38#4	0.82
10	12	1.95	4.97	0.65	0.95	10#7	38#5	0.74
9	12	2.03	5.19	0.65	0.99	10#7	38#5	0.99
8	12	2.10	5.35	0.73	0.93	16#8	34#6	0.82
7	12	2.25	5.75	0.73	1.00	16#8	34#6	0.96
6	12	2.55	6.50	0.92	0.95	16#10	34#7	0.80
5	12	2.94	7.50	1.03	1.00	16#10	34#7	0.91
4	16	2.52	6.42	0.92	0.94	22#10	30#8	0.84
3	16	2.81	7.15	1.03	0.95	22#10	30#8	0.97
2	16	3.01	7.67	1.03	1.0	22#11	30#11	0.87
1	16	3.08	7.84	1.03	1.0	22#11	30#11	0.99

As this study aims to compare the collapse results of uncoupled versus coupled walls, nonlinear pushover analyses and IDAs were performed using consistent failure criteria and designs based on the new ACI 318-19 provisions. Although the collapse performance of structural walls has been assessed in previous studies, this study employs a systematic evaluation approach with failure criteria that are based on the more recent findings from earthquakes and experimental databases. In the NIST GCR 10-917-8 (NIST, 2010) study on special reinforced concrete shear walls, "collapse" was defined when the IDA reached a drift of 5%, based on consensus opinion of the ATC 76 project team and observations that collapse of buildings with structural walls has rarely been observed following strong earthquake shaking. For this study, roof drift values at strength loss, used to conservatively define collapse for flexural failure, were about 3%. Also, shear failures for this study are less likely than in the 2010 study due to consideration of wall shear amplification.

IDA results indicate that when consistent design and collapse assessment criteria are used, the 12-story Ductile Coupled Wall Archetype has higher median collapse intensity and ACMR values than the comparable uncoupled wall Archetypes (see Table 6-5). Using the failure criteria in this study, the uncoupled Archetypes pass the FEMA P695 20% probability of collapse acceptability criteria, but the ACMR values fall slightly below the 10% probability of collapse acceptability. The results of this limited study suggest that studies of cantilever wall Archetypes are very likely to produce a higher R-value than currently used for many designs (i.e., ***R*** = 5).

However, for a more comprehensive study, a less conservative criteria for flexural failures and collapse may be required to produce acceptable ACMRs.

Table 6-5: IDA results of Uncoupled Wall Archetypes

Archetype ID	IDA Results					Acceptability	
	S_{MT} [T]	S_{CT} [T]	CMR	SSF	**ACMR**	$ACMR_{20}$	$ACMR_{10}$
CW-12H-DR-3.0	0.89	1.33	1.50	1.36	2.03	> 1.56, Pass	> 1.96, Pass
SW-12H-RSA		1.19	1.34	1.36	**1.82**	> 1.56, Pass	< 1.96, Fail
SW-12H-ELF		1.26	1.42	1.32	**1.87**	> 1.56, Pass	< 1.96, Fail

When the uncoupled Archetypes are designed for shear amplification, the median collapse intensity values are at a ground motion scaling factor exceeding the MCE level shaking; at MCE only 12 of 44 records reach failure (namely, flexural failures at about 2% drift). Moreover, it is interesting to note that if the uncoupled Archetypes had not been designed for amplified shear demands, about 30% of records (14 out of 44) would reach failure at DE level shaking whereas 80% of records would reach failure at MCE level shaking due to a high number of shear failures.

6.3 Low-rise Archetypes

In the initial study, use of coupled walls for buildings shorter than 8-stories was not viewed as practical; however, several Archetypes with fewer stories were studied for completeness. Two sets of Archetypes were studied, i.e., one set of 6- and 4-story Archetypes having a consistent floor plan as the 8 to 30 story coupled wall Archetypes, and a second set of 2-story Archetypes with an enlarged floor plan to increase wall shear demands close to ACI 318 limits. Design details and analysis results for the low-rise Archetypes are presented in the following subsections.

6.3.1 6- and 4-Story Archetypes

The performance of the 6- and 4-story Archetypes were studied following the same design and analysis approach as before using the same floor loading and building floor plan with two sets of coupled walls in each principal building direction. The Archetype variations include designs with coupling beam aspect ratios (ℓ_n/h) of 2.0 and 5.0. The Archetype design details are summarized in Table 6-6 and in the Appendix, and a sample wall detail is presented in Figure 6.5. The wall piers are optimally designed to be as thin and short as possible with amplified shear stresses ranging from about 6 to $7.4\sqrt{f_c'}A_{cv}$ (close to ACI 318 limits) and wall drift capacities in the range of 3 percent. The coupling beam shear stresses range from about 4 to $7\sqrt{f_c'}A_{cv}$ with a trend of decreasing shear stress with decreasing building height and coupling beam aspect ratio. The degree of coupling (DOC) of the coupled wall system is lower than the DOC of the taller Archetypes and decreases for the designs with conventionally reinforced coupling beams.

Table 6-6: Design summary of the 6- and 4-story Archetypes

Archetype	l_w (ft)	t_w (in.)	Wall c_{max}	Wall $V_{e,max}$	Wall $P_{u,max}$	CB $V_{u,max}$	δ_c/h_w	DOC
6H-DR-2.0	8	L1-4: 14 L5-6: 10	0.42 l_w	$7.4\sqrt{f'_c}A_{cv}$	0.28 $A_gf'_c$ P_D =0.1$A_gf'_c$	$7.1\sqrt{f'_c}A_{cv}$	2.93%	0.60
6H-CR-5.0			0.34 l_w	$6.9\sqrt{f'_c}A_{cv}$	0.23 $A_gf'_c$ P_D =0.1$A_gf'_c$	$5.2\sqrt{f'_c}A_{cv}$	3.03%	0.49
4H-DR-2.0	7	12	0.32 l_w	$6.3\sqrt{f'_c}A_{cv}$	0.21 $A_gf'_c$ P_D =.08$A_gf'_c$	$5.4\sqrt{f'_c}A_{cv}$	3.10%	0.54
4H-CR-5.0			0.30 l_w	$5.7\sqrt{f'_c}A_{cv}$	0.17 $A_gf'_c$ P_D =.09$A_gf'_c$	$3.7\sqrt{f'_c}A_{cv}$	3.18%	0.43

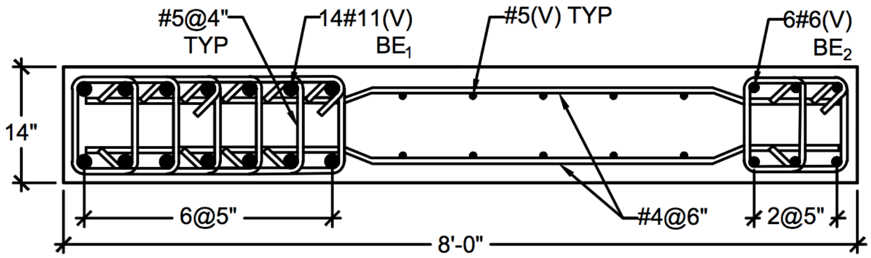

Figure 6.5: Archetype 6H-DR-2.0 Level 1 Wall Detail

The analysis results for these Archetypes are summarized in Table 6-7. Although the degree of coupling is lower for the 4 and 6-story low-rise Archetypes, they still meet the FEMA P695 acceptability criteria with ACMRs exceeding the 10% probability of collapse acceptable ACMR.

Table 6-7: Analysis results of the 6- and 4-story Archetypes

Archetype	**Ω_0**	**μ_T**	**S_{MT}**	**S_{CT}**	**Failures**	**ACMR**	**$ACMR_{20}$**	**$ACMR_{10}$**
6H-DR-2.0	2.28	7.54	1.49	2.68	19 Flexure 2 Shear	2.42	> 1.56	> 1.96
6H-CR-5.0	1.73	7.97	1.49	2.55	20 Flexure 0 Shear	2.32	> 1.56	> 1.96
4H-DR-2.0	2.49	10.5	1.50	3.19	18 Flexure 3 Shear	2.83	> 1.56	> 1.96
4H-CR-5.0	1.86	11.3	1.50	2.73	19 Flexure 1 Shear	2.42	> 1.56	> 1.96

For theses low-rise Archetypes, alternative collapse criteria could have been considered, e.g., defining collapse to occur at 5 percent drift, thus resulting in higher ACMRs. However, given the low degree of coupling for the low-rise Archetypes, the impact of considering different collapse criteria was not studied, and instead a minimum height of 60 feet is proposed for a Ductile Coupled Wall in ASCE 7 to ensure adequate degree of coupling and significant energy dissipation provided by the coupling beams.

6.3.2 2-Story Archetypes

The collapse performance of two additional 2-story Archetypes were assessed using the same design and analysis approach used before. However, instead of optimizing the length of the wall piers to be as short as possible, the wall pier lengths were established as 10 feet at the minimum allowable height to length ratio from the definition of a Ductile Coupled Wall, i.e., $h_{wcs}/\ell_w = 2.0$ intended to promote wall flexural yielding versus abrupt failure modes. In order to increase the wall shear stress demands to be close to the ACI limiting design value of $8\sqrt{f_c'}A_{cv}$, the building seismic weight was increased by increasing the floor area by a factor of almost 4 compared to the taller Archetypes as shown in Figure 6.6; the superimposed dead load also was increased to 50 psf compared to the typical 25 psf for the taller Archetypes. The designs with this wall length represent the worst-case 2-story Ductile Coupled Wall system that can be designed.

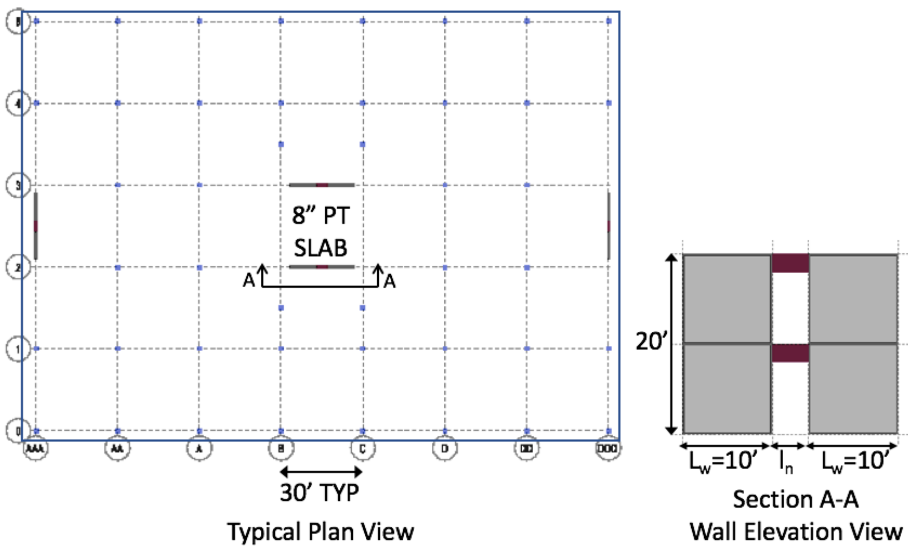

Figure 6.6: 2-Story Archetype Floor Plan and Elevation View

The 2-story Archetype variations include designs with coupling beam aspect ratios (ℓ_n/h) of 2.0 and 5.0. The design details of the Archetypes are summarized in Table 6-8 and the Appendix. The 10 foot long wall piers are 10 in. thick with amplified shear stresses of about $6.5\sqrt{f_c'}A_{cv}$ (close to ACI 318 limits) and wall drift capacities of about 2.7 percent. The maximum coupling beam shear stresses are $5.7\sqrt{f_c'}A_{cv}$ for the design with $\ell_n/h = 2$ but only $3.4\sqrt{f'_c}A_{cv}$ for the design with $\ell_n/h = 5$. The degree of coupling (DOC) of the coupled wall system is significantly lower than the DOC of the taller Archetypes, especially for the design with conventionally reinforced coupling beams ($\ell_n/h = 5$) for which the DOC is only about 10 percent.

Table 6-8: Design summary of the 2-story Archetypes

Archetype	l_w (ft)	t_w (in.)	Wall c_{max}	Wall $V_{e,max}$	Wall $P_{u,max}$	CB $V_{u,max}$	δ_c/h_w	DOC
2H-DR-2.0	10	10	0.25 l_w	$6.5\sqrt{f'_c}A_{cv}$	$0.10\ A_g f'_c$ $P_D = 0.05 A_g f'_c$	$5.7\sqrt{f'_c}A_{cv}$	2.63%	0.23
2H-CR-5.0			0.23 l_w	$6.4\sqrt{f'_c}A_{cv}$	$0.09\ A_g f'_c$ $P_D = 0.05 A_g f'_c$	$3.4\sqrt{f'_c}A_{cv}$	2.70%	0.11

Pushover analysis results presented in Figure 6.7 demonstrate the onset of strength loss begins at roof drift values of about 2 to 2.4 percent for the 2-story Archetypes as compared to values closer to 3% for the taller Archetypes. Although the degree of coupling is low for the 2-story Archetypes, analysis results presented in

Table 6-9 indicate that the ACMRs meet the 20% probability of collapse acceptability criteria; however, if the 2-story Archetypes are grouped into their own performance group, they would not pass the 10% probability of collapse acceptability criteria. These 2-story Archetypes experience shear failures for more ground motion records than the taller Archetypes do; moreover, the records that experience shear failures typically have flexural failures around the same time step in the nonlinear response history.

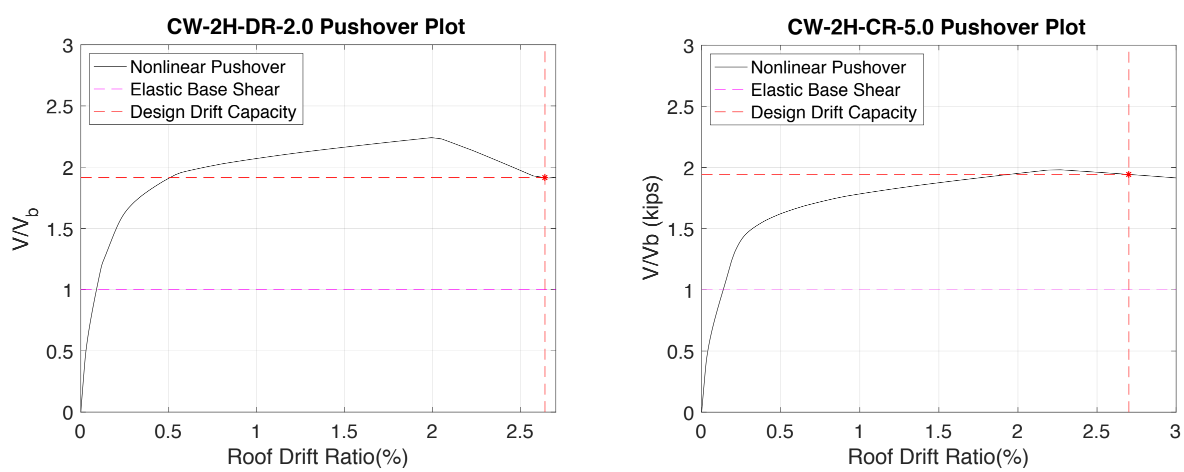

Figure 6.7: 2-Story Archetype pushover analysis results

The use of alternative collapse criteria defining failure at 5% drift would have resulted in higher ACMRs within the FEMA P695 acceptability range. However, given the lower degree of coupling from design and the lower ACMRs obtained from analysis results reinforce the consensus to set a minimum height of 60 feet in ASCE 7 for Ductile Coupled Walls to ensure adequate participation of the coupling beams in the energy dissipation mechanism of the system.

Table 6-9: Analysis results of the 2-story Archetypes

Archetype	**Ω_0**	**μ_T**	**S_{MT}**	**S_{CT}**	**Failures**	**ACMR**	**$ACMR_{20}$**	**$ACMR_{10}$**
2H-DR-2.0	2.24	> 8	1.50	2.11	13 Flexure 9 Shear	1.87	> 1.56	< 1.96
2H-CR-5.0	2.00	> 8	1.50	1.95	9 Flexure 13 Shear	1.73	> 1.56	< 1.96

IDA Results	**2H-DR-2.0**				**2H-CR-5.0**			
EQ	SF = 2.7, Dir1		SF = 2.7, Dir2		SF = 2.7, Dir1		SF = 2.7, Dir2	
	Flexure	Shear	Flexure	Shear	Flexure	Shear	Flexure	Shear
1	969	969	977	988	971	970	980	979
2	584	NaN	593	591	586	NaN	595	591
3	NaN	NaN	1192	1191	NaN	NaN	1197	1191
4	NaN	NaN	752	NaN	NaN	NaN	756	NaN
5	NaN	NaN	3148	NaN	NaN	NaN	3146	NaN
6	NaN	NaN	NaN	NaN	NaN	NaN	NaN	NaN
7	1149	NaN	900	NaN	1161	NaN	NaN	NaN
8	NaN	NaN	NaN	NaN	NaN	1596	NaN	NaN
9	NaN	NaN	NaN	NaN	NaN	NaN	1736	NaN
10	NaN	NaN	NaN	NaN	NaN	NaN	NaN	NaN
11	921	920	NaN	NaN	922	921	NaN	NaN
12	NaN	NaN	5192	6271	NaN	NaN	5195	6276
13	1831	NaN	NaN	NaN	1829	1818	NaN	NaN
14	NaN	1077	1090	NaN	NaN	1077	1090	1092
15	NaN	NaN	636	610	NaN	NaN	637	610
16	2743	2739	NaN	NaN	2748	2739	NaN	NaN
17	740	NaN	NaN	NaN	742	NaN	NaN	NaN
18	386	NaN	NaN	NaN	386	393	NaN	NaN
19	NaN	NaN	NaN	NaN	NaN	NaN	NaN	NaN
20	9175	NaN	9124	9043	NaN	NaN	9140	9043
21	624	615	NaN	NaN	625	568	NaN	NaN
22	NaN	NaN	900	898	NaN	NaN	907	894
# Failures:	7	4	6	5	4	7	5	6
Result:	**22**	GMs fail	→ 50%	fail	**22**	GMs fail	→ 50%	fail

6.4 Sensitivity studies with Shear-Flexure Interaction effects

A preliminary study was done to assess a subset of Archetypes using the model capturing shear-flexure interaction effects (SFI-MVLEM) developed by Kolozvari et al. (2018) as described in section 3.1.2 in order to compare results with those of the uncoupled MVLEM which instead used an elastic horizonal spring with an effective shear stiffness of 0.5G. The model with SFI effects uses an evolving shear stiffness that allows coupling of wall axial/flexural and nonlinear shear behavior. Incorporating SFI can better predict the distribution of wall shear demands and tends to result in reduced wall shears and higher interstory drifts than predicted with an uncoupled model.

Two Archetypes are assessed considering SFI effects, namely the 8 and 12-story buildings with coupling beam aspect ratio $l_n/h = 3.0$. Nonlinear pushover results, as presented in Figure 6.8 for the 8-story Archetype, indicate that including Shear-Flexure interaction effects captures a decrease in shear at the base of the tension pier but an increase in shear at the base of the compression pier. Moreover, capturing SFI effects reduces the strains at the wall extreme fibers (as shown with the dashed lines in Figure 6.9) due to capturing nonlinear shear deformations. Although the reduction in the wall shear demand is typically in the range of 15 to 20 percent, the effects on neutral axis depth, axial load, and wall shear responses can result in a reduced ACMR compared to an uncoupled model.

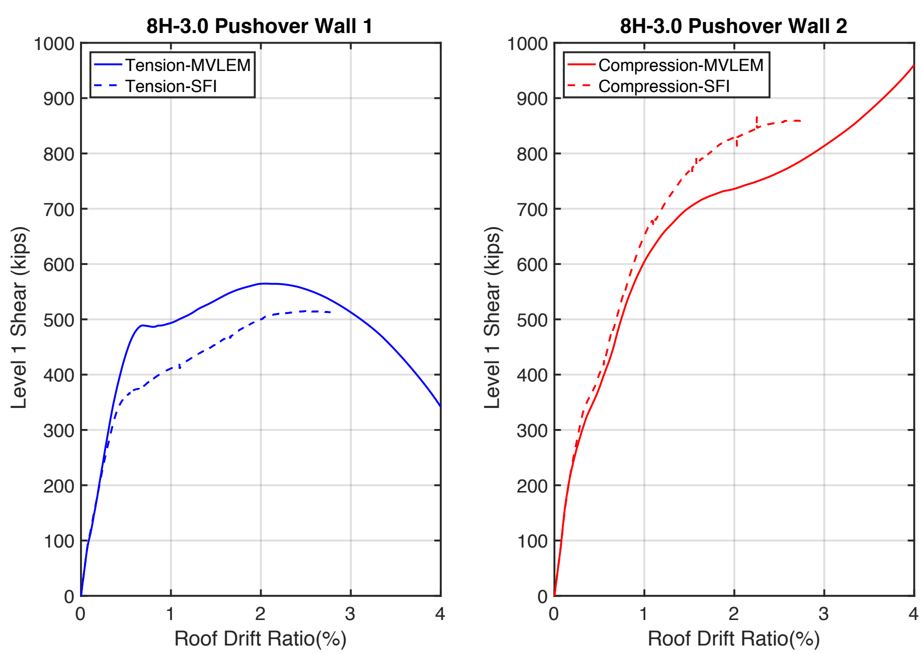

Figure 6.8: Wall shears with SFI effects for Archetype 8H-DR-3.0

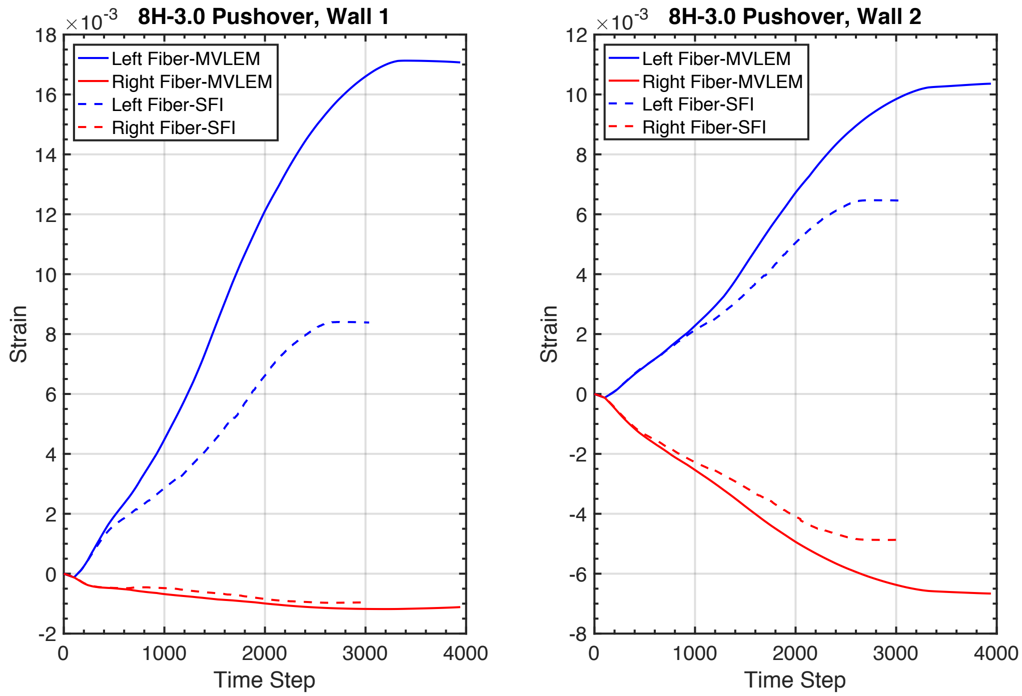

Figure 6.9: Wall strains with SFI effects for Archetype 8H-DR-3.0

Preliminary IDA results for the 8- and 12-story Archetypes suggest that reduced wall shears and tensile strains predicted with the SFI model lead to the Archetypes having slightly higher drift capacities and therefore slightly higher collapse margin ratios. Moreover, reduced wall shear demands predicted with the SFI model due to nonlinear shear deformations lead to slightly fewer shear failures experienced. Although nonlinear shear deformations predicted using the SFI model are larger than those of the MVLEM with linear elastic shear behavior, higher occurrences of shear failures are not predicted. For these particular 8 and 12 story Archetypes, the increase in the median collapse intensity and collapse margin ratio considering SFI effects is not greater than 5 percent. The small difference in ACMR is due to the fact that the Archetypes considered in this study are designed for amplified shear demands, have lower probabilities of shear failures as their collapse potential is captured mostly through the drift capacity model. However, prior nonlinear dynamic studies comparing the MVLEM and SFI-MVLEM for walls showed that neglecting SFI effects underestimates the interstory drift and overestimates the shear demand by up to 30 percent due to underestimating nonlinear shear deformations (Kolozvari et. al, 2018). Additional future studies are warranted to assess the extent of increase in ACMR of more coupled wall Archetypes (including taller Archetypes) and to assess the impact of varying failure criteria.

Chapter 7 - Summary and Conclusions

This study presents an application of the FEMA P695 methodology in efforts to propose appropriate values for seismic response modification factors for Reinforced Concrete Ductile Coupled Walls, as defined in ACI 318-19. A series of forty-one coupled wall Archetype buildings are designed for Seismic Design Category hazard D_{max} as defined in FEMA P695 in conformance with the most recent code provisions of ASCE 7-16 and ACI 318-19. The Archetypes considered address a range of variables expected to influence the collapse margin ratio, with primary variables of building height (i.e., 6, 8, 12, 18, 24, and 30 stories), wall cross section (i.e., planar and flanged walls), coupling beam aspect ratio (ln/h) ranging from 2.0 to 5.0, and coupling beam reinforcement arrangement (i.e., diagonally and conventionally reinforced). The range of variables are chosen considering those used to define a Ductile Coupled Wall system in ACI 318-19, as noted above. Archetypes with similar characteristics are assigned to Performance Groups.

Important design considerations include using a drift capacity model to verify the wall piers have sufficient drift capacity to resist Design Earthquake (DE) demands with a low (roughly 10%) probability of strength loss and applying wall shear force amplification to reduce the likelihood of shear failure with an approach similar to that used in the New Zealand NZ 3101 code. Wall shear amplification is applied because preliminary analysis results indicated that Archetypes, using $\boldsymbol{R} = \boldsymbol{C_d} = 8$ and designed conforming to ACI 318-14 shear provisions, did not meet the FEMA P695 acceptability criteria due to a high number of shear failures experienced during incremental dynamic analysis. Both of these design requirements, the wall drift capacity check and wall shear amplification, have been approved and will appear in ACI 318-19.

Two-dimensional nonlinear models are created for each Archetype with the OpenSees computational platform in which fiber elements with uniaxial material relations and linear shear springs are used to model the wall piers, while beam-column elements and nonlinear shear springs are used to model the coupling beams. Seismic weight is assigned at the element nodes at each story level, while gravity loads tributary to the wall are assigned at the same nodes. P-delta effects are considered by using a column with zero lateral stiffness. The modeling approaches used for the structural elements are validated with experimental data from isolated wall tests, isolated coupling beam tests, and from a 12-story coupled wall test. Three primary failure modes are considered to capture lateral strength loss and collapse, i.e., 1) flexural failure (crushing of concrete, buckling of rebar, tensile fracture of longitudinal reinforcement) is assessed using a statistical drift capacity model developed based on an extensive database of wall tests, 2) shear failure (diagonal tension/compression) is based on the relationship between wall shear force versus tensile strain of wall longitudinal reinforcement based on LATBSDC (2017) recommendations, and 3) axial failure is estimated using a shear-friction model. For this study, collapse is defined as being associated with either flexure or shear, i.e., the axial failure model did not govern because the lateral drift values at axial failure generally exceed 5% and have not been verified (although collapse of buildings with reinforced concrete walls has rarely been reported following strong earthquakes). Overall, the criteria used for collapse assessment in this study are conservative since the failure models predict the onset of strength loss (as a 20 percent drop in lateral strength) and not necessarily collapse. This approach is conservative because loss of axial load carrying capacity typically does not occur until lateral strength drops to near zero. In some studies, axial failure has been assumed to occur at a specified roof drift ratio, which has been typically defined as 4 to 5% (NIST GCR-10-917-8), whereas, in this study, the conservative approach used resulted in drift ratios at failure that were typically not more than about 3%.

Nonlinear static pushover (NSP) analyses and incremental dynamic analyses (IDA) using the 44 far-field ground motion records defined in Appendix A.9 of FEMA P695 are conducted for each Archetype. The pushover analysis is used to obtain an estimate of the system overstrength factor ($\boldsymbol{\Omega_0}$) and system ductility (μ_T), whereas IDA results are used to determine the median collapse intensity and collapse margin ratio for each Archetype. Uncertainties associated with ground motion records (β_{RTR}=0.4), code design requirements (β_{DR}=0.2), available test data (β_{TD}=0.2), and computational modeling approaches (β_{MDL}=0.2) are estimated to determine a total system uncertainty value of about 0.525 per FEMA P695 Table 7.2a. Based on this total system uncertainty value of 0.525, the acceptable adjusted collapse margin ratios as specified in FEMA P695 Table 7-3 are 1.56 for each Archetype and 1.96 for the mean of each performance group.

Because shear amplification of ASCE 7-16 wall demands (with factors ranging from 2.35 to 2.7) is applied in design, shear failures are mostly suppressed, and flexure-related collapse is typically defined by the drift capacity model for most Archetypes. Analysis results indicate that the most common collapse mode for Archetypes with diagonally-reinforced coupling beams is flexural compression failure at the base of each of the wall piers. This is generally the case for the 8- and 12-story Archetypes, where very few wall shear failures are observed due to the design for amplified wall shear demands. For the taller, flanged wall Archetypes, higher ACMRs are observed relative to the 8 and 12-story Archetypes, with failure defined by either flexure or shear failure, possibly because a wall shear amplification value of 2.7 is applied for the design of the taller Archetypes. The Archetypes designed with conventionally-reinforced coupling beams generally experience strength degradation at lower drifts and have lower ACMRs than the Archetypes with diagonally-reinforced coupling beams due to the lower coupling beam rotation capacity at strength loss.

As a result of this study, a system overstrength factor of $\boldsymbol{\Omega_0}$ = 2.5 is proposed based on nonlinear static pushover analysis results indicating that mean overstrength values of the performance groups range from 1.3 and 2.2. The proposed response modification factor $\boldsymbol{R}$ = 8 is validated based on incremental dynamic analysis results indicating that mean Adjusted Collapse Margin Ratio values of the performance groups range from 2.09 to 2.91 corresponding to collapse probabilities of less than ten percent based on using a conservative definition of collapse as noted in the prior paragraph. The deflection amplification factor of $\boldsymbol{C_d}$ = 8 is proposed based on damping considerations and the assessment of median roof drift responses from DE level shaking compared to design roof drifts. A minimum height limit of 60 feet is recommended for Ductile Coupled Wall systems with the proposed seismic response parameters to be adopted in ASCE 7 because coupled walls are generally not efficient lateral force-resisting systems for shorter buildings. Overall, results of this study suggest that an overstrength factor of $\boldsymbol{\Omega_0}$ = 2.5, a response modification factor $\boldsymbol{R}$ = 8, and a deflection amplification factor of $\boldsymbol{C_d}$ = 8 are appropriate seismic design parameters for RC Ductile Coupled Wall systems that are designed per ASCE 7-16 and ACI 318-19 provisions.

Appendix

Notes: l_w is the wall length, t_w is the wall thickness, and A_{sb} is the wall longitudinal reinforcement in the Outer, Web, and Inner segments of a wall pier; l_n is the clear span of the coupling beam and h is the total depth of the coupling beam section; coupling beam width is the same dimension as the wall thickness; the coupling beams either consist of two bundles of diagonal (diag.) reinforcement (A_{vd}) for Archetypes with DR beams or top and bottom longitudinal (long.) reinforcement for Archetypes with CR beams.

Table A-1: Low-rise Archetype Designs

Archetype ID	Floor Level	f'_c (ksi)	Wall Pier Design						Coupling Beam Design		
			l_w (ft)	t_w (in.)	Outer A_{sb}	Web A_{sb}	Inner A_{sb}	Shear Reinf.	l_n (ft)	h (in.)	CB Reinf.
6H-DR-2.0	5-6	6.00	8.00	10	8#5	14#4	6#5	2#6@9”	5.00	30	6#8 diag.
	3-4			14	12#8	12#4	6#5	2#6@6”			8#8 diag.
	1-2			14	14#11	10#5	6#6	2#6@6”			8#8 diag.
6H-CR-5.0	5-6	6.00	8.00	10	8#5	14#4	6#5	2#6@10”	11.25	27	6#9 long.
	3-4			14	12#7	12#5	6#6	2#6@6”			6#10 long.
	1-2			14	14#10	10#5	6#6	2#6@6”			6#10 long.
4H-DR-2.0	3-4	6.00	7.00	12	8#6	10#4	6#4	2#6@10”	5.00	30	4#9 diag.
	1-2				8#9	10#5	6#6	2#6@9”			4#10 diag.
4H-CR-5.0	3-4	6.00	7.00	12	8#5	10#4	6#4	2#6@12”	11.25	27	3#11 long.
	1-2				8#9	10#5	6#6	2#6@10”			3#11 long.
2H-DR-2.0	1-2	4.00	10.00 (H/l_w = 2)	10	8#7	18#5	8#7	2#5@8”	4.00	24	4#7 diag.
2H-CR-5.0	1-2	4.00		10	10#6	14#4	10#6	2#5@9”	10.00	24	3#8 long.

Table A-2: 8-Story Ductile Coupled Wall Archetype Designs

Archetype ID	Floor Level	f'_c (ksi)	Wall Pier Design						Coupling Beam Design			
			l_w (ft)	t_w (in.)	Outer A_{sb}	Web A_{sb}	Inner A_{sb}	Shear Reinf.	l_n (ft)	h (in.)	A_{vd}	$A_{long.}$
8H-DR-3.0	7-8	6.00	8.50	10	6#7	10#4	6#4	2#5@8”	7.50	30	6#8 6#9	-
	6 5	6.00		10 12	8#9	16#4	6#5	2#6@8”			6#9 6#10	
	3-4	6.00		14	12#10	16#5	6#6	2#6@7”			6#11 6#11	
	1-2	7.00		14	16#11	12#6	6#7	2#6@6”			6#11 6#11	
8H-DR-2.4	7-8	6.00	8.50	10	6#7	10#4	6#4	2#5@7”	6.00	30	6#7 6#8	-
	6 5	6.00		10 12	8#9	16#4	6#5	2#6@8”			6#9 6#10	
	3-4	6.00		14	12#10	16#5	6#6	2#6@7”			6#10 6#10	
	1-2	7.00		14	16#11	12#6	6#7	2#6@6”			6#10 6#10	
8H-DR-2.0	7-8	6.00	8.50	10	6#7	10#4	6#4	2#5@7”	5.50	33	6#7 6#8	-
	6 5	6.00		10 12	8#9	16#4	6#5	2#6@8”			6#8 6#9	
	3-4	6.00		14	12#10	16#5	6#6	2#6@7”			6#10 6#10	
	1-2	7.00		14	16#11	12#6	6#7	2#6@6”			6#10 6#10	
8H-DR-3.3 and CR-3.3	7-8	6.00	8.50	10	6#7	10#4	6#4	2#5@8”	8.25	30	6#9 6#9	4#9 4#10
	6 5	6.00		10 12	8#9	16#4	6#5	2#6@8”			6#9 6#10	4#10 4#11
	3-4	6.00		14	12#10	16#5	6#6	2#6@7”			6#11 6#11	6#10 6#10
	1-2	7.00		14	16#11	12#6	6#7	2#6@6”			6#11 6#11	6#10 6#10
8H-CR-4.0	7-8	6.00	8.50	10	6#7	10#4	6#4	2#5@8”	10.00	30	-	4#10 4#10
	6 5	6.00		10 12	8#9	16#4	6#5	2#6@8”				4#10 6#10
	3-4	6.00		14	12#10	16#5	6#6	2#6@7”				6#10 6#10
	1-2	7.00		14	14#11	14#6	6#7	2#6@6”				6#10 6#10
8H-CR-5.0	7-8	6.00	8.50	10	6#7	10#4	6#4	2#5@8”	11.25	27	-	4#10 4#10
	6 5	6.00		10 12	8#9	16#4	6#5	2#6@8”				4#11 6#10
	3-4	6.00		14	12#10	16#5	6#6	2#6@7”				6#10 6#10
	1-2	7.00		14	14#11	14#6	6#7	2#6@6”				6#10 6#10

Table A-3: 12-Story Archetype Designs

Archetype ID	Floor Level	f'_c (ksi)	Wall Pier Design: l_w (ft)	t_w (in.)	Outer A_{sb}	Web A_{sb}	Inner A_{sb}	Shear Reinf.	Coupling Beam Design: l_n (ft)	h (in.)	A_{vd}	$A_{long.}$
12H-DR-3.0	11-12	6.00	9.25	12	8#5	14#4	8#4	2#5@10”	7.50	30	6#8 6#9	-
	9-10			12	12#7	14#4	8#4	2#6@10”			6#9 6#10	
	7-8			12	12#8	14#5	8#5	2#6@9”			6#10 6#10	
	5-6			12	14#9	14#6	8#6	2#6@8”			6#10 6#10	
	3-4			16	16#10	14#7	8#7	2#6@6”			6#11 6#11	
	1-2			16	1#11	10#8	8#8	2#6@6”			6#11	
12H-DR-2.4	11-12	6.00	9.25	same as DR-3.0	same as DR-3.0…			same as DR-3.0	6.00	30	6#8 6#8	-
	9-10										6#9 6#9	
	7-8										6#9 6#10	
	1-6										…	
12H-DR-2.0	11-12	6.00	9.25	12	same as DR-3.0			same as DR-3.0	5.50	33	6#7	-
	9-10			12							6#8	
	5-8			12							6#9	
	1-4			16							6#10	
12H-DR-3.3 and CR-3.3	11-12	6.00	10.00	12	same as CR-5.0			same as CR-5.0	8.33	30	6#9 6#9	4#9 4#10
	9-10	6.00		12							6#10 6#10	4#10 4#11
	5-8	6.00		12							6#10	4#11
	1-4	7.00		16							6#11	5#11
12H-CR-4.0	11-12	6.00	10.00	12	same as CR-5.0			same as CR-5.0	10.00	30	-	4#10
	8-10			12								4#11
	5-7			12								5#11
	1-4			16								5#11
12H-CR-5.0	11-12	6.00	10.00	12	8#5	14#4	8#4	2#5@10”	12.5	30	-	4#10 4#11
	9-10			12	10#7	14#4	8#5	2#5@8”				4#11
	7-8			12	12#8	14#4	8#5	2#6@10”				5#11
	5-6			12	12#9	14#5	8#6	2#6@8”				5#11
	3-4			16	14#10	14#6	8#7	2#6@7”				6#11
	1-2			16	18#11	14#7	8#8	2#6@6”				6#11

Table A-4: 18-Story Archetype Designs

Archetype ID	Floor Level	f'_c (ksi)	Wall Pier Design l_w (ft)	Wall Pier Design t_w (in.)	Wall Pier Design A_{sb}	Wall Pier Design Shear Reinf.	Coupling Beam Design l_n (ft)	Coupling Beam Design h (in.)	Coupling Beam Design A_{vd}	Coupling Beam Design $A_{long.}$
18H-DR-3.0	18 17	8.00	9.00	16	2#5@12”	2#5@14” 2#6@8”	7.50	30	6#8	-
	15-16			16	2#5@9”	2#6@6”			6#9	
	12-14			16	2#6@6”	2#6@6”			6#10	
	9-11			16	2#7@6”	2#6@5”			6#10	
	6-8			20	3#7@6”	2#7@6”			6#11	
	3-5			24	3#9@6”	2#7@5”			8#10	
	1-2			24	3#10@6”	2#7@5”			8#10	
18H-DR-2.4	18 17	8.00	9.00	16	same as DR-3.0	same as DR-3.0	6.00	30	6#7 6#8	-
	16 15			16					6#8 6#9	
	12-14			16					6#9	
	9-11			16					6#10	
	6-8			20					6#11	
	1-5			24					6#11	
18H-DR-2.0	18 17	8.00	9.00	16	same as DR-3.0	2#5@12” 2#6@8”	5.50	33	6#6 6#7	-
	14-16			16		same as DR-3.0			6#8	
	9-13			16					6#9	
	7-8			16					6#10	
	6			20					6#11	
	1-5			24		2#7@4.5”			6#11	
18H-DR-3.3 and CR-3.3	18 17	8.00	9.00	16	same as DR-3.0	2#5@14” 2#6@8”	8.33	30	6#8 6#9	4#9 4#10
	16 15			16		2#6@7”			6#9 6#10	4#10
	12-14			16		2#6@6”			6#10	4#11
	9-11			16		2#6@5”			6#11	5#11
	6-8			16		2#7@6”			8#10	6#11
	3-5			20		2#7@5”			8#10	6#11
	1-2			24		2#7@5”			8#10	6#11

Table A-4 continued…

Archetype ID	Floor Level	f'_c (ksi)	Wall Pier Design				Coupling Beam Design			
			l_w (ft)	t_w (in.)	A_{sb}	Shear Reinf.	l_n (ft)	h (in.)	A_{vd}	$A_{long.}$
18H-CR-4	18 17	8.00	9.00	16	2#5@12”	2#5@14” 2#5@9”	10.00	30	-	4#10
	16 15			16	2#5@9” 2#5@6”	2#6@9” 2#6@7”				4#11
	14 13 12			16		2#6@6”				4#11 5#11 5#11
	9-11			16		2#6@5”				5#11
	6-8			16	same as CR-3.3	2#7@6”				6#11
	5 4			20		2#7@5”				6#11
	3 2 1			24		2#7@5”				6#11
18H-CR-5	18 17 16	8.00	9.00	16	2#5@12” 2#5@12” 2#5@9”	2#5@14” 2#5@10” 2#6@10”	12.50	30	-	4#11
	15			16	2#5@6”	2#6@8” 2#6@7”				5#11
	14 13 12			16	same as CR-3.3	2#6@6”				5#11
	9-11			16		2#6@5”				6#11
	6-8			16		2#7@6”				8#10
	3-5			20	3#10@6”	2#7@5”				8#10
	1-2			24	3#11@6”	2#7@5”				8#10

Table A-5: 24-Story Archetype Designs

Archetype ID	Floor Level	f'_c (ksi)	Wall Pier Design				Coupling Beam Design			
			l_w (ft)	t_w (in.)	A_{sb}	Shear Reinf.	l_n (ft)	h (in.)	A_{vd}	$A_{long.}$
	22-24			18	2#4@12”	2#5@12” 2#5@12” 2#5@8”			6#8 6#8 6#9	
	19-21			18	2#6@12”	2#6@6”			6#9 6#9 6#10	
	17-18			24	3#6@12”	2#6@6”			6#11	
	14-16			24	#7@12”	2#6@6”			6#11	
24H-DR-3.0	11-13	10.00	9.00	24	3#7@12”	2#7@8”	7.50	30	6#11 6#11 8#10	-
	8-10			24	3#8@12”	2#7@6”			8#10 8#11 8#11	
	5-7			24	3#8@6”	2#8@6”			8#11	
	3-4			24	3#9@6”	2#8@6”			8#11	
	1-2			24	3#10@6”	2#8@6”			8#11	
24H-DR-2.4	23-24 21-22 19-20 12-18 7-11 1-6	10.00	9.00	18 18 18 24 24 24	same as DR-3.0	same as DR-3.0	6.00	30	6#7 6#8 6#9 6#10 6#11 8#10	-
24H-DR-2.0	24 22-23 19-21 13-18 8-12 1-7	10.00	9.00	18 18 18 24 24 24	same as DR-3.0	same as DR-3.0	5.50	33	6#6 6#7 6#8 6#9 6#10 6#11	-
	23-24			18		2#5@12”			6#8	4#9
	21-22			18		2#5@6”			6#9	4#9 4#10
	19-20			18		2#5@6” 2#6@8”			6#9 6#10	4#10
24H-DR-3.3 and CR-3.3	17-18 14-16 12-13	10.00	9.00	24	same as DR-3.0	2#6@8” 2#6@6” 2#7@8”	8.33	30	6#11	5#11
	10-11			24		2#7@8” 2#7@6”			8#10	5#11 6#11
	7-9			24		2#7@6”			8#11	6#11
	1-6			24		2#8@6”			8#11	6#11

Table A-5 continued…

Archetype ID	Floor Level	f'_c (ksi)	Wall Pier Design				Coupling Beam Design			
			l_w (ft)	t_w (in.)	A_{sb}	Shear Reinf.	l_n (ft)	h (in.)	A_{vd}	$A_{long.}$
24H-CR-4	23-24	10.00	9.00	18	2#4@12”	2#5@12”	10.00	30	-	4#9 4#10
	21-22			18	2#5@12”	2#5@8” 2#5@6”				4#10
	19-20			18	2#6@12”	2#5@6” 2#6@8”				4#11
	16-18 15 14 12-13			24	same as DR-3.0	2#6@8” 2#6@6” 2#6@6” 2#7@8”				5#11 5#11 6#11 6#11
	10-11			24		2#7@8”				6#11
	9 6-8			24		2#7@6”				6#11 8#10
	1-5			24		2#8@6”				8#10
24H-CR-5	23-24	10.00	9.00	18	2#4@12”	2#5@12”	12.50	30	-	4#10 4#11
	21-22			18	2#5@12”	2#5@9” 2#5@6”				4#11
	19-20			18	2#7@12”	2#5@6” 2#6@8”				5#11
	16-18 14-15 12 13			24	same as DR-3.0	2#6@8” 2#6@6” 2#7@8” 2#7@8”				6#11 8#10 8#10 8#11
	10-11			24		2#7@8”				8#11
	6-9			24		2#7@6”				8#11
	5 3-4 1-2			24	3#8@6” 3#9@6” 3#10@6”	2#8@6”				8#11

Table A-6: 30-Story Archetype Designs

Archetype ID	Floor Level	f'_c (ksi)	Wall Pier Design				Coupling Beam Design			
			l_w (ft)	t_w (in.)	A_{sb}	Shear Reinf.	l_n (ft)	h (in.)	A_{vd}	$A_{long.}$
	29-30			18	2#4@9”	2#5@10”			6#8	
	27-28				2#5@9”	2#6@8”			6#9	
	25			18	2#6@9”	2#6@6”			6#9	
	26								6#10	
	24			18	2#7@9”	2#6@6”			6#10	
	23					2#7@7”				
	21-22			18	2#8@9”	2#7@7”			6#10	
30H-DR-3.0	15-20	11.25	9.00	24	3#6@6”	2#7@7”	7.50	30	6#11	-
	14					2#7@6”				
	11-13			24	3#7@6”	2#7@6”			8#10	
	9-10			30	3#7@6”	2#8@7”			8#11	
	7-8				3#8@6”	2#8@6”				
	5-6			30	3#9@6”	2#8@6”			8#11	
	3-4			30	3#10@6”	2#8@5.5”			8#11	
	1-2			30	3#11@6”	2#8@5.5”			8#11	
	30			18	2#4@9”				6#7	
	27-29								6#8	
	26			18	2#5@9”	same as DR-3.0			6#9	
	24-25				2#6@9”				6#9	
	23				2#7@9”				6#9	
	22				2#7@9”				6#10	
	21				2#8@9”				6#10	
30H-DR-2.4	16-20	11.25	9.00	24	3#6@6”		6.00	30	6#10	-
	11-15								6#11	
	9-10			30	3#6@6”				8#11	
	7-8				3#7@6”					
	5-6			30	3#8@6”	2#8@6”			8#11	
	3-4				3#9@6”					
	1-2			30	3#10@6”	2#8@5.5”			8#11	
	28-30			18	2#4@9”				6#7	
	27								6#8	
	25-26			18	2#5@9”	same as DR-2.4 except			6#8	
	24			18	2#7@9”				6#9	
	21-23				2#7@9”					
30H-DR-2.0	15-20	11.25	9.00	24	3#6@6”	2#8@7” at L12 and 2#7@6” at L15	5.50	33	6#10	-
	11-14				3#6@6”				6#11	
	9-10			30	3#6@6”				8#10	
	7-8				3#7@6”					
	5-6				3#8@6”					
	3-4				3#9@6”					
	1-2			30	3#10@6”				8#10	

Table A-6 continued…

Archetype ID	Floor Level	f'_c (ksi)	Wall Pier Design				Coupling Beam Design			
			l_w (ft)	t_w (in.)	A_{sb}	Shear Reinf.	l_n (ft)	h (in.)	A_{vd}	$A_{long.}$
30H-DR-3.3 and CR-3.3	30 29 28	11.25	9.00	18	same as DR-3.0	2#5@12” 2#5@12” 2#5@8”	8.33	30	6#9 6#9 6#10	4#9 4#10 4#10
	26-27 25			18		2#6@8” 2#6@6”			6#10	4#10
	23-24 21-22			18		2#6@6” 2#7@8”			6#11	4#10
	17-20 15-16 14 11-13			24		2#7@8” 2#7@7” 2#7@7” 2#7@6”			8#10 8#11 8#11 8#11	4#10 4#10 4#11 4#11
	9-10 8			30		2#8@7”			10#11	5#11 6#11
	4-7 1-3			30		2#8@6” 2#8@5.5”			10#11	6#11
30H-CR-4	30 29	11.25	9.00	18	same as DR-3.0	2#5@12” 2#5@12”	10.00	30	-	4#10 4#11
	27-28			18		2#6@9”				4#11
	26 23-25 22 21			18		2#6@8” 2#6@6” 2#7@8” 2#7@8”				5#11 5#11 5#11 6#11
	17-20 14-16 11-13			24		2#7@8” 2#7@7” 2#7@6”				6#11 8#10 8#10
	7-10 5-6			30		2#8@7” 2#8@6”				8#11
	3-4 1-2			30	3#10@6” 3#11@6”	2#8@5.5”				8#11
30H-CR-5	30 29	**12.00**	9.00	18	2#4@9”	2#5@12”	12.50	30	-	4#11 5#11
	27-28			18	2#5@9”	2#6@9”				5#11
	25-26 24 21-23			18	2#6@9” 2#6@9” 2#7@9”	2#6@8” 2#6@6” 2#7@9”				5#11 6#11 6#11
	19-20 14-18 11-13			24	3#6@6”	2#7@9” 2#7@8” 2#7@7”				8#10 8#11 8#11
	9-10 7-8 5-6			30	3#6@6” 3#7@6” 3#9@6”	2#8@8” 2#8@6” 2#8@6”				10#11
	3-4 1-2			30	3#10@6” 3#11@6”	2#8@6”				10#11

References

[1] Abdullah S., and Wallace, J.W. (2019). “Drift Capacity of Structural Walls with Special Boundary Elements”, *ACI Structural Journal,* Vol. 116, No. 1, pp.183-194.

[2] ACI. (2014). “Building code requirements for structural concrete.” *ACI 318-14*, Farmington Hills, MI.

[3] ACI. (2018). “Building code requirements for structural concrete.” *ACI 318-19, Public Review*, Farmington Hills, MI.

[4] Adebar, P., Hindi, R., and Gonzalez, E., “Seismic Behavior of a Full-Scale Diagonally Reinforced Slender Coupling Beam,” Techncal Report, Dept. of Civil Engineering, The University of British Columbia, Vancouver, Canada, 2001.

[5] Aktan, A., and Bertero, V. (1984). Seismic Response of R/C Frame-Wall Structures. *Jounral of Structural Engineering , 110* (8), 1803-1821.

[6] ASCE/SEI. (2016). “Minimum design loads for buildings and other structures.” *ASCE/SEI 7-16*, Reston, VA.

[7] ASCE 41-13, “Seismic Evaluation and Retrofit of Existing Buildings.” American Society of Civil Engineers, Reston, Virginia.

[8] Barney, K., Rabbat, B., Fiorato, A. E., Russell, H. G., and Corley, W. G. (1980). Behavior of Coupling Beams under Load Reversals. *Portland Cement Association*.

[9] Belarbi, A. and Hsu, T.C. (1994). “Constitutive Laws of Concrete in Tension and Reinforcing Bars Stiffened By Concrete”, *ACI Structural Journal*, Vol. 91, No. 4, pp. 465-474.

[10] Binney, J. (1972). *Diagonally Reinforced Coupling Beams.* MS Thesis, University of Canterbury, Christchurch, New Zealand.

[11] Bower, O. (2008). *Analytical Investigation into the Effect of Axial Restraint on the Stiffness and Ductility of Diagonally Reinforce Concrete Coupling Beams.* Masters Thesis, University of Cincinnati.

[12] Brena, S., and Ihtiyar, O. (2011). Preformance of conventinoally reinforced coupling beams subjectd to cyclic loading. *Journal of Structural Engineering, 137*, 665-676.

[13] Bristowe, S. (2000). *Seismic response of normal and high-strength concrete members.* PhD Thesis, McGill University, Canada.

[14] Canadian Standards Association (CSA) (2014). *CAN/CSA-A23.3-14 Design of Concrete Structures*.

[15] Canbolat, A., Parra-Montesinos, G.J., and Wight, J.K. (2005). Expeirmental Study on Seismic Behavior of High Performance Fiber-Reinforced Cement Composite Coupling Beams. *ACI Structural Journal, 102-S17*, 159-166.

[16] Dugas, D. (2003). *Seismic response of diagonally reinforced coupling beams with headed bars.* MS Thesis, McGill University, Canada.

[17] Elwood KJ, Moehle JP (2003). “Shake Table Tests and Analytical Studies on the Gravity Load Collapse of Reinforced Concrete Frames.”, PEER report 2003/01, Berkeley: Pacific Earthquake Engineering Research Center, University of California, 2003.

[18] FEMA. (2009). “Quantification of building seismic performance factors.” *FEMA P695*, Washington, DC.

[19] Filippou, F.C.; Popov E.G.; and Bertero, V.V., 1983, “Effects of Bond Deterioration on Hysteretic Behavior of Reinforced Concrete Joints”, EERC Report No. UCB/EERC-83/19, Earthquake Engineering Research Center, University of California, Berkeley.

[20] Fortney, P. (2005). *The Next Generation of Coupling Beams.* PhD Thesis, University of Cincinnati.

[21] Galano, L., and Vignoli, A. (2000). Seismic behavior of short coupling beams with different reinforcement layouts. *ACI Structural Journal, 97*, 876-885.

[22] Iguchi, M., and Luco, J.E., 1982, “Vibration of flexible plate on viscoelastic medium,” *Journal of Engineering Mechanics*, Vol. 108, No. 6, pp. 1103-1120.

[23] Kanakubo, T., Fujisawa, M., Sako, N., and Sonobe, Y. (1996). “Ductility of Short Span RC Beams.” *Proceedings, Eleventh World Conference on Earthquake Engineering*, 1369.

[24] Kent, D.C. and Park, R., 1971, “Flexural Members with Confined Concrete”, *Journal of the Structural Division*, ASCE, V. 97, No. ST7, pp. 1969-1990.

[25] Kimura, Y. (1996). Experimental Study on Seismic Behavior of R/C Diagonally Reinforced Short Beams. Proceedings, *Eleventh World Conference on Earthquake Engineering.*

[26] Kolozvari K, Orakcal K, and Wallace JW (2018). "New OpenSees Models for Simulating Nonlinear Flexural and Coupled Shear-Flexural Behavior of Reinforced Concrete Walls and Columns", *Computers and Structures Journal*, 196: 246-262.

[27] K. Kolozvari, V. Terzic, R. Miller, and D. Saldana (2018), “Assessment of Dynamic Behavior and Seismic Performance of a High-Rise RC Coupled Wall Building”, Engineering Structures, 176:606-620.

[28] Kolozvari K and Wallace JW (2016). "Practical Nonlinear Modeling of Reinforced Concrete Structural Walls", *ASCE Journal of Structural Engineering*, Vol. 142, No. 12.

[29] Kolozvari K, Orakcal K, and Wallace, JW (2015a). "Modeling of cyclic shear-flexure interaction in reinforced concrete structural walls. Part I: Theory." *ASCE J. of Struct. Eng*., 141(5) 04014135.

[30] Kolozvari K, Orakcal K, Wallace JW (2015c). "Shear-Flexure Interaction Modeling for Reinforced Concrete Structural Walls and Columns under Reversed Cyclic Loading," Pacific Earthquake Engineering Research Center, PEER Report No. 12/2015.

[31] Kolozvari K, Tran T, Orakcal K. and Wallace JW (2015b). "Modeling of cyclic shear-flexure interaction in reinforced concrete structural walls - Part II: Experimental validation." *ASCE Journal of Structural Engineering*, 141 (5) 04014136.

[32] Kwan, A., and Zhao, Z. (2002). Cyclic behaviour of deep reinforced concrete coupling beams. *Proc Inst Civil Eng: Struct Build, 152*, 283-293.

[33] Kwan, A., and Zhao, Z. (2002). Testing of coupling beams with equal end rotations maintained and local joint deformation allowed. *Proc Inst Civil Eng: Struct Build, 152*, 67-78.

[34] Lequesne, R. D., Parra-Montesinos, G. J. and Wight, J. K. (2009), "Test of a Coupled Wall with High Performance Fiber Reinforced Concrete Coupling Beams," Thomas T. C. Hsu Symposium: Shear and Torsion of Concrete Structures, SP-265, American Concrete Institute, Farmington Hills, MI.

[35] Lim, E., Hwang, S.-J., Cheng, C.-H., and Lin, P.-Y. (2016). Cyclic Tests of Reinforced Concrete Coupling Beam with Intermediate Span-Depth Ratio. *ACI Structural Journal, 113*(03), 515-524.

[36] Los Angeles Tall Buildings Structural Design Council (LATBSDC) (2017). "An Alternative Procedure for Seismic Analysis and Design of Tall Buildings Located in the Los Angeles Region."

[37] Mansour, M.Y., Hsu T.C., and Lee J.Y. (2002). "Pinching Effect in Hysteretic Loops of R/C Shear Elements." *ACI Special Publications*, Vol. 205, pp. 293-321.

[38] McKenna F, Fenves GL, Scott MH, and Jeremic B. Open System for Earthquake Engineering Simulation (OpenSees). Pacific Earthquake Engineering Research Center, University of California, Berkeley

[39] Menegotto, M. and Pinto, E., 1973, "Method of Analysis for Cyclically Loaded Reinforced Concrete Plane Frames Including Changes in Geometry and Non-Elastic Behavior of Elements Under Combined Normal Force and Bending", *Proceedings*, IABSE Symposium on Resistance and Ultimate Deformability of Structures Acted on by Well-Defined Repeated Loads, Lisbon, Portugal.

[40] Naish, D., Fry, A., Klemencic, R., Wallace, J. (2013). Reinforced Concrete Coupling Beams – Part II: Modeling. *ACI Structural Journal*. 110:6, 1067-1075.

[41] Naish D, Wallace JW, Fry JA, Klemencic R. Reinforced concrete link beams: alternative details for improved construction, SGEL Report, University of California, Los Angeles CA, 2009.

[42] Naish, D. A. (2010). *Testing and Modeling of Reinforced Concrete Coupling Beams.* PhD Thesis, University of California, Los Angeles.

[43] NIST GCR 10-917-8 (2010). Evaluation of the FEMA P-695 Methodology for Quantificaiton of Building Seismic Performance Factors. NEHRP Consultants Joint Venture.

[44] NIST GCR 12-917-21. (2012). *Soil-Structure Interaction for Building Structures by NEHRP Consultants Joint Venture.* U.S. Department of Commerce. National Institute of Standards and Technology.

[45] NZS 3101 (2006). *Concrete Structures Standard, Part 1: The Design of Concrete Structures: Part 2: Commentary on the Design of Concrete Structures*, Standards New Zealand, Wellington, New Zealand. ISBN 1-86975-043-8.

[46] Orakcal K and Wallace JW (2006). "Flexural Modeling of Reinforced Concrete Walls - Experimental Verification." *ACI Structural Journal*, 103 2 196-206.

[47] Orakcal K, Conte JP, and Wallace JW (2004). "Flexural Modeling of Reinforced Concrete Structural Walls - Model Attributes." *ACI Structural Journal*, 101 (5) 688-698.

[48] Orakcal K, Massone LM, Wallace JW (2009). "Shear Strength of Lightly Reinforced Wall Piers and Spandrels." ACI Structural Journal, V. 106, No. 5, pp 455-465.

[49] Orakcal, K., Ulugteking, D., and Massone, L. M. (2012). "Constitutive Modeling of Reinforced Concrete Panel Behavior under Cyclic Loading." *Proceedings, 15th World Conference on Earthquake Engineering*, Lisbon, Portugal, No. 3573.

[50] Paulay, T. (1971). Coupling Beams of Reinforced Concrete Shear Walls. *Journal of the Structural Division, American Society of Civil Engineers, 97*(3), 843-862.

[51] PEER (2017). "Guidelines for Performance-Based Seismic Design of Tall Buildings." Berkeley, CA.

[52] PEER Report 2014/18. (2014). *Three-Dimensional Beam-Truss Model for Reinforced-Concrete Walls and Slabs Subjected to Cyclic Static or Dynamic Loading* . Lu, Y.; Panagiotou, M.; Koutromanos, I.;. Berkeley, CA: Pacific Earthquake Engineering Research Center .

[53] Perform 3D, 3D Performance Based Design Software, Computers and Structures Inc.

[54] Poudel, A., Lequesne, R., and Lepage, A. (2018). "Diagonally Reinforced Concrete Coupling Beams: Effects of Axial Restraint". SL Report No. *18-3 2018-09*, University of Kansas Center for Research, Inc., 39pp.

[55] Rodriguez, ME, Botero JC, and Villa J (1999). "Cyclic Stress-Strain Behavior of Reinforcing Steel including Effect of Buckling." Journal of Structural Engineering, June 1999, pp 605-612.

[56] Santhakumar, A. R. (1974). *The Ductiltiy of Coupled Shear Walls.* PhD Thesis, University of Canterbury, Christchurch, New Zealand.

[57] Scott, B.D.; Park, R.; and Priestley, M.J.N., 1982, "Stress-Strain Behavior of Concrete Confined by Overlapping Hoops at Low and High Strain Rates", *Journal of the American Concrete Institute*, V. 79, No. 1, pp. 13-27.

[58] Segura, C. L., and Wallace, W. J., 2018a, "Seismic Performance Limitations and Detailing of Slender Reinforced Concrete Walls," *ACI Structural Journal*, V. 115, No. 3, May, pp. 849-860. doi: 10.14359/51701918

[59] Segura, C. L., and Wallace, W. J., 2018b, "Impact of Geometry and Detailing on Drift Capacity of Slender Walls," *ACI Structural Journal*, V. 115, No. 3, May, pp. 885-896. doi: 10.14359/51702046

[60] Sugaya, K. (2003). Experimental Study on Variation Mechanism of Carrying shear force at the time of the earthquake of Coupling Beams with T-shaped Continuous Layer Coupled Wall. PhD Thesis, Japan.

[61] Sugaya, Teshigawara, and Kato. (2000). Experimental Study on Carrying Shear Force Ratio of 12 Story Coupled Shear Wall. *12WCEE.*

[62] Tassios, T., Moretti, M., and Bezas, A. (1996). On the behavior and ductility of reinforced concrete coupling beams of shear walls. *ACI Structural Journal, 93*, 711-720.

[63] Taucer F.F., Spacone E., and Filippou F.C. (1991). "A fiber beam-column element for seismic response analysis of reinforced concrete structures." Rep. No. UCB/EERC-91/17, Earthquake Engineering Research Center, College of Engineering, University of California, Berkeley, CA.

[64] Tegos, I.A. and Penelis, G. Gr. (1988). Seismic Resistance of Short Columns and Coupling Beams Reinforced with Inclined Bars. *ACI Structural Journal, 85-S10*, 82-88.

[65] Tran TA and Wallace JW (2012). "Experimental Study of Nonlinear Flexural and Shear Deformations of Reinforced Concrete Structural Walls." Proceedings of the 15th World Conference on Earthquake Engineering, Lisbon, Portugal.

[66] Ulugtekin D (2010). "Analytical Modeling of Reinforced Concrete Panel Elements under Reversed Cyclic Loadings," M.S. Thesis, Department of Civil Engineering, Bogazici University.

[67] Vecchio, F.J., and Collins, M.P. (1993). "Compression Response of Cracked Reinforced Concrete." *ASCE Journal of Structural Engineering*, Vol. 83, No. 2, pp. 219-231.

[68] Wallace JW, Elwood KJ, Massone LM, (2008) “An Axial Load Capacity Model for Shear Critical RC Wall Piers.” Journal of Structural Engineering, ASCE, Vol. 134, No. 9, pp 1548-1557.

[69] Wallace, J. W.; Moehle, J. P., Ductility and Detailing Requirements of Bearing Wall Buildings, Journal of Structural Engineering, ASCE, Vol. 118(6): 1625- 1644, (June 1992).

[70] Yassin, M.H.M., 1994, “Nonlinear Analysis of Prestressed Concrete Structures Under Monotonic and Cyclic Loads”, Dissertation, University of California, Berkeley.

[71] Zhou, J., 2003, “Effect of Inclined Reinforcement on Seismic Response of Coupling Beams”, Dissertation, McGill University, Montreal, Canada.

[72] Zhu, Y., Zhou, F.L., and Su, R.K.L. (2008). “Seismic Effects on Coupled Shear Wall Structure by Coupling Beams with Side Bolted Steel Plates.” *Proceedings, 14th World Conference on Earthquake Engineering*, Beijing, China.